Master's Thesis

Màster en Enginyeria de l'Energia

Numerical modeling and experimental analysis of the desorption process in a metal hydride hydrogen storage system

PROJECT REPORT

Author: Raquel Busqué Somacarrera
Directors: Attila Husar, Ricardo Torres Cámara

Call: June 2017

Escola Tècnica Superior
d'Enginyeria Industrial de Barcelona

Abstract

The highly increasing energy demand and reduction of available fossil energy sources have made it important to develop a new technique for energy storage, hydrogen being a good alternative for the future. That is the reason why within this project, the storage of hydrogen as an adsorbed element in metal hydride bottles has been studied, more specifically hydrogen desorption and discharge.

To this end, a two-dimensional axisymmetric model is developed to study the hydrogen desorption reaction and resultant mass and heat transport phenomena inside a metal hydride canister. Moreover, the work has also been focused on experimental tests performed on an in-house fabricated setup using different heating scenarios.

It is important to mention that the studied system has a lot of unknowns, as the metal inside the bottle, as well as the internal canister structure and morphology are not known. That is the reason why an extensive study on the effects of the metal properties on desorption performance is carried out through non-destructive testing (NDT). The numerical model results are explained in detail and compared with experimental data as well, obtaining a good agreement.

Finally, the results obtained can not only be used to select metal hydride materials but also to evaluate the degradation of the canisters in terms of total hydrogen storage capacity.

Resumen

El gran aumento de la demanda energética y la reducción de las fuentes de energía fósil disponibles han hecho que sea importante desarrollar una nueva técnica para almacenar energía, siendo el hidrógeno una buena alternativa para el futuro. Por esa razón, en este proyecto se ha estudiado el almacenamiento de hidrógeno como elemento adsorbido en botellas de hidruro metálico, más concretamente la desorción y descarga de hidrógeno.

Con esta finalidad, se ha desarrollado un modelo 2D axisimétrico para estudiar la reacción de desorción y los fenómenos resultantes de transporte de masa y energía dentro de la botella de hidruro metálico. Este trabajo también se ha centrado en ensayos experimentales realizados en un montaje de fabricación propia, teniendo en cuenta distintos escenarios caloríficos.

Es importante mencionar que el sistema estudiado tiene muchas incógnitas, ya que el metal dentro de la botella, al igual que la estructura y morfología interna del contenedor no son conocidos. Esta es la razón por la que un exhaustivo estudio de los efectos de las propiedades del metal en la desorción se ha desarrollado a través de ensayos no destructivos. Los resultados del modelo numérico están detalladamente explicados, y comparados con los datos experimentales obteniendo una buena concordancia entre los datos.

Finalmente, los resultados obtenidos pueden usarse para seleccionar hidruros metálicos, pero también para evaluar la degradación de las botellas en términos de capacidad total de almacenamiento de hidrógeno.

Acknowledgements

I would like to thank all those who made possible the realization of this project. First and foremost, I would like to express my gratitude to the fuel cell laboratory of the Institut de Robòtica i Informàtica Industrial (CSIC/UPC) for giving me the opportunity to do the necessary research work in their institution and also giving me all the necessary resources and elements to do so.

Additionally I would like to thank Professor Dr. Ricardo Torres for his suggestions and for helping throughout the entire research process. I would also like to thank Dr. Attila Husar for the project supervision and help during the development of the project.

I want to give an acknowledgement to Vicente Roda, Uxía Reija and Alejandro Cifuentes for their help, support, interest and valuable insight, and for providing me with the possibility of collaboration in a friendly and stimulating environment.

Finally I would like to give my special thanks to my friends and family, for their continuous moral support and encouragement during the making of this project as well as throughout my entire studies.

CONTENTS

LIST OF FIGURES

LIST OF TABLES

Nomenclature

a	—	Speed of sound (m s^{-1})
A	—	Area (m^2)
b	—	Critical pressure ratio (-)
C_a	—	Adsorption rate constant (s^{-1})
C_d	—	Desorption rate constant (s^{-1})
c_p	—	Pressure specific heat capacity (J $kg^{-1}K^{-1}$)
c_v	—	Volume specific heat capacity (J $kg^{-1}K^{-1}$)
E	—	Energy (J)
E_a	—	Adsorption activation energy (J mol^{-1})
E_d	—	Desorption activation energy (J mol^{-1})
$\vec{f}$	—	Field body forces (N)
g	—	Gravity (m s^{-2})
$grille$	—	Outlet flow resistance (kg $m^{-4}s^{-1}$)
h	—	Convection heat transfer coefficient (W $m^{-2}K^{-1}$)
(H/M)	—	Hydrogen to metal ratio (-)
K	—	Permeability (m^2)
k	—	Specific thermal conductivity (W $m^{-1}K^{-1}$)
k_a	—	Adsorption velocity rate constant
K_{AV}	—	Available volume fraction (-)
k_d	—	Desorption velocity rate constant
K_{eq}	—	Equilibrium constant (-)
m	—	Mass (kg)
$\dot{m}$	—	Mass flow rate (kg s^{-1})
M	—	Molecular weight (g mol^{-1})
Ma	—	Mach number (-)
n	—	Number of mols (mol)
$\vec{n}$	—	Normal vector (-)
p	—	Pressure (Pa)
$\dot{Q}$	—	Heat flux (W)
$\dot{q}_i$	—	Conductive heat flux (W m^{-2})
R	—	Universal gas constant (J $mol^{-1}K^{-1}$)
R'	—	Specific gas constant (J $kg^{-1}K^{-1}$)
Re	—	Reynolds number (-)
S_m	—	Mass source/sink term (kg $m^{-3}s^{-1}$)
S_T	—	Energy source/sink term (W m^{-3})
t	—	Time (s)
T	—	Temperature (K)
$\vec{u}$	—	Velocity field (m s^{-1})
V	—	Volume (m^3)
$\dot{V}$	—	Volumetric flow (m^3s^{-1})
W	—	Work (W)

Greeks

γ	—	Adiabatic coefficient (-)
Δe_c	—	Kinetic energy (J)
Δe_p	—	Potential energy (J)
ΔG	—	Gibbs free energy (J)
Δh	—	Enthalpy (J)
ΔH	—	Formation enthalpy (J mol^{-1})
ΔS	—	Entropy (J $mol^{-1}K^{-1}$)
ε	—	Porosity (-)
θ	—	Desorbed hydrogen fraction (-)
θ_s	—	Surface coverage fraction (-)
μ	—	Dynamic viscosity (kg $m^{-1}s^{-1}$)
ρ	—	Density (kg m^{-3})
$\dot{\sigma}$	—	Irreversibilities
τ	—	Tortuosity (-)

Subscripts

0	—	Initial
emp	—	Empty
eq	—	Equilibrium
MH	—	Metal hydride
sat	—	Saturation

Superscripts

eff	—	Effective
g	—	Gas
m	—	Metal
ref	—	Reference

Chapter 1

Introduction and objectives

As energy consumption increases, society, industry and governments have become aware of the necessities to invest in sustainable energies that can decrease the problems associated with the use of fossil fuels and other non-renewable sources. Recent studies [36] show that the use of hydrogen as an energy vector can aid to satisfy the present and future energy demands without additional carbon emissions.

Due to its calorific value and being environmentally friendly, hydrogen energy has become a possible replacement for fossil fuels, depending on how it is produced. As hydrogen is abundant in water and in various hydrocarbons, it could be easily produced using renewable energy sources. Hence, it can facilitate the transition from the present fossil fuel energy economy to a future hydrogen based economy [17, 27].

A major concern that needs to be addressed to make hydrogen technology economically feasible is the safe storage of hydrogen in vessels with the desirable weight, volume and cost. The future of hydrogen as an energy vector will strongly depend on these technologies [33].

Hydrogen has the particularity of having a very low energy density per unit of volume, so it requires a lot of volume to store a large amount of energy in gaseous state. This is a problem when there is a limited amount of storage space available, for example in automotive applications.

Hydrogen can be stored in many ways, for example as a compressed gas inside high-pressure tanks. In order to satisfy space limitations and energy requirements depending on the application, pressures are typically around 700 bars. These levels of pressure cause safety concerns and a high energy cost when pressurizing the tanks.

Liquid storage in cryogenic tanks constitutes another possible alternative. The problem is that it would require extremely low temperatures and also a cooling system that would have high energy costs as well.

Hydrogen can also be stored as an adsorbed element in solid porous materials (metal hydride) [18]. Metal hydride based hydrogen storage offers certain advantages compared to high-pressure gaseous or cryogenic liquid storage systems in terms of compactness, storage at ambient

conditions, possibility of tailoring metal hydrides to suit different temperature-pressure requirements, as well as being inherently safe because hydrogen is stored at low pressure [3,31,34]. The disadvantage is that it offers low energetic density per unit of mass due to the weight of the metal itself. But on the contrary, it offers a high energy density per unit of volume.

A primary application of hydrogen storage is proton exchange membrane fuel cells (PEMFCs), which use pure hydrogen as their fuel [6].

Although considerable efforts have been made regarding the modeling of hydrogen adsorption and desorption in metal hydride vessels, a detailed analysis of its complex transport mechanisms, and mass and heat transfer is in great demand not only to enrich the current understanding of these processes, but also to efficiently design, to select suitable materials and to evaluate the degradation of the canisters for any industrial application involving metal hydrides.

This work is the continuation of a previous project titled: *Metal hydride state of charge estimator. Development and experimental validation of the hydrogen storage system model* [9], where the adsorption and charging of the bottles was studied.

In the current project, the objective is to study hydrogen desorption and subsequent discharge of a metal hydride hydrogen storage tank. Therefore, it provides an extensive study on the effects of each individual metal property through non-destructive testing (NDT), which has not been thoroughly analyzed in previous numerical studies. It is also important to mention that a detailed experimental setup has been designed and assembled emulating a real application using commercially available metal hydride canisters, which has not been widely investigated in prior studies.

The structure of this project is the following. First an introduction to the theoretical fundamentals, including charge and discharge mechanisms, transport in porous media, as well as adsorption isotherms, storage materials and discharge of pressurized tanks, is presented in Chapter 2. Next, in Chapter 3, there is a description of the mathematical model implemented, including a mesh independence study. As said, some experimental tests are performed, so, in Chapter 4, a definition of the experimental setup implemented, as well as the data acquisition system is introduced. Chapter 5 includes the numerical and experimental results, as well as the non-destructive studies of the metal properties that help calibrate the model, as the metal hydride and morphology of the bottle is unknown. This chapter also contains the relationship and comparison between simulation and experimental results. Finally, Chapters 6, 7 and 8 include the budget, the environmental impact and the planning of the project.

Chapter 2

Theoretical fundamentals

2.1 Charge and discharge mechanisms

First thing that is important to take into account is that the metal hydride bottle is assumed to be composed mainly by two regions. First, there is a porous region where the powdery metal is located and where adsorption/desorption take place, and then there is a buffer zone where hydrogen is accumulated waiting to enter the porous region or exit the bottle.

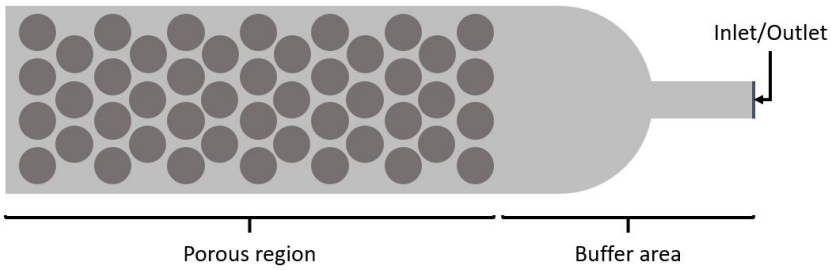

Figure 2.1: Scheme of the metal hydride bottle

Charging and discharging the bottles include two processes. In charge situation, the hydrogen first has to enter the bottle and then get adsorbed. On the contrary, in discharge situation the hydrogen has to get desorbed and then leave the bottle.

Focusing on the charge process, the first thing that needs to happen is that hydrogen enters inside the bottle. This process is pressure driven. Inside the bottle pressure is close to atmospheric conditions (as it was previously discharged leaving the outlet open to atmospheric pressure), and the supplied hydrogen is at a higher pressure, in the studied case around 6.5 bars. This pressure gradient forces the hydrogen to go towards the lower pressure zone, i.e. inside the bottle.

Once hydrogen is inside the bottle, the adsorption process can begin, as explained in section 2.3. At this point it is important to take into account that the adsorption reaction is exothermic, thus the temperature in the bottle will increase, exciting the hydrogen molecules and producing an increase in the pressure of the bottle. This increase in the bottle pressure will reduce the

difference between interior and exterior pressure (gradient), thus reducing the inlet rate, and consequently the adsorption process. For this reason, a good strategy is to remove the excess heat produced by the reaction. Using a fan, the bottle keeps cool, and so there is a pressure gradient that allows hydrogen to enter and get adsorbed at a higher rate, eventually storing larger amounts of hydrogen at a shorter charging time.

Regarding the discharge process the inverse situation happens. First hydrogen needs to get desorbed, and these released hydrogen molecules will increase the pressure inside the bottle. This way, a pressure gradient is generated, as the pressure inside the bottle is higher than the one outside (atmospheric pressure). This pressure difference forces the hydrogen to leave the bottle. Again, these processes can be improved, in this case using a heater. Supplying heat to the metal hydride bottles will make the particles inside the bottle to get excited and desorb at a much faster rate, increasing the pressure and so the discharge rate. This way, a more effective and faster discharge is accomplished.

This being said, the desorbed mass flow is not the same than the one exiting the bottle, as they follow two different kinetics. First, hydrogen is desorbed, following desorption kinetics generating a desorbed mass flow inside the bottle. These hydrogen molecules inside the bottle are in gas form, and so they will increase the pressure inside the bottle, creating a pressure gradient and allowing discharge.

2.2 Transport in a porous medium

Porous media are solid materials with internal pore structures. These pores can be either empty or filled with fluids.

2.2.1 Porosity, tortuosity and available volume fraction

One of the main characteristics of porous media is porosity, which can be defined as:

$$\varepsilon = \frac{\text{void volume}}{\text{total volume}} \tag{2.1}$$

Where, the void volume is the total volume of the void penetrable space in a porous medium.

Porosity may vary both spatially and temporally as material deformation can change its spatial distribution. If a porous material is homogeneous, its porosity can be easily calculated. Otherwise, if it is heterogeneous, the porosity is equal to the volume fraction of local interstitial fluid [38].

Porosity is only a measure of the average void volume fraction in a specific region of porous medium. It does not provide any information on how different pores are connected or on how many pores are available for fluid transport.

The path length between points A and B in a porous medium is measured by the distance between these points through connected pores. The shortest path length L_{min} can be characterized by the geometric tortuosity.

$$\tau = \left(\frac{L_{min}}{L}\right)^2 \tag{2.2}$$

Where L is the straight-line distance between A and B. By definition, τ is always greater than or equal to unity.

Not all penetrable pores are accessible to solutes. Such accessibility will depend on the molecular properties of the solutes. For example, a pore will be inaccessible to a solute if the solute molecule is larger than the pore or if the pore is surrounded by other pores that are smaller than the solute molecule. The portion of accessible volume that can be occupied by the solute is called the available volume. For a solute, the ratio of the available volume to the total volume is defined as the available volume fraction [38].

$$K_{AV} = \frac{\text{available volume}}{\text{total volume}} \tag{2.3}$$

By definition, K_{AV} is molecule-dependent and always smaller than the porosity ε.

2.2.2 Fluid flow in porous media

The movement of fluid molecules in porous media follows tortuous pathways in the void space. To describe the fluid flow in porous media two approaches can be used [38].

At fundamental microscale, the general Navier-Stokes equations can be applied and provide a complete description of the entire flow field. However, as a result of the complex and often only statistically known geometry of the solid surfaces in the medium, solution of the Navier-Stokes equations is generally very difficult.

On the macroscopic level, Darcy's law is a simple approximation that performs appropriate volume averages of the Navier-Stokes equations and it can also be applied in some cases. Between the complexity of the Navier-Stokes equations and the simplicity of Darcy's law there is a third possibility. The Brinkman equation suggests a general approach that interpolates between the Navier-Stokes equation and the Darcy's law.

2.2.2.1 Darcy's Law

The interaction between solid and liquid phases in porous media was first quantified by Darcy in 1856. Darcy discovered that the flow rate was proportional to the pressure gradient. This relationship is valid in many porous media, but is invalid for non-Newtonian fluids, for Newtonian liquids at high velocity, and for gases at very low and very high velocities. Darcy's Law also neglects the friction within the fluid and the exchange of momentum between fluid and solid phases.

The equation for momentum balance in porous media is Darcy's Law, which in a homogeneous and isotropic medium can be written as:

$$u = -K\nabla p \tag{2.4}$$

Where ∇p is the gradient of the hydrostatic pressure and K is a constant defined as the hydraulic conductivity. For non-isotropic and heterogeneous media, K is a tensor and it depends upon the location in the medium [38].

If the gravitational force is not negligible, Darcy's law must be modified as shown below:

$$u = -K(\nabla p - \rho g) \tag{2.5}$$

Where ρ is the density of the fluid and g is the acceleration due to gravity.

The hydraulic conductivity is inversely proportional to the viscosity of the fluid (μ), and the product of K and μ is defined as the specific hydraulic permeability (k) and depends only on microscopic structures of the porous medium.

$$k = K\mu \tag{2.6}$$

2.2.2.2 Brinkman Equation

Fluid flow in porous media may not be correctly modeled by Darcy's law because, from the physical point of view, Darcy's law assumes that the viscous resistance at the fluid-solid interface is much larger than that within the fluid, which implies a low specific permeability (k). The viscous stress within the fluid may not be negligible when k is large. In this case, the new momentum equation is called the Brinkman equation [38]:

$$\mu\nabla^2 u - \frac{1}{K}u - \nabla p = 0 \tag{2.7}$$

Darcy's law equation can be considered a special case of the Brinkman equation where the first term can be neglected.

2.2.2.3 Navier-Stokes Equation

Another possibility would be to directly use the Navier-Stokes equation, which is a much more complex expression, shown in equation (2.8). This expression takes into account all the geometry details by means of pores and narrow channels where the fluid would flow through.

$$\rho\frac{\partial \mathbf{u}}{\partial t} = \nabla\left[-p\mathbf{I} + \mu(\nabla\mathbf{u} + (\nabla\mathbf{u})^T) - \frac{2}{3}\mu(\nabla\mathbf{u})\mathbf{I}\right] + \mathbf{F} \tag{2.8}$$

This approach would require having the exact geometry that is being considered to be able to obtain results regarding how the fluid moves inside the interstices of the geometry, and the velocity in every single point of the domain.

The other two methods, Darcy's Law and Brinkman Equation, are approximations of the Navier-Stokes equation adapted to porous media and considering the material properties as constant parameters applied to the bulk.

2.3 Hydrogen storage in metal hydrides

Many metals and alloys can form metal hydrides with hydrogen leading to solid-state which can be used as a storage system under moderate temperature and pressure.

Metal hydrides can be formed reversibly according to the following reaction:

$$M + \frac{x}{2}H_2 \leftrightarrows MH_x + \Delta H$$

Where M represents the metal, MH_x is the respective hydride and x the ratio of hydrogen to metal. Finally ΔH is the heat of reaction.

2.3.1 Thermodynamic considerations

A spontaneous process requires Gibbs free energy, ΔG, to be negative. Taking into account that the entropy of the adsorbate, ΔS, is negative, and according to the following equation:

$$\Delta G = \Delta H - T\Delta S \tag{2.9}$$

In order for ΔG to be negative, ΔH must be negative. This means that the adsorption process should be exothermic and the degree of adsorption increases with decreasing temperature. Consequently the reverse reaction is endothermic and therefore heat is required for hydrogen release [41].

2.3.2 Adsorption and desorption phenomena and isotherms

Many physical and chemical processes occur at the interface. Adsorption (not to be confused with absorption) is one of the main and basic surface phenomena. Adsorption is found to occur in many natural physical, biological and chemical systems.

Solid surfaces show strong affinity for gas molecules that come in contact with them, and some of them get trapped on the surface.

In an adsorption process, spontaneous accumulation of a gas (adsorbate, in this case hydrogen) occurs at the solid surface (adsorbent or substrate, which is usually a porous material of large specific surface (m^2/g), in this case a metal alloy) as compared to the bulk phase.

There is a clear difference between the adsorption and absorption phenomena. Whilst in absorption there is physical penetration of one phase into the other, adsorption only occurs at the surface. However it is possible that both phenomena occur simultaneously, and in this case it can be difficult to separate the effects of each one of them, and even one phenomenon can affect the other, and that is why the term sorption is used [40].

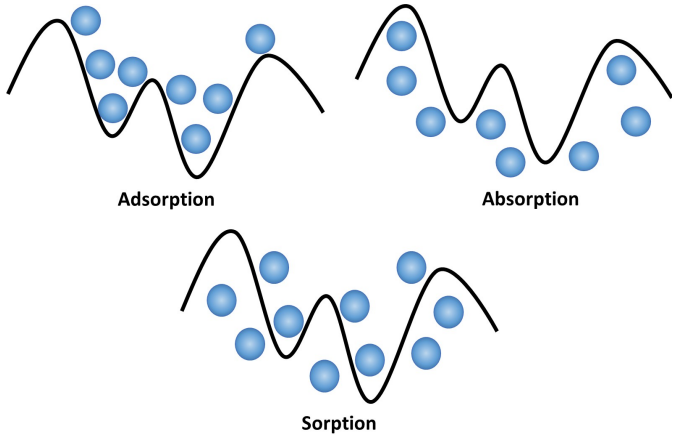

Figure 2.2: Difference between adsorption, absorption and sorption [40]

2.3.2.1 Physical and chemical adsorption

The adsorption process is generally classified as either:

- Physisorption (physical adsorption): gas molecules are attached to the solid surface through van der Waals forces (dipole interactions, dispersion and/or induction).
- Chemisorption (chemical adsorption): forces involved are valence forces of the same kind as those operating in the formation of chemical compounds.

The problem distinguishing between chemisorption and physisorption is basically the same as distinguishing chemical and physical interaction in general.

The main differences between chemisorption and physisorption are summarized in table 2.1.

In the case of hydrogen stored in metal hydrides, the adsorption process is physisorption, as it is reversible, enthalpies of adsorption are low and also the desorption product (hydrogen) is the same as the one that was adsorbed.

Physisorption	**Chemisorption**
Intermolecular forces of attraction are van der Waals forces	Valence forces of attraction are chemical bonds
Low enthalpy of adsorption $(5-50kJ/mol)$	High enthalpy of adsorption $(100-500kJ/mol)$
Reversible process (desorption)	Irreversible process
Multi-molecular layers may be formed	Generally, a mono-molecular layer is formed
Observed under low temperature conditions	Takes place at high temperatures
Non-activated, with equilibrium achieved relatively quickly. Increasing temperature always reduces surface coverage	Can be activated, in which case equilibrium can be slow and increasing temperature can favor adsorption.
Desorption produces products identical as the ones that were adsorbed	Desorption produces products different as the ones that were adsorbed
Multilayer adsorption: BET isotherm	Monolayer adsorption: Langmuir isotherm

Table 2.1: Differences between physisorption and chemisorption [39–41]

2.3.2.2 Adsorption equilibrium

Between the adsorbate (hydrogen) and adsorbent (metal) dynamic equilibrium is established, which results from the equalization of the number of adsorbed molecules with that of molecules undergoing desorption [41]:

$$A \leftrightarrows A_{ads}$$

Where A are the hydrogen molecules in the gas phase, and A_{ads} are in the adsorbed state.

In adsorption equilibrium these quantities depend on the gas temperature and pressure.

When studying adsorption equilibrium one of the parameters (quantity of adsorbed gas, pressure or temperature) remains unchanged. Usually this parameter is temperature and so, adsorption isotherms are used for these kind of systems.

2.3.2.3 Adsorption isotherms or Pressure-Composition-Temperature (PCT)

An adsorption isotherm or Pressure-Composition-Temperature (PCT) is the general relationship at constant temperature between the equilibrium adsorbed amount of gas and the gas pressure.

Metal hydride systems are pressure and temperature dependent since the thermodynamic conditions vary according to the solid phase structural and thermo-physical properties. Thus, characterization of this thermodynamic behavior is very important for metal hydride studies.

Langmuir isotherm:

In 1916, Irving Langmuir developed an adsorption model that is the most common one used to quantify the amount of adsorbate adsorbed on an adsorbent as function of partial pressure at a given temperature.

The Langmuir adsorption isotherm is based on the following assumptions [41]:

- The adsorbent surface consists of a certain number of active sites (proportional to the surface area), at each of which only one molecule may be adsorbed.
- No lateral interaction between the adsorbed molecules, thus the heat of adsorption is constant and independent of coverage.
- The adsorbed molecule remains at the site of adsorption until it is desorbed (the adsorption is localized).
- At maximum adsorption, only a monolayer is formed: molecules of adsorbate do not deposit on top of the already adsorbed ones, only on the free surface of adsorbent.

The dynamic adsorption process of a gas A can be represented as:

$$A_{(g)} + M_{surface} \underset{k_d}{\overset{k_a}{\leftrightarrows}} A_{ads} - M_{surface}$$

Where k_a is the adsorption velocity rate constant and k_d the desorption rate constant.

To express the degree of adsorption, the surface coverage fraction (θ) is introduced. Taking into account that in every position only one molecule can be adsorbed:

$$\theta_s = \frac{\text{N. adsorbed molecules}}{\text{N. adsorption positions}} = \frac{\text{N. occupied positions}}{\text{N. adsorption positions}} \tag{2.10}$$

At an instant t:

- Number of occupied adsorption positions $= \theta_s N$
- Number of free adsorption positions $= N - \theta_s N = N(1 - \theta_s)$

Where N is the total number of adsorption positions at the surface.

If first order kinetics are considered, the adsorption velocity is proportional to the number of collisions between gas molecules and empty adsorption positions, as only a monolayer is formed [39]:

$$u_a = k_a p(1 - \theta_s)N \tag{2.11}$$

Desorption velocity is proportional to the number of adsorbed molecules:

$$u_d = k_d N \theta_s \tag{2.12}$$

When equilibrium is reached, both velocities are equal:

$$k_a p N(1-\theta_s) = k_d N \theta_s \tag{2.13}$$

That can be simplified to:

$$k_a - k_a p \theta_s = k_d \theta_s \tag{2.14}$$

If the surface coverage fraction is isolated:

$$\theta_s = \frac{k_a p}{k_d + k_a p} \tag{2.15}$$

And finally, defining the equilibrium constant as $K_{eq} = k_a/k_d$ the Langmuir isotherm is obtained:

$$\theta_s = \frac{K_{eq} p}{1 - K_{eq} p} \tag{2.16}$$

Experimentally, the surface coverage fraction can be obtained using the relationship between volume of adsorbed gas at pressure p and adsorbed volume when the monolayer is saturated, that is, when it fully covers the surface: $\theta_s = V/V_{mon}$. Depending on the pressure, the behavior of θ_s is obtained. When $p = 0$, $\theta_s = 0$. When p is small, $\theta_s \approx K_{eq} p$ and when p is large, $\theta_s \to 1$, as shown in 2.3.

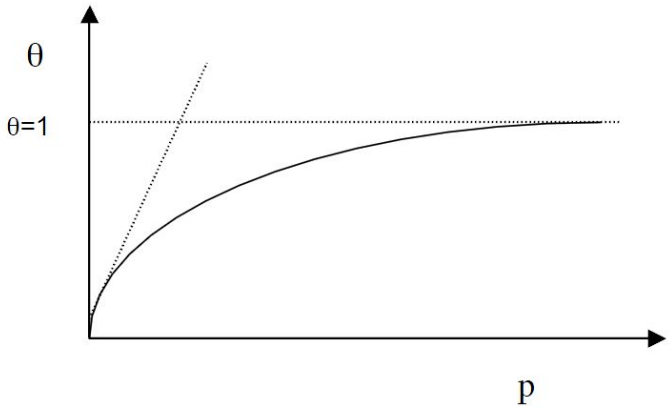

Figure 2.3: Langmuir adsorption isotherm (Tuñón, 2015) [39]

Brunauer-Emmett-Teller (BET) isotherm:

Langmuir isotherm ignores the possibility of creating physisorbed layers over the first layer. If the possibility of multilayer formation is considered, the most used isotherm to analyze multilayer adsorption is the one proposed by S. Brunauer, P. Emmett, and E. Teller (1938) called BET isotherm, and based on the Langmuir model.

The basic assumption of the BET theory is the Langmuir equation applied to each layer with the added postulate that for the first layer the heat of adsorption may have a special value, whereas for all the subsequent layers it is equal.

The results of the BET isotherm can be summarized in:

$$\theta_s = \frac{V}{V_{mon}} = \frac{Cx}{(1-x)(1-x+Cx)} \tag{2.17}$$

Where V is the adsorbed gas volume and V_{mon} is the gas volume necessary to fill the first layer. Constant C only depends on the temperature: $C = K_{eq}/K^*_{eq}$, K_{eq} is the equilibrium constant for the positions with an adsorbed molecule and K^*_{eq} the ones that have more than one adsorbed molecule. x can be deduced from [39]:

$$x = K^*_{eq} p = \frac{p}{p^*} \tag{2.18}$$

Being p gas pressure and p^* equilibrium pressure. And so, BET isotherm can also be expressed as a function of p, K_{eq} and K^*_{eq}:

$$\theta_s = \frac{V}{V_{mon}} = \frac{K_{eq} p}{(1 - K^*_{eq} p)(1 - K^*_{eq} p + K_{eq} p)} \tag{2.19}$$

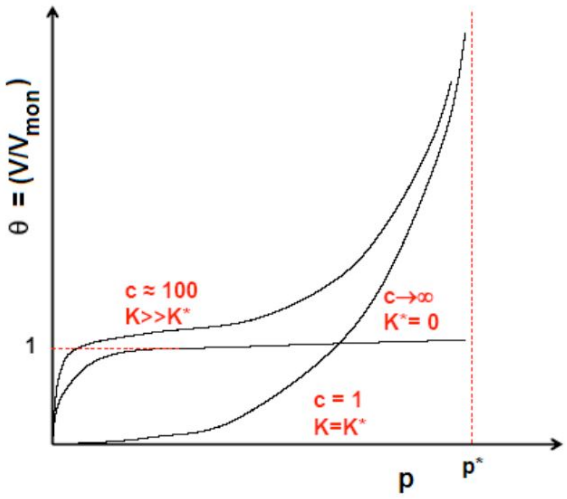

Figure 2.4: BET adsorption isotherm (Tuñón, 2015) [39]

Adsorption isotherm models for Metal Hydrides

In figure 2.5 a PCT based on the BET isotherm is shown for the hydrogen adsorption in metal hydrides. In this specific case it is the relationship between hydrogen pressure in thermodynamic equilibrium (equilibrium pressure) and hydrogen concentration, expressed as a ratio of hydrogen to metal (H/M) at a certain temperature.

The slope of the isotherm plateau and the hysteresis between adsorption and desorption isotherms are inherent characteristics and vary among different metal hydrides. These also depend on experimental variables such as pressure, temperature and mass flow rate [24].

For the adsorption process hydrogen initially diffuses into the metal interstices, and so the equilibrium pressure rises sharply. After the empty space in the bottle is saturated, the metal

hydride begins to form at constant pressure, so a plateau is observed. When the adsorption is complete, another sharp pressure rise is seen as more hydrogen is added to the volume [20]. For the desorption process, the reaction is reversed.

As said, the adsorption reaction is exothermic, if at any time the temperature increases (for example heat is supplied), the equibrium of the reaction will shift to the left, making the reaction endothermic (desorption) and trying to recover equilibrium. On the contrary, if temperature decreases (for example a fan is connected), the reaction will compensate this change in temperature shifting to the right, making the reaction exothermic (adsorption) [26].

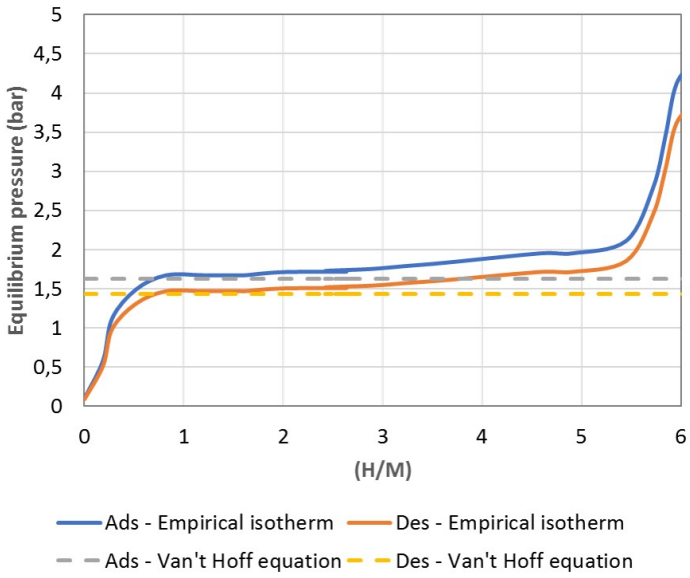

Figure 2.5: Adsorption and desorption PCT of $LaNi_5 - H_2$ system at 296 K [26]

The equilibrium pressure will indicate the direction of the chemical reaction. If the hydrogen gas pressure increases over the equilibrium pressure, the reaction proceeds to the right trying to balance out the pressure difference, hence forming a metal hydride. If the gas pressure decreases below the equilibrium pressure, the equilibrium shifts to the left, hydrogen is released and the metal returns to its original state. The equilibrium pressure itself depends on temperature; it increases with increasing temperature and vice versa.

The equilibrium pressure for hydrogen adsorption on $LaNi_5$ has been measured experimentally as a function of the H/M and temperature and presented in the literature [17]. In these studies, the focus has been on the determination of the H/M-dependent term in equation (2.20). The equilibrium pressure expression given by Dhaou et al. [17], which approximates $f(H/M)$ as a ninth-order polynomial function for hydrogen desorption on $LaNi_5$ is shown in equation (2.20).

$$p_{eq_d} = exp\left(\frac{\Delta H}{RT} - \frac{\Delta S}{R}\right) = \left(a_0 + \sum_{n=1}^{9} a_n \left(\frac{H}{M}\right)^n\right) exp\left(\frac{\Delta H}{R}\left(\frac{1}{T} - \frac{1}{T_{ref}}\right)\right) \tag{2.20}$$

$$\begin{array}{lllll} a_0 = 0.421 & a_1 = -4.114 & a_2 = 14.180 & a_3 = -13.109 & a_4 = 4.557 \\ a_5 = 0.166 & a_6 = -0.592 & a_7 = 0.179 & a_8 = -0.023 & a_9 = 1.126E-3 \end{array}$$

On the other hand, several other researchers [10, 12, 42] have used a simplified version of the equilibrium pressure following the conclusion of Ben Nasrallah and Jemni [4]. In the simplified version, called Van't Hoff equation, the equilibrium pressure is assumed to be a function of only the reference pressure and temperature as follows:

$$p_{eq} = p_{ref} \cdot exp\left(A - \frac{B}{T_{ref}}\right) \tag{2.21}$$

In equation (2.21), the values of A and B are given by Chung and Ho [10] for hydrogen desorption on $LaNi_5$ (A = 10.57 and B = 3704.6). The Van't Hoff equation in this form is only valid for a limited temperature range in which ΔH does not change much with temperature.

Fig. 2.5 clearly illustrates that the difference between Eqs. (2.20) and (2.21) may result in different hydrogen absorption/desorption behaviors in a $LaNi_5 - H_2$ system. Also, the difference between adsorption and desorption isotherms is due to the hysteresis between adsorption and desorption. For the $LaNi_5 - H_2$ system, the hysteresis is $ln\left(\frac{p_{eq_a}}{p_{eq_d}}\right) = 0.13$ [10].

2.4 Storage materials

While the metal hydride material used to store the hydrogen typically does not determine fundamental equations used to model the storage system, details of properties of the storage material are required in some equations to accurately model aspects such as thermal conductivity, thermodynamics and kinetics of the interaction of the material with hydrogen.

The material used may be a simple metal, such as magnesium, an intermetallic or alloy or other complex hydrides such as alanates or borohydrides. Each of these material classes has advantages and disadvantages [26].

The most common metal hydride used for modeling purposes is $LaNi_5$ or a variant of this AB_5 intermetallic. For this reason, intermetallic materials are further discussed below.

2.4.1 Intermetallic materials

Intermetallic materials have proven to be practical hydrogen storage alloys. The simplest intermetallic materials are binary phases, often represented as A_xB_y.

It has been found that good prospective hydrogen storage materials are often formed where A is a metal which readily forms a hydride, such as La, Ca, Ti, Y, Zr and B represents a metal which does not hydride or only weakly hydrides such as Ni, Fe, Mn, Co, Cr, V. Common intermetallic materials for hydrogen storage include AB, AB_2, A_2B and AB_5 materials [35].

$LaNi_5$ is a classic intermetallic of the AB_5 family. Partial substitution for both the A and B metals is possible and this can be used to tailor the temperature and pressure properties of the material. Intermetallic materials have the advantage that most can be modified by inclusion of another metal or modification of the relative proportions of elements to tailor the characteristics in order to meet the fuel cell requirements.

For example, in $LaNi_5$, Lanthanum is often replaced by mischmetal (Mm), a naturally occurring mix of rare earth elements, which is cheaper to produce due to the cost of separating the similar large mass elements [21], or lighter metals such as magnesium and cerium ($La_{1-x}Mg_xNi_5$ and $La_{1-x}Ce_xNi_5$) [14, 15, 29].

2.5 Compressible flow. Discharge of a pressurized tank

2.5.1 Introduction

A large amount of industrial applications work with gases where the effects of compressibility are important, and its behavior and mathematical description greatly differs from incompressible fluids.

Relation between pressure, temperature and gas volume in a real application is complex, but, excluding high pressure or low temperature systems, gas behavior can be approximated to ideal gas. In this situation, ideal gas law can be applied [1].

$$pV = nRT \tag{2.22}$$

Entropy has the following definition (2.23):

$$\dot{m}\Delta S = \int \frac{\delta \dot{Q}}{T} + \dot{\sigma} \tag{2.23}$$

If the process is adiabatic (without release or absorption of heat) $\delta \dot{Q} = 0$ and if it is reversible $\dot{\sigma} = 0$. This means that an adiabatic reversible process is isentropic ($\Delta S = 0$), and so the following equations can be used instead.

$$pV^{\gamma} = ct \tag{2.24}$$

$$\frac{T^{\gamma}}{p^{\gamma-1}} = ct \tag{2.25}$$

Where the coefficient γ is:

$$\gamma = c_p/c_v \tag{2.26}$$

Heat capacities of ideal gases depend only on temperature, and real gases behave approximately as ideal gases if its pressure is low.

Sound is a small perturbation in the density and pressure of a medium (gas, liquid or solid) that propagates faster or slower depending on the elastic properties of the medium itself. Flows at velocities comparable to the speed of sound present important changes in fluid densities: convergent and divergent nozzles, wind tunnels, aviation engines, rocket propulsion...

These flows are difficult to obtain on liquids as pressure levels up to 1000 bars are needed.

Although in the studied case, velocities are very slow in comparison with the speed of sound, and the use of Mach number is not mandatory, when dealing with compressible flow, Mach number is an important parameter, as it relates the velocity of the flow (u) to the speed of sound (a) in that medium, as follows:

$$Ma = \frac{u}{a} \tag{2.27}$$

If ideal gas and constant c_p are considered, speed of sound in a substance can be calculated:

$$a = \sqrt{\gamma R' T} \tag{2.28}$$

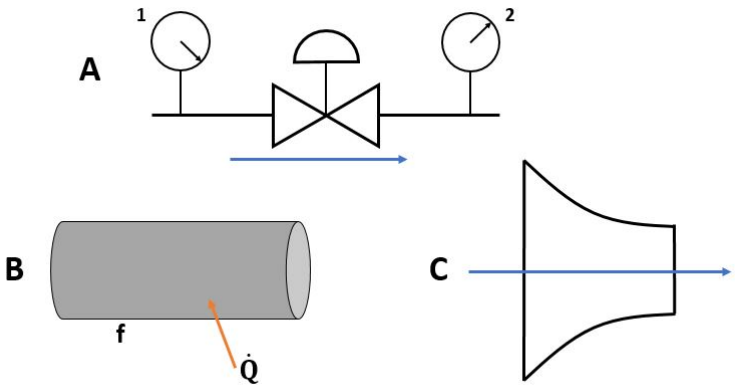

Figure 2.6: Elements affected by compressibility effects

Figure 2.6 shows three different situations where compressibility effects play a key role. Element A is a pneumatic valve, where pressures at the inlet and outlet are obviously different and the gas behaves differently depending on them. Element B is a straight tube where the gas is affected by temperature and friction. Element C is a convergent nozzle that in many cases could be placed as an outlet of a tank. These three elements represent three different situations with analogous effects in terms of compressibility and gas behavior so only the third case will

be studied in detail, considering the discharge of gas from a pressurized tank.

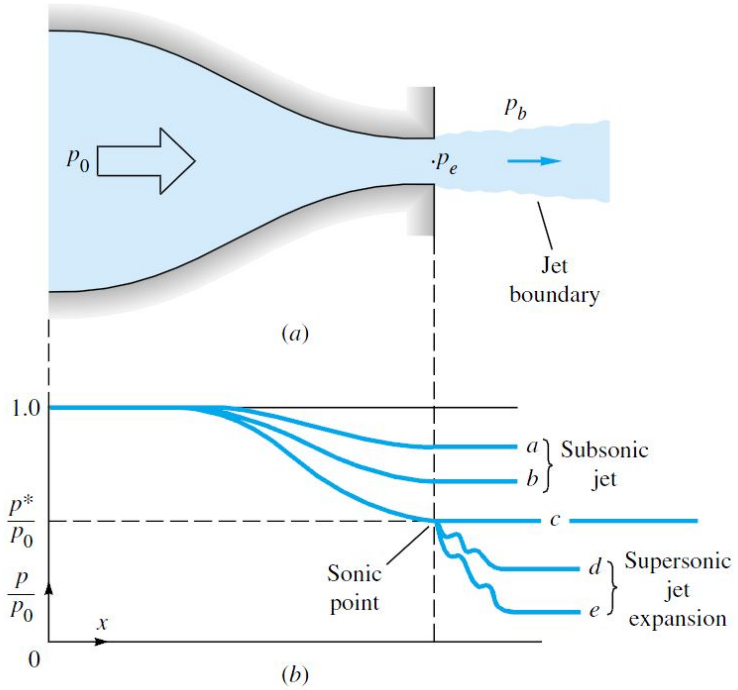

Figure 2.7: Behavior of pressure in a convergent nozzle (White, 1998) [44]

Following the 1st law of thermodynamics inside the tank in Fig. 2.7:

$$Q = \Delta h + W + \Delta e_c + \Delta e_p \tag{2.29}$$

In this case the tank is adiabatic ($Q = 0$), there is no work produced ($W = 0$) and potential energy has no effect ($\Delta e_p = 0$), so:

$$0 = \Delta h + \Delta e_c \tag{2.30}$$

$$h_0 = h + \frac{u^2}{2} \tag{2.31}$$

If ideal gas is considered:

$$T_0 = T + \frac{u^2}{2c_p} \tag{2.32}$$

Knowing that $c_p = \frac{\gamma R'}{\gamma - 1}$, equation (2.32) can be written in the following way, so that the Mach number can appear [44]:

$$\frac{T_0}{T} = 1 + \frac{\gamma - 1}{2} Ma^2 \tag{2.33}$$

If the flux is isentropic, using equations (2.25) and (2.33):

$$\frac{p_0}{p} = \left(1 + \frac{\gamma - 1}{2} Ma^2\right)^{\frac{\gamma}{\gamma - 1}} \tag{2.34}$$

Equation (2.31) implies that the gas inside the tank is at stagnation state. Stagnation is the state achieved by a fluid when it is brought to rest state isentropically (without friction nor heat transfer). As seen in Eqs. (2.30) and (2.31), enthalpy inside the tank (produced by pressure and/or temperature) will be transformed into kinetic energy, and so a mass flow will exit the tank.

This created mass flow exiting the tank is driven by a pressure gradient. Inside the tank pressure is stagnation pressure p_0, whilst on the outlet section pressure is p_e and outside the tank pressure is called back pressure p_b. On the graph on figure 2.7 there is a representation of p/p_0 over the length of the nozzle.

If pressure inside (p_0) is kept constant and back pressure (p_b) is reduced, a pressure gradient is produced that forces the gas to exit the tank. In these cases (a, b) the flow is subsonic and $p_e = p_b$, and so Mach number $Ma < 1$. If p_b keeps decreasing, p_e will reach a critical value p^* in which the outlet velocity is equal to the speed of sound in that substance. This is called sonic conditions (situation c), and in this case $Ma = 1$. If p_b continues to decrease below p^* the system tries to balance the pressure differences expanding in a complex way until it reaches the back pressure value (situations d and e).

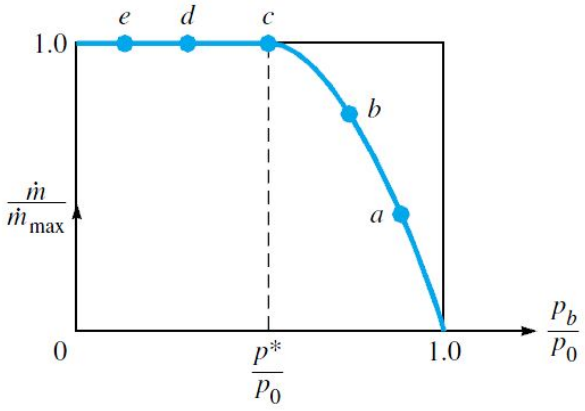

Figure 2.8: Relationship between pressure and mass flow in a convergent nozzle (White, 1998) [44]

It is also important to look at the pressure and mass flow relationship in figure 2.8. At subsonic conditions, situations a and b, ($p_b > p^*$) mass flow keeps increasing until p_b reaches critical pressure (sonic conditions, situation c), where the mass flow becomes the maximum mass flow. When this point is reached the flow is choked. At this point if p_b is reduced even more, the mass flow will continue being the maximum one.

That being said, it is important to know in which region (choked or subsonic) the system is working, because the mass flow will be one or another.

2.5.2 Analytical model of the discharge of a pressurized tank

A hydrogen tank of volume V and characteristic length $V^{1/3}$ is initially at p_0 and T_0. At t =0 it begins exhausting through a converging nozzle to sea-level conditions (p_a and T_a). The throat area is A and its characteristic length is $A^{1/2}$. The gas storage tank is insulated and with negligible kinetic and potential energy within. Under certain conditions it is possible to find the pressure and temperature evolution during discharge of this pressurized gas.

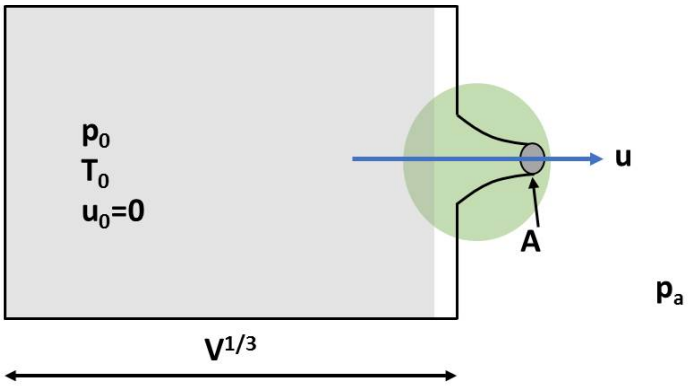

Figure 2.9: Scheme of the gas tank

When the relation between characteristic lengths of the outlet and tank is small and so, the gas in the tank is at resting state except in the region close to the outlet, it can be assumed that the process occurs following a series of quasi-static equilibrium states where the local thermal equilibrium hypothesis is valid. Local thermodynamic equilibrium means that physical properties are varying in space and time, but are varying so slowly that, for any point, one can assume thermodynamic equilibrium in the surroundings of that point [13].

If the discharge is quasi-static, it can be assumed that the mean pressure varies in a continuous way, without important spatial variations (as shown in equations 2.35 and 2.36). Pressure is almost uniform inside, but temperature is not, as the local density differences generated by the emergence of flow and the effect of the heat transfer in the wall cause variable temperature fields. In any case, these spatial pressure variations are negligible inside the tank in comparison with the spatial and temporal variations of pressure in the outlet region.

Spatial variations of pressure in the tank can be in the order of:

Turbulent flow

$$\Delta p \approx \rho \left(\frac{\sqrt[3]{V}}{t_c} \right)^2 \rightarrow \Delta p \approx K_{turb} \dot{V}^2 \tag{2.35}$$

Laminar

$$\Delta p \approx \frac{\mu}{t_c} \rightarrow \Delta p \approx K_{lam} \dot{V} \tag{2.36}$$

2.5.2.1 Mass flow calculation

To calculate the mass flow $\dot{m}$ that exits the tank depending on the pressure inside, it has been seen in figure 2.8 that the discharge of a pressurized gas to ambient pressure follows an almost exponential relaxation in which outlet mass flow is not constant. If spatial density variations are negligible (which is true for many practical applications, except in the outlet region whose mass is not relevant), then mass conservation equation is used inside the tank [13]:

$$\frac{dm}{dt} = \dot{m}_{in} - \dot{m}_{out} \tag{2.37}$$

As the tank is being discharged, $\dot{m}_{in} = 0$, and m can be expressed as density per volume.

$$\frac{d}{dt}(\rho_0 V) = -\dot{m}_e \tag{2.38}$$

Defining $\dot{m}_e$ as:

$$\dot{m}_e = \rho_e u_e A \tag{2.39}$$

If the gas is considered ideal:

$$\dot{m}_e = \frac{p_e}{R'T_e} u_e A \tag{2.40}$$

If sonic conditions at the outlet are achieved velocity will be speed of sound defined in equation (2.28). In this case, the mass flow is choked, being the maximum one. Here it is important to notice that the mass flow is being fixed and so the pressure evolution can be obtained. If mass flow evolution were to be obtained analytically, the pressure would need to be constant.

$$\dot{m}_{max} = \frac{p_e}{R'T_e} a A^* = \frac{p_e}{R'T_e}\sqrt{\gamma R'T_e} A^* = p_e\sqrt{\frac{\gamma}{R'T_e}} A^* \tag{2.41}$$

Using equations (2.33) and (2.34) p_e and T_e can be related with stagnation pressure and temperature, and the following expression is obtained:

$$\dot{m}_{max} = A^* \gamma^{1/2} \left(\frac{2}{\gamma+1}\right)^{\frac{\gamma+1}{2(\gamma-1)}} \frac{p_0}{\sqrt{R'T_0}} \tag{2.42}$$

When the discharge takes place under subsonic conditions, that is to say, when the pressure ratio $r = p_0/p$ is larger than the critical one (b), the mass flow can be calculated using Saint-Venant's expression.

$$\dot{m} = \frac{A^* \gamma^{1/2} Ma \frac{p_0}{\sqrt{R'T_0}}}{\left[1 + \frac{(\gamma-1)Ma^2}{2}\right]^{\frac{\gamma+1}{2(\gamma-1)}}} \tag{2.43}$$

Equation 2.44 shows that the value of the critical pressure ratio depends on k, although this dependence is weak. For values of $\gamma = 1.4$ b is 0.53, and for values of $\gamma = 1.3$ b is 0.55.

$$b = \left(\frac{p_a}{p}\right)_{crit} = \left(\frac{2}{\gamma+1}\right)^{\frac{\gamma}{\gamma-1}} \tag{2.44}$$

Back to the studied tank, initially, the flow is choked, so $\dot{m}_e = \dot{m}_{max}$ from equation (2.42):

$$\dot{m}_e = \dot{m}_{max} = A^* \gamma^{1/2} \left(\frac{2}{\gamma+1} \right)^{\frac{\gamma+1}{2(\gamma-1)}} \frac{p_0}{\sqrt{R'T_0}} \underbrace{=}_{\gamma_{H_2}=1.41} 0.6864 A^* \frac{p_0}{\sqrt{R'T_0}} \tag{2.45}$$

So, combining equations (2.38) and (2.45):

$$\frac{d}{dt}(\rho_0 V) = -0.6864 A^* \frac{p_0}{\sqrt{R'T_0}} = -0.6864 A^* \rho_0 \sqrt{R'T_0} \tag{2.46}$$

Equation (2.46) is only valid when the flow is choked, and consequently the mass flow is constant.

Obviously the amount of mass inside the tank at a certain instant t is calculated as follows:

$$m = -\int_0^t \dot{m} dt \tag{2.47}$$

So, mean density is $\rho = m/V$, where the volume of the tank is constant, and the initial mass is given by the initial conditions and the state equation.

2.5.2.2 Temperature calculation

To calculate the temperature evolution, considering an initial tank temperature $T_0(0)$, exterior temperature of T_a and choked flow at the outlet (as in equation (2.46)), it is necessary to start with the energy conservation equation:

$$\frac{dE}{dt} = \dot{H}_{in} - \dot{H}_{out} + \dot{W} + \dot{Q} \tag{2.48}$$

In this case $\dot{H}_{in}$, $\dot{W}$ and $\dot{Q}$ are zero, so:

$$\frac{d}{dt}(\rho_0 V c_v T_0) = -\dot{m}_e c_p T_0 \tag{2.49}$$

Then, equations (2.46) and (2.49) can be combined:

$$c_v T_0 \frac{d}{dt}(\rho_0 V) + c_v \rho_0 V \frac{dT_0}{dt} = -0.6864 A^* \rho_0 \sqrt{R'T_0} c_p T_0 \tag{2.50}$$

Considering V and ρ_0 as constant:

$$c_v \rho_0 V \frac{dT_0}{dt} = 0.6864 A^* \rho_0 \sqrt{R'T_0} (c_v - c_p) T_0 \tag{2.51}$$

And isolating the temperature evolution:

$$\frac{dT_0}{dt} = \underbrace{\frac{0.6864A^*}{V}(1-k)\sqrt{R'}}_{K_1} T_0^{3/2} \tag{2.52}$$

The equation can be integrated:

$$\frac{-2}{T_0(t)} = K_1 t + K_2 \tag{2.53}$$

Taking into acount that at $t = 0$, $T_0(t) = T_0(0)$, the value of K_2 is:

$$K_2 = \frac{-2}{\sqrt{T_0(0)}} \tag{2.54}$$

And so, the evolution of temperature is:

$$T_0(t) = \left[-\frac{1}{2}K_1 t + \frac{1}{\sqrt{T_0(0)}}\right]^{-2} \tag{2.55}$$

Replacing the value of K_1:

$$T_0(t) = \left[\frac{1}{2}\frac{0.6864A^*\sqrt{R'}}{V}(\gamma-1)t + \frac{1}{\sqrt{T_0(0)}}\right]^{-2} \tag{2.56}$$

2.5.2.3 Pressure calculation

To calculate the pressure evolution it is necessary to take into account if the temperature varies throughout the discharge of the tank or not.

Constant temperature

Considering a constant temperature means that $T_0 = T_a$ during blowdown, as there is no heat generated or extracted from the system, the tank is at the same temperature as the exterior medium. Starting from equation (2.46), it is possible to go back and solve $p_0(t)$, as follows:

$$\frac{d}{dt}\left(\frac{p_0}{R'T_0}V\right) = -0.6864A^*\frac{p_0}{\sqrt{R'T_0}} \tag{2.57}$$

Constant properties can be taken out of the derivative:

$$\frac{dp_0}{dt} = \frac{-0.6864A^*}{V}\sqrt{R'T_0}p_0 \tag{2.58}$$

Isolating pressure:

$$\frac{1}{p_0}\frac{dp_0}{dt} = \frac{-0.6864A^*}{V}\sqrt{R'T_0} \tag{2.59}$$

Integrating the last expression, the pressure evolution can be obtained:

$$\ln\left(\frac{p_0(t)}{p_0(0)}\right) = \frac{-0.6864A^*}{V}\sqrt{R'T_0}t \tag{2.60}$$

Rearranging this expression, it can be clearly seen that the tank pressure decreases exponentially with time:

$$p_0(t) = p_0(0)\exp\left(\frac{-0.6864A^*}{V}\sqrt{R'T_0}t\right) \tag{2.61}$$

Variable temperature

In this case, temperature decreases during blowdown (as demonstrated in equation (2.56)). To calculate the pressure evolution, it is possible to go back to equation (2.46) again and solve $p_0(t)$ considering variable temperature, but knowing $T_0(t)$ it is easier to find $p_0(t)$ from the isentropic flow equation (2.25):

$$\frac{p_0(t)}{p_0(0)} = \left[\frac{T_0(t)}{T_0(0)}\right]^{\frac{\gamma}{\gamma-1}} \tag{2.62}$$

Rearranging and combining this equation with equation (2.56):

$$\frac{p_0(t)}{p_0(0)} = \left[\frac{\left(\frac{K_1}{2}t + \frac{1}{\sqrt{T_0(0)}}\right)^{-2}}{\frac{1}{\left(\sqrt{T_0(0)}\right)^{-2}}}\right]^{\frac{\gamma}{\gamma-1}} \tag{2.63}$$

So, the pressure evolution is:

$$\frac{p_0(t)}{p_0(0)} = \left[\frac{K_1}{2}\sqrt{T_0(0)}t + 1\right]^{\frac{-2\gamma}{\gamma-1}} \tag{2.64}$$

$$\frac{p_0(t)}{p_0(0)} = \left[\frac{1}{2}\frac{0.6864A^*\sqrt{R'}}{V}(\gamma-1)\sqrt{T_0(0)}t + 1\right]^{\frac{-2\gamma}{k\gamma-1}} \tag{2.65}$$

Clearly, tank pressure also decreases with time as the tank blows down.

The combined resolution of all the previous equations is complex and it is mandatory to use computational simulation. Anyway, this procedure does not allow a fast estimation of the discharge time which is usually the main objective.

2.5.3 Validity of the analytical model and results

2.5.3.1 Scope of the analytical model and assumptions

As explained in previous sections, the analytical model is very limited and only possible under certain conditions, and most of them are not true in the case of the discharge of hydrogen in a real metal hydride system [13, 44].

First and foremost, mass flow and pressure are related, but it is only possible to obtain the

evolution of one of them if the other one is fixed, as there is only one equation. In the previous explanation, mass flow rate has been kept constant (considering choked flow at the outlet) and the pressure evolution has been calculated.

Other assumptions considered in the analytical model that do not represent the studied metal hydride storage system are:

- Characteristic lengths of the tank and the outlet are similar, and so it is more difficult to justify the consideration of a series of quasi-static equilibrium states where the local thermal equilibrium hypothesis is valid.
- As said before, in the analytical model the flow is choked. Mass flow is constant and the maximum one, while pressure decreases, as seen in the first part of plot 2.8. In the real studied case, both mass flow and pressure are variable.
- There is a desorption endothermic reaction, which means that $\dot{Q}$ in equation (2.48) is not zero, and temperature will follow a different dynamic as the one considered above. The reaction also implies that a hydrogen mass flow is being generated inside the bottle.
- Storage tank contains a porous media, so the spatial pressure variations in the tank (equations (2.35) and (2.36)) may not be negligible.

As stated before, the system is way to complex to be effectively modeled analytically and so it is mandatory to use computational simulation. Nevertheless, the presented simple analytical study, is useful to understand the physical phenomenon that is the discharge of a pressurized tank as well as a first estimation of the pressure evolution.

2.5.3.2 Analytical model results

As deduced from the previous section 2.5.3.1, the results given by the analytical model will not effectively explain the hydrogen discharge from a metal hydride canister.

The results have been obtained using the following parameters on table 2.2:

$\mathbf{p_0(0)}$ **[bar]**	3
$\mathbf{A^*}$ **[m^2]**	7.92E-6
V [m^3]	0.05
$\mathbf{R'}$ **[Jkg^{-1}K^{-1}]**	4124
$\mathbf{T_0(0)}$ **[K]**	298

Table 2.2: Parameters used on analytical pressure evolution

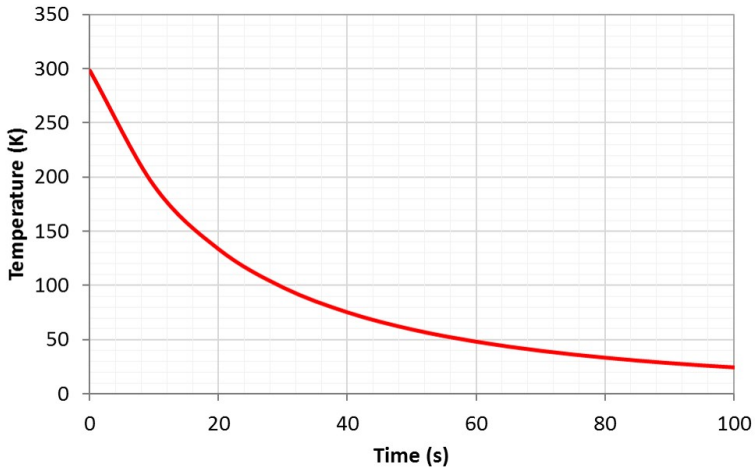

Figure 2.10: Temperature of the tank during discharge

In figure 2.10 the analytical evolution of temperature during the discharge of the pressurized tank is depicted. Fig. 2.11 the evolution of pressure during the blow down of a hydrogen tank can be seen. These two curves have been calculated using real experimental data from the metal hydride bottles (table 2.2) and equations (2.61) and (2.64).

As can be seen, hydrogen discharge is fast and following an exponential relaxation function. In the metal hydride situation, this discharge is way slower as the hydrogen needs to be desorbed from the metal matrix and then circulate through the porous medium until it reaches the outlet.

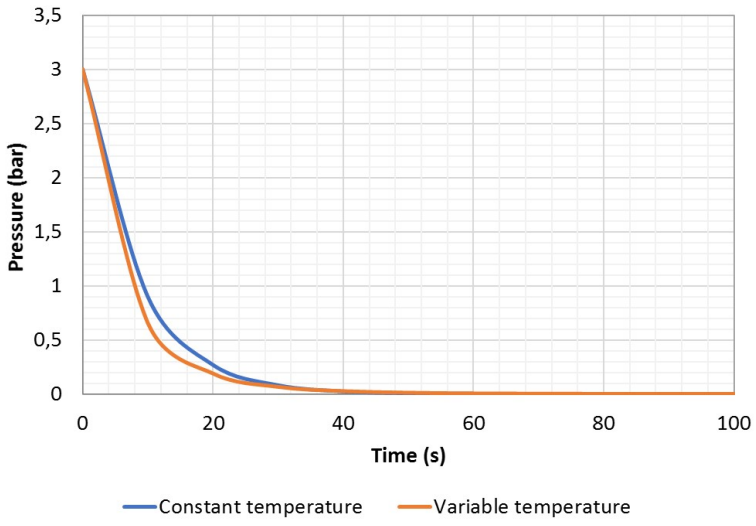

Figure 2.11: Pressure of the tank during discharge

Chapter 3

Model description

For this project modeling is an essential part due to the complexity of the metal hydride storage system. There are numerous parameters and several interactions of physical and chemical phenomena occurring within the metal hydride bottle. Moreover, all these processes are linked creating a sophisticated model that has to be solved.

Modeling is a required process in the development of this project as the system that will be studied, i.e. the bottle, is sealed and therefore it is impossible to get inside to see the phenomena that are occurring. However, through computer simulation that is not a problem, as the necessary equations can be implemented in order to observe, in a clear and visual way, velocity, temperature or concentration distributions, for example. The results can then be compared with experimental values taken from laboratory tests.

Moreover, simulation is a versatile process, meaning that once created the model it can be easily extrapolated to other work conditions. For example, it could be seen how results change if exterior temperature increases or decreases. But not only work conditions could be changed, but also the dimensions of the bottle.

3.1 Overview of the model

3.1.1 Model assumptions

1. Gas phase (hydrogen) is considered as an ideal gas.
2. Powdery metal hydride is treated as an isotropic and homogeneous porous medium.
3. Local thermal equilibrium is assumed between the solid metal and the hydrogen gas. That means that the gas temperature and the metal temperature inside the vessel will be the same.
4. Volumetric expansion of the metal hydride during desorption is neglected.
5. Metal hydride properties such as porosity, permeability and thermal conductivity remain constant during the desorption process.

3.1.2 Geometry

Two different geometries are used. Firstly a cylindrical shape (3.1a) is implemented into COMSOL Multiphysics as its simplicity allows a faster calculation to initially build and test the numerical model.

Once the model works effectively, a bottle-like geometry (3.1b) to match the real metal hydride vessels available in the lab is implemented instead.

Both geometries are modeled as two-dimensional axisymmetric domains, which have two differentiated sections: the top section is a void region acting as a buffer for the hydrogen particles and the larger bottom section is a porous region which contains the metal hydride and is where the reaction takes place.

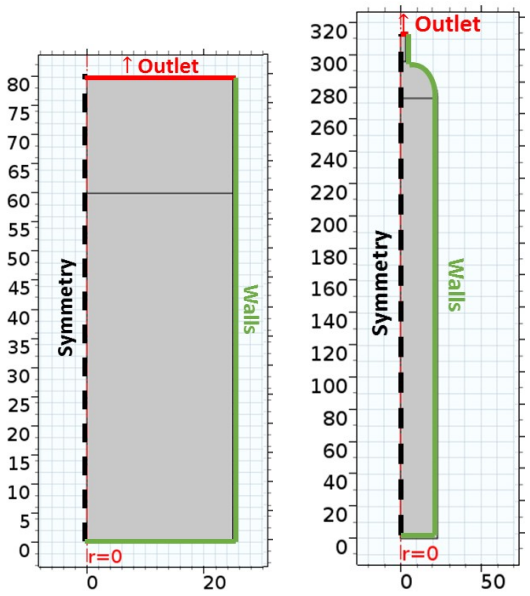

(a) Cylindrical geometry (b) Bottle geometry

Figure 3.1: Geometries with boudary conditions (mm)

3.1.3 Material

As said in section 2.4, regarding the metal inside the bottle, most of the literature reviewed use $LaNi_5$ as the hydride forming metal. The reaction then is:

$$LaNi_5 + 3H_2 \leftrightarrows LaNi_5H_6 + \Delta H$$

So, in order to simplify the simulations, the same metal is adopted, this way the results can be easily compared with the ones presented in other papers. Let's remember that the metal inside the metal hydride canisters in the lab is unknown, and to deal with this lack of information, a detailed and systematic numerical analysis on the characteristics of various metal properties is needed, as well as an exhaustive study on external cooling level and heating supply both numerical and experimentally.

3.2 Discharge model

3.2.1 Governing equations and source terms

Under those assumptions, the metal hydride container is governed by the conservation of mass, momentum and thermal energy.

3.2.1.1 Mass conservation

The equation governing mass conservation is the continuity equation, which is the following:

$$\varepsilon\frac{\partial\rho^g}{\partial t} + \underbrace{\nabla(\rho^g\vec{u})}_{\text{compressible flow}} = \Phi_{source} + \Phi_{sink} \tag{3.1}$$

During hydrogen desorption the mass source term of the equation is zero, as there only is a consumption of hydrogen which is being released from the metal.

Sink term of the equation will be called S_m, so the final equation for hydrogen is:

$$\varepsilon\frac{\partial\rho^g}{\partial t} + \nabla(\rho^g\vec{u}) = -S_m \tag{3.2}$$

Where the gas density, ρ^g, can be described by the ideal gas law:

$$\rho^g = \frac{p^g M^g}{RT} \tag{3.3}$$

For the metal hydride, the equation is the following:

$$(1-\varepsilon)\frac{\partial\rho^m}{\partial t} = S_m \tag{3.4}$$

It can be noticed that in equations (3.2) and (3.4) there is ε, which indicates the porosity of the metal hydride container. On the other hand, S_m is a sink term which represents the local hydrogen desorption rate per unit volume.

Mass and energy source terms are based on the Arrhenius expression which is a simple formula for the temperature dependence of reaction rates. The Arrhenius expression is the following:

$$k = Ae^{\left(\frac{-E_d}{RT}\right)} \tag{3.5}$$

Where: k is the rate constant of a chemical reaction, A is the pre-exponential factor, E_d is the activation energy for desorption and R is the universal gas constant.

Based upon that expression, mass and energy source terms can be deduced so S_m can be expressed:

$$S_m = C_d \exp\left(\frac{-E_d}{RT}\right)\left(\frac{p^g - p_{eq}}{p_{eq}}\right)(\rho^m - \rho^m_{emp}) \tag{3.6}$$

Where, C_d is the rate constant for desorption, E_d the activation energy for desorption, ρ^m_{emp} the density of the metal hydride powder when it does not have hydrogen, and p_{eq} is the equilibrium pressure for hydrogen desorption.

Equilibrium pressure has been defined and detailed in section 2.3.2.3, the simplified version of equilibrium pressure has been chosen for the desorption of hydrogen in metal hydrides. It is also important to take into account that p^g has to be an absolute pressure, as p_{eq} is also an absolute pressure.

3.2.1.2 Momentum conservation

At this point, the model could follow two different approaches: Navier-Stokes equation or Brinkman equation.

Navier-Stokes equation 2.8 would take into account the geometry of the metal hydride by means of pores and narrow channels where hydrogen would flow through. Using this approach would require taking a photograph (a tomography or similar, example on figure 3.2) of the inside geometry so that it can be implemented into COMSOL to solve Navier-Stokes equations inside the bottle.

This method would provide information on how the hydrogen moves inside the metal and the velocity in every single point of the domain, as can be seen in the example on 3.2.

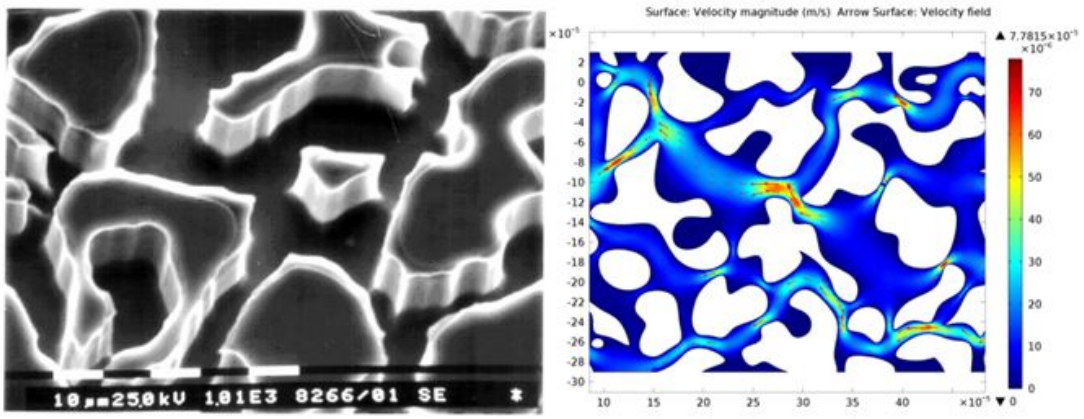

Figure 3.2: Left: Scanning electron microscope image of the repeat pattern in a silicon wafer [5]. Right: Surface and arrow plots of the velocity field calculated by COMSOL's Creeping Flow interface [11].

On porous media it is typical to represent fluid flow as a continuum process using average properties for the bulk rather than detailing the shape and orientation of each solid particle within a porous medium. Inserting the bulk properties into an equation, such as Brinkman equations, gives an average flow rate for the total volume. Bulk approximations typically produce excellent estimates, sufficient for considering flow over large areas, like the one that is being considered in this project [11].

In this case, a combination of both equations is used. Navier-Stokes equation is used in the hydrogen buffer area, as there is not any complex geometry or pattern that complicates its resolution. On the other hand, Brinkman equation is used for the momentum conservation in the porous media region, and is explained in detail below:

$$\frac{\rho}{\varepsilon}\frac{\partial \vec{u}}{\partial t} + \underbrace{\frac{\rho}{\varepsilon}\vec{u}\nabla\vec{u}}_{\text{Inertial term}} = -\underbrace{\nabla p}_{\text{Pressure gradient}} + \underbrace{\nabla\left[\frac{\mu}{\varepsilon}(\nabla\vec{u} + (\nabla\vec{u})^T) - \frac{2\mu}{3\varepsilon}\nabla\vec{u}I\right]}_{\text{Deviatoric stress tensor}} - \underbrace{\frac{\mu}{K}\vec{u}}_{\text{Source term}} - \underbrace{\beta_F|\vec{u}|\vec{u}}_{\text{Forchheimer drag}} - \underbrace{\frac{S_m}{\varepsilon^2}\vec{u}}_{\text{Mass source term}} + \underbrace{\rho\vec{g}}_{\text{Gravitational term}} \tag{3.7}$$

Brinkman equation can be simplified and re-written so that it is easier to understand.

First of all, hydrogen will move through the metal in a creeping flow (or Stokes flow), which is a type of fluid flow where advective inertial forces are small compared with viscous forces. That happens when the Reynolds number is low ($Re \ll 1$), which is a typical situation in flows where the fluid velocity is very slow.

Taking that into account, the inertial term can be neglected as it will be small compared with the viscous forces.

Next there are the terms regarding the effect of stress in the fluid, represented by the pressure gradient and the deviatoric stress tensor.

∇p is called pressure gradient and appears due to the isotropic part of Cauchy stress tensor. This means that pressure gradient depends on normal stresses that intervene in almost all situations.

The anisotropic part of the stress tensor is represented by $\nabla\tau$, which is called deviatoric stress tensor (τ) and usually describes viscous forces. $\nabla\tau$ corresponds to the following expression:

$$\nabla\tau = \nabla\left[\frac{\mu}{\varepsilon}(\nabla\vec{u} + (\nabla\vec{u})^T) - \frac{2\mu}{3\varepsilon}\nabla\vec{u}I\right] \tag{3.8}$$

The next term in the equation is the source term. For the porous metal hydride region, the source term follows Darcy's law and so it can be expressed as function of permeability (K) and dynamic viscosity (μ).

The Forchheimer drag term represents the kinetic energy of the fluid. Forchheimer observed that as the flow velocity increases, the inertial effects start dominating the flow. The parameter β_F is called the Forchheimer coefficient, and although in most cases the parameter is obtained from best fit to experimental data, Ergun proposed an expression for β_F which is:

$$\beta_F = \frac{C_E}{\sqrt{K}} \tag{3.9}$$

The Ergun coefficient C_E is strongly dependent on the flow regime and for slow flows C_E is very small.

Taking into account all being said about the Forchheimer drag, as hydrogen velocity inside the canister is very small, the effect of Forchheimer drag can be neglected ($\beta_F = 0$).

The mass source term accounts for mass deposit and mass creation in domains. The mass exchange is assumed to occur at zero velocity.

Finally, the last term represents body forces which in this case consist of only gravity forces, but may include others, such as electromagnetic forces. The vector field of body forces is called f, which in this case is:

$$\vec{f} = \rho\vec{g} \tag{3.10}$$

In conclusion, the simplified and re-written equation for momentum conservation is:

$$\frac{\rho^g}{\varepsilon}\frac{\partial\vec{u}}{\partial t} = -\nabla p + \nabla\tau - \frac{\mu}{K}\vec{u} - \frac{S_m}{\varepsilon^2}\vec{u} + \rho^g\vec{g} \tag{3.11}$$

3.2.1.3 Thermal energy conservation

Regarding the temperature field, it has been assumed local thermal equilibrium between the gas phase and the solid metal hydride; so, the energy equation can be expressed with a single temperature variable as follows:

$$\rho\bar{c}_p\frac{\partial T}{\partial t} + \underbrace{\rho^g c_p^g u\vec{\nabla}T}_{\substack{\text{Convective}\\ \text{term}}} = \underbrace{\nabla(k^{eff}\nabla T)}_{\substack{\text{Conductive}\\ \text{term}}} + \underbrace{\tau : S}_{\substack{\text{Viscous}\\ \text{heating}}} - \underbrace{\frac{T}{\rho}\frac{\partial\rho}{\partial T}|_p\left(\frac{\partial p}{\partial t} + (\vec{u}\nabla)p\right)}_{\substack{\text{Pressure}\\ \text{work}}} + \underbrace{S_T}_{\substack{\text{Source}\\ \text{term}}} \tag{3.12}$$

First off there is an evolutionary term, which obviously depends on time, and also depends on the effective heat capacity ($\rho\bar{c}_p$), which is a function of porosity:

$$\rho\bar{c}_p = (1-\varepsilon)\rho^m c_p^m + \varepsilon\rho^g c_p^g \tag{3.13}$$

Next there is a convective term, which transports the heat content in a fluid through the fluid's own velocity.

The conductive term is represented through Fourier's law, which states that the conductive heat flux (q) is proportional to the temperature gradient:

$$q_i = -k\frac{\partial T}{\partial x_i} \tag{3.14}$$

Where k is the thermal conductivity which can be anisotropic. If that's the case k would become a tensor. It will be assumed that the metal hydride inside the bottle is isotropic and so the thermal conductivity is constant, and depends on the porosity and the thermal conductivities of hydrogen and the metal itself, following the expression:

$$k^{eff} = (1 - \varepsilon)k^m + \varepsilon k^g \tag{3.15}$$

The second term on the right of equation (3.12) represents viscous heating of the fluid and the third term represents pressure work and is responsible for the heating of a fluid under adiabatic compression. It is generally small for low Mach number flows. So in this case, as the Mach number will be small, pressure work can be neglected.

Finally, S_T is the volumetric energy source term, which represents the heat taken by the endothermic hydrogen desorption reaction.

In the current project viscous heating and pressure work are ignored, and therefore the heat equation can be written as:

$$\frac{\partial \rho \bar{c}_p T}{\partial t} + \nabla(\rho^g c_p^g \vec{u} T) = \nabla(k^{eff} \nabla T) + S_T \tag{3.16}$$

To deduce the energy source term it has to be considered that S_T represents the loss of heat through the endothermic hydrogen desorption reaction. Then S_T can be expressed as the product of the enthalpy change during hydrogen desorption and the volumetric hydrogen desorption rate (S_m) as follows:

$$S_T = S_m[\Delta H - T(c_p^g - c_p^m)] \tag{3.17}$$

Finally, hydrogen to metal ratio is defined by equation (3.18), and the desorbed hydrogen fraction (θ) can be defined according to equation (3.19), where $(H/M)_{sat}$ is the saturated hydrogen to metal atomic ratio. Therefore θ ranges from 0 to 1.

$$(H/M) = \frac{2(\rho^m - \rho_{emp}^m)/M_{H2}}{\rho_{emp}^m / M_m} \tag{3.18}$$

$$\theta = \frac{(H/M)}{(H/M)_{sat}} \tag{3.19}$$

3.2.2 Initial and boundary conditions

3.2.2.1 Initial conditions

At first, the metal hydride container is assumed to be in thermodynamic equilibrium, so the initial conditions are the following:

$$T = T_0 \quad p = p_0 \quad \rho^m = \rho_{ini}^m \tag{3.20}$$

Where ρ^m_{ini} represents the initial metal hydride density, which may be equal to the hydrogen-saturated metal hydride density or lower if the metal is only partially filled.

Also, the initial velocity of hydrogen gas is zero.

$$\vec{u} = 0 \tag{3.21}$$

3.2.2.2 Boundary conditions

As for boundary conditions, boundary walls are assumed to be impermeable so, no-slip velocity and no-flux conditions are valid.

For the energy equation a convection boundary condition is applied between the bottle walls and exterior air.

$$k^{eff}\frac{\partial T}{\partial \vec{n}} = h(T_{ext} - T) \tag{3.22}$$

Where $\vec{n}$ is the unit normal vector out of the vessel wall and T_{ext} is the exterior air temperature.

Besides the convection with surrounding air, a thin stainless steel layer has been added to the exterior boundaries, emulating the metallic container. Thickness and thermal conductivity of the conductive material are specified considering stainless steel 304L (UNS S30403) as a material.

Hydrogen is discharged to the ambient, so pressure at the outlet has been set to atmospheric. However, it is important to consider that exiting hydrogen mass flow circulates through a circuit that generates pressure losses and then reaches the exterior (atmospheric pressure). To emulate that, an hydraulic resistance has been set at the outlet (*grille*). These pressure differences (gradient) between the interior of the bottle and the exterior drive the evacuation of hydrogen from the bottle.

3.2.3 Other considerations

As stated before (section 2.3.2.3), the reaction will proceed to the right (adsorption) or to the left (desorption) depending on the equilibrium pressure.

For adsorption to occur, the pressure of the bottle must be higher than the adsorption equilibrium pressure ($p^g > p_{eq_a}$). As the pressure of the bottle in this case, is almost the same as the inlet pressure, it can be guaranteed that the adsorption reaction will take place just controlling inlet pressure.

On the contrary, for the desorption process the gas pressure needs to be smaller than the desorption equilibrium pressure ($p^g < p_{eq_d}$). As the pressure in the bottle will vary during discharge, the condition above cannot always be guaranteed.

To ensure that the numerical model fulfills the equilibrium conditions and decides accordingly to adsorb or desorb, some constrains have been added:

- If $p^g > p_{eq_a}$: Adsorption

$$S_m = C_a \exp\left(-\frac{E_a}{RT}\right) \ln\left(\frac{p^g}{p_{eq_a}}\right) (\rho^m_{sat} - \rho^m)$$

- If $p_{eq_a} > p^g > p_{eq_d}$:

$$S_m = 0$$

- If $p^g < p_{eq_d}$: Desorption

$$S_m = C_d \exp\left(-\frac{E_d}{RT}\right) \left(\frac{p^g - p_{eq_d}}{p_{eq_d}}\right) (\rho^m - \rho^m_{emp})$$

3.3 Mesh

An important part of the numerical model is the mesh, which has to be carefully defined and selected.

3.3.1 Mesh definition

The studied domain is composed of three differentiated parts: a large rectangle at the bottom, where the metal is located; a quarter of a circle above it, which represents the buffer area; and finally a smaller rectangle which is the outlet.

For the two straight domains, a mapped mesh type is selected. A mapped mesh is composed of structured quadrilateral elements forming a grid, and is suitable for non-curve domains as the ones selected.

Regarding the curvy part, a free triangular mesh type is selected. This mesh is composed of unstructured triangular elements that can easily be adapted to the shape of the domain.

Finally, a boundary layer is also added to the exterior boundaries for the domains. A boundary layer is a mesh with dense element distribution in the normal direction along specific boundaries. This type of mesh is typically used for fluid flow problems to resolve the thin boundary layers along the no-slip boundaries.

3.3.2 Mesh independence study

Once the mesh types are selected it is mandatory to adjust the size of the elements composing the mesh. To select the appropriate mesh two conditions are required:

- Mesh convergence: meaning that a solution is obtained with an absolute error below a set value (in the studied case the absolute tolerance is 5E-4).
- Mesh independence: the solution is independent on the selected mesh size.

Regarding convergence, all the tested meshes have converged with an error below 5E-4.

Focusing on mesh independence, 5 different meshes have been built, going from an extra coarse mesh to an extra fine mesh (Fig. 3.3), whose characteristics are detailed in table 3.1.

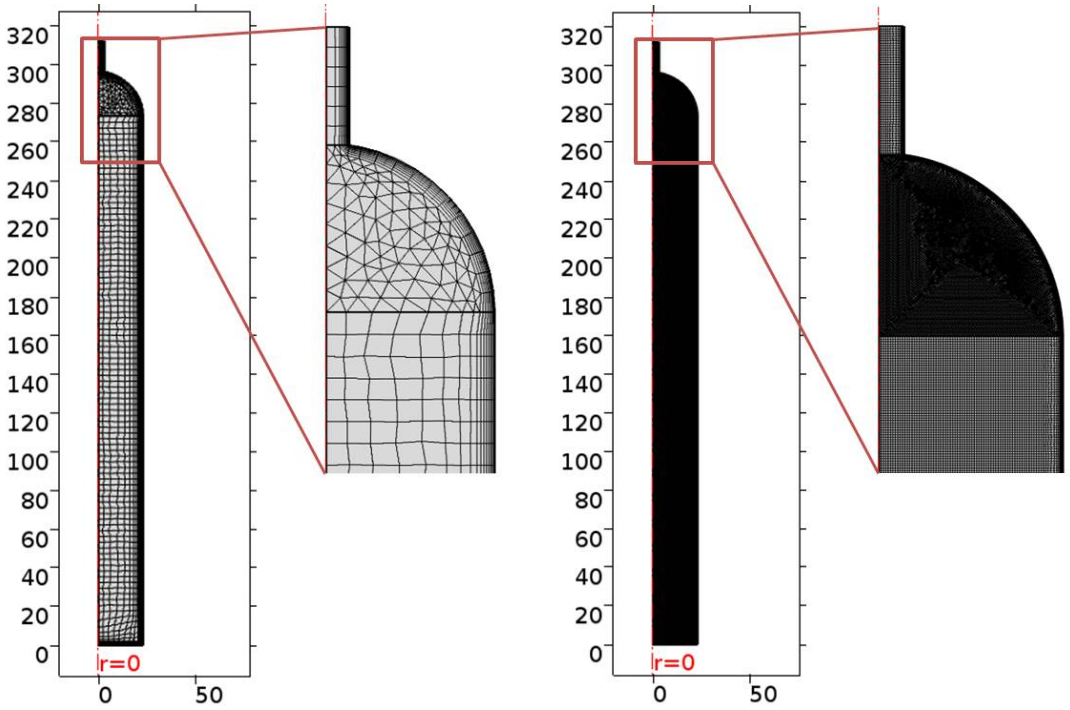

(a) Extra coarse (b) Extra fine

Figure 3.3: Extra coarse and extra fine meshes

	Extra coarse	**Coarse**	**Normal**	**Fine**	**Extra fine**
DOF	21412	57914	113717	174136	1055918
t_{sim} (s)	69	206	328	491	2272
Max. element size (mm)	2.99	1.54	1.04	0.805	0.299
Min. element size (mm)	0.115	0.069	0.046	0.023	0.00345
Max. element growth rate	1.3	1.2	1.15	1.13	1.08
Curvature factor	0.8	0.4	0.3	0.3	0.025
Number of elements	1851	5025	9893	15186	93125
Triangular elements	152	507	1101	1799	12898
Quadrilateral elements	1699	4518	8792	13387	80227
Edge elements	268	483	698	888	2332
Vertex elements	8	8	8	8	8

Table 3.1: Specifications of the tested meshes

Then, the simulation is run using the different meshes and the results obtained for the monitored variables ($p^g, T, \theta, S_m ...$) are compared. At first sight, the result curves seem identical, regardless of the selected mesh, but a detailed analysis is presented below.

The variable that seemed to have higher discrepancies depending on the chosen mesh is S_m. It has been considered that the finer mesh (extra fine mesh) has the more accurate result, and so it has been calculated the relative error of the results obtained by the other meshes compared to the extra fine mesh.

The relative error is calculated for each time instant, and some of them are depicted in figure 3.4, including t =1200 s which is the the time instant where the solution deviates the most from the extra fine mesh result. The first point of the plot corresponds to the extra coarse mesh, and then coarse, normal, fine and finally extra fine.

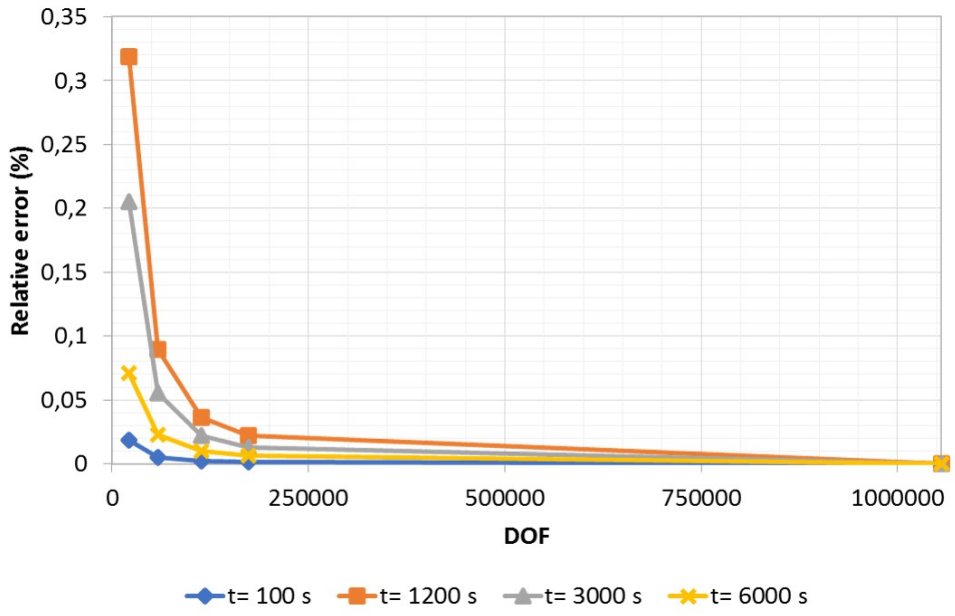

Figure 3.4: Relative error of the meshes

As shown in Fig. 3.4, all meshes have a relative error below 0.35% in all the studied time instants. As expected, the extra coarse mesh is the less accurate of them all, and progressively refining, the results become more similar to the extra fine mesh.

Taking into account the accuracy (in the terms explained above) and also the computing time, it has been decided to use the coarse mesh for further simulations.

3.4 Communications to run the simulations remotely

Most of the simulations of this project were performed remotely, in a server located at EEBE Campus. This server is called Machine-31.

To achieve this, SSH (Secure Shell) protocol is used, which allows access to computers remotely using the net via UNIX's command interpreter, since Machine-31 uses Linux (Fig. 3.5).

In order to connect to the server using SSH, it is necessary to know its public address, that is to say, the IP of the network where the server is connected to.

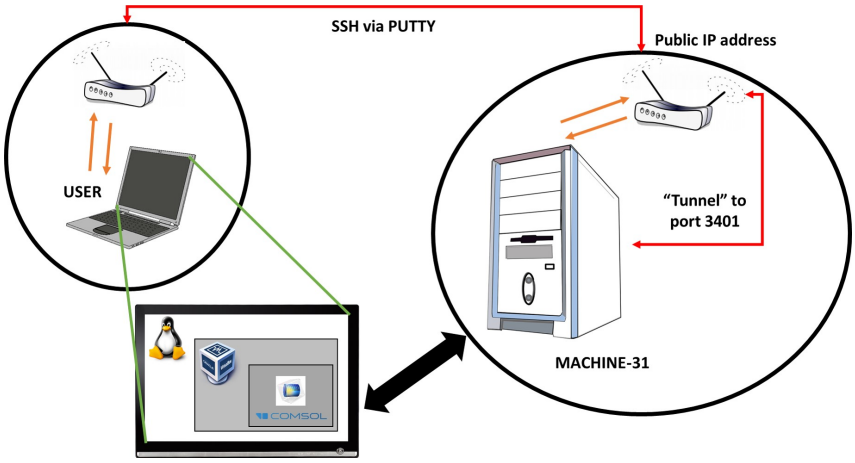

Figure 3.5: Scheme of the network communications

To establish an SSH connection to Machine-31 PUTTY is used, which is a free SSH and telnet client for Windows. It is necessary to specify the server's network public IP address and indicate that the connection will be established using SSH protocol (which corresponds to port 22).

Besides that, a tunnel is created to the port 3401 of Machine-31, which is the enabled port in the server for SSH connections. Now the username and password of the Machine-31 is asked, and then an SSH connection is finally established and so it is possible to access UNIX's terminal of the user in Machine-31.

Then, a virtualization of Windows OS over Linux is needed, as COMSOL Multiphysics is executed on Windows. To that end, VirtualBox will be used. VirtualBox is a program that allows virtualizing an operative system (Windows, in this case), inside another mother system (in this case Linux). It is important to understand that the features and specifications available on the Windows OS (in VirtualBox) will not be the same as the full native Linux, as VirtualBox defines how many resources are dedicated to Windows (Table 3.2).

To visualize graphically the virtualized Windows OS, a program called Parallels Client will be used, which is a solution for sending desktops and virtual applications remotely. At this point, Windows interface can be seen, and COMSOL Multiphysics can run effectively to perform the simulations.

Finally, to copy files from any computer and Machine-31, or the other way around, WinSCP is used. WinSCP is a SCP (Secure Copy Protocol) client for Windows. This protocol allows the safe transfer of files between a host machine and a remote one, using the SSH protocol.

	Machine-31	**VirtualBox in Machine-31**
Processor	Intel® core™ i7-6700 Processor	Intel® core™ i7-6700 Processor
CPU	4 cores, 8 threads = 8 CPU	4 CPU
RAM	16 GB	8 GB

Table 3.2: Specifications of Machine-31 and VirtualBox in Machine-31

Chapter 4

Experimental Characterization

4.1 Experimental setup

The easiest way to study the behavior of the metal hydride during cyclic charge and discharge processes is to design an experimental setup that allows monitoring the most important variables of the system.

To this end, an experimental setup has been designed and assembled, as well as its data acquisition system and its schematic representation is shown in Fig. 4.1. The system has been designed to allow easy transitions between charge and discharge processes, without having to disassemble any parts of the setup to change the operating mode.

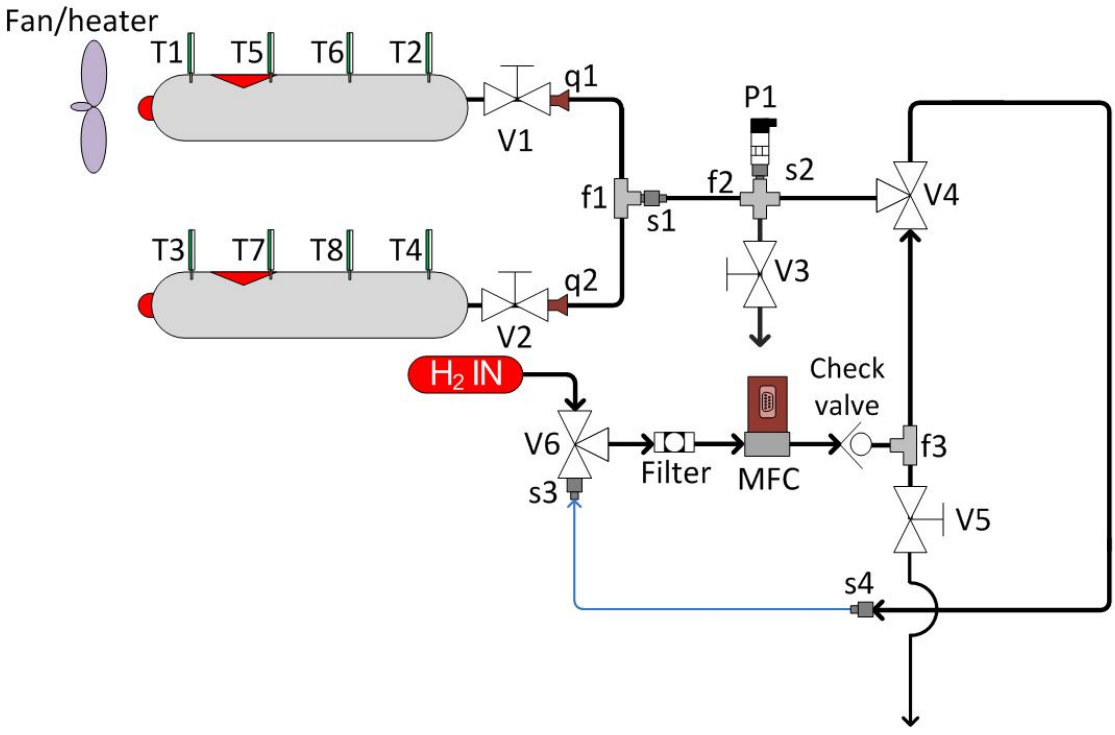

Figure 4.1: Experimental setup scheme

All the list of elements is detailed in Appendix A, and regarding piping there are two different types of pipes. Pipes drawn in black correspond to 1/4" stainless steel tubes and the small section in blue corresponds to 1/4" Teflon tube, as it is more flexible. Finally, at the outlet - and not drawn in the scheme-, there is a Teflon tube connected that carries the exiting hydrogen up to the ceiling, where a bigger tube is placed to carry this hydrogen out of the building.

Through this experimental setup, temperatures at the surface of the bottles, pressure at the inlet/outlet and entering/exiting mass flow can be measured.

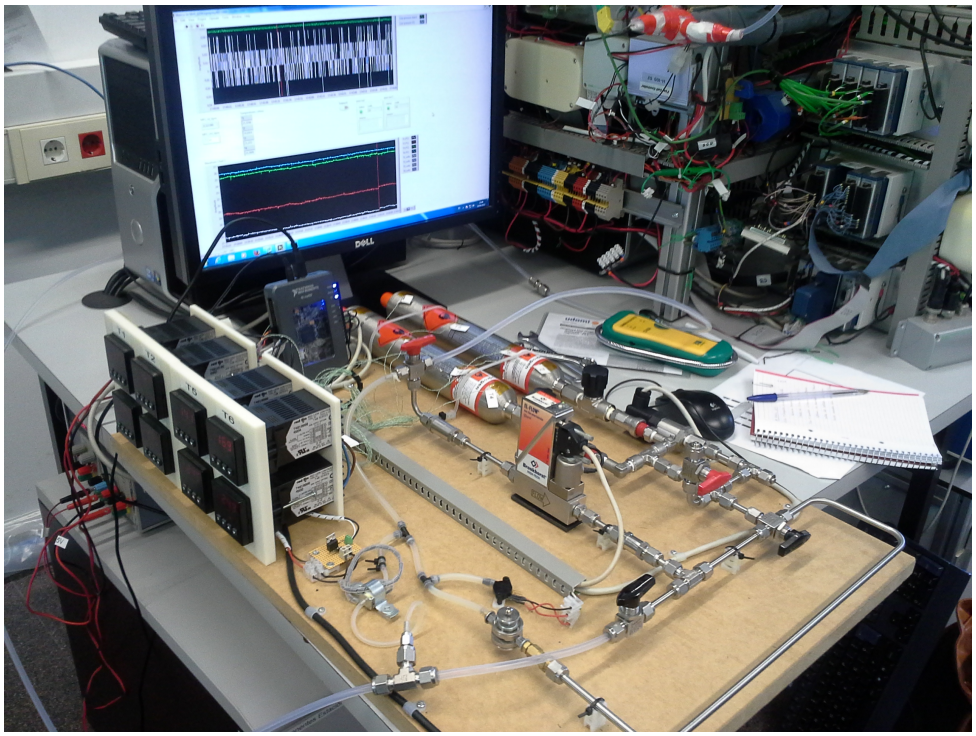

Figure 4.2: Real experimental setup

The experiments have been carried out in two different scenarios: leaving the system in contact with ambient air (natural convection - NC) and connecting a heater (H).

The heater is a Hot air blower HOTWIND SYSTEM from Leister Technologies AG. At the outlet of this air blower a flexible tube and a PVC pipe are connected (Fig. 4.3). The metal hydride bottle perfectly fits inside the PVC pipe, and so the canister walls are heated.

Obviously, if the heater is connected, the temperature of the bottles will increase. It has to be taken into account, though, that the thermocouples that used to monitor temperature are connected on the surface of the bottles. So, the obtained measurement when the heater is connected is basically because of the heater.

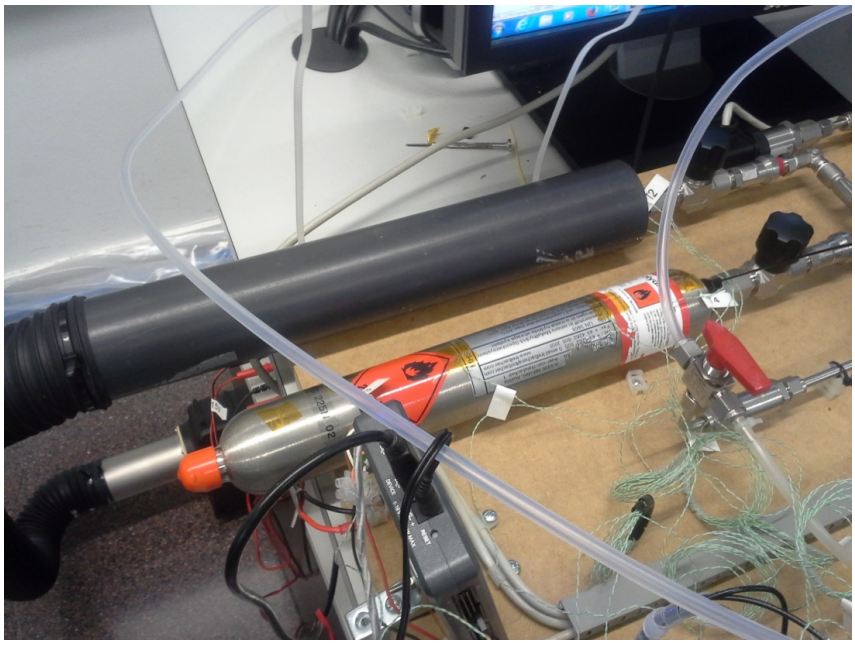

Figure 4.3: Heater connection in the experimental setup

4.2 Charge and discharge experimental protocols

4.2.1 Charge protocol

First, it is necessary to make sure that the circuit is completely empty and there is no air in the pipes, so a purge with hydrogen of the whole system is required. Also, it is mandatory that the bottle that is going to be studied in each of the experiments is empty. A canister is considered empty when during discharge a steady asymptotic situation is achieved, which means that a relatively small amount of hydrogen is released. The last step before starting charging process is to make sure that all valves are closed.

Once the setup protocol is completed, the charging process can start (Fig. 4.4). First, the valve corresponding to the selected bottle is opened, being it $V1$ or $V2$. Then, $V4$ is opened in the direction that allows hydrogen flow from the red circuit. The last step is to release the hydrogen into the system and towards the MFC by opening $V7$ valve.

At this instant the bottle is in charging mode, and the system will continue working until the hydrogen charging curve is saturated, which means that it has reached a steady asymptotic situation in which a large amount of time is required to adsorb any new hydrogen molecules. At this point, the bottle is considered charged.

When the bottle is full, charge process is completed and so the inlet valve $V7$ is closed, followed by $V4$ and the bottle valve ($V1$ or $V2$).

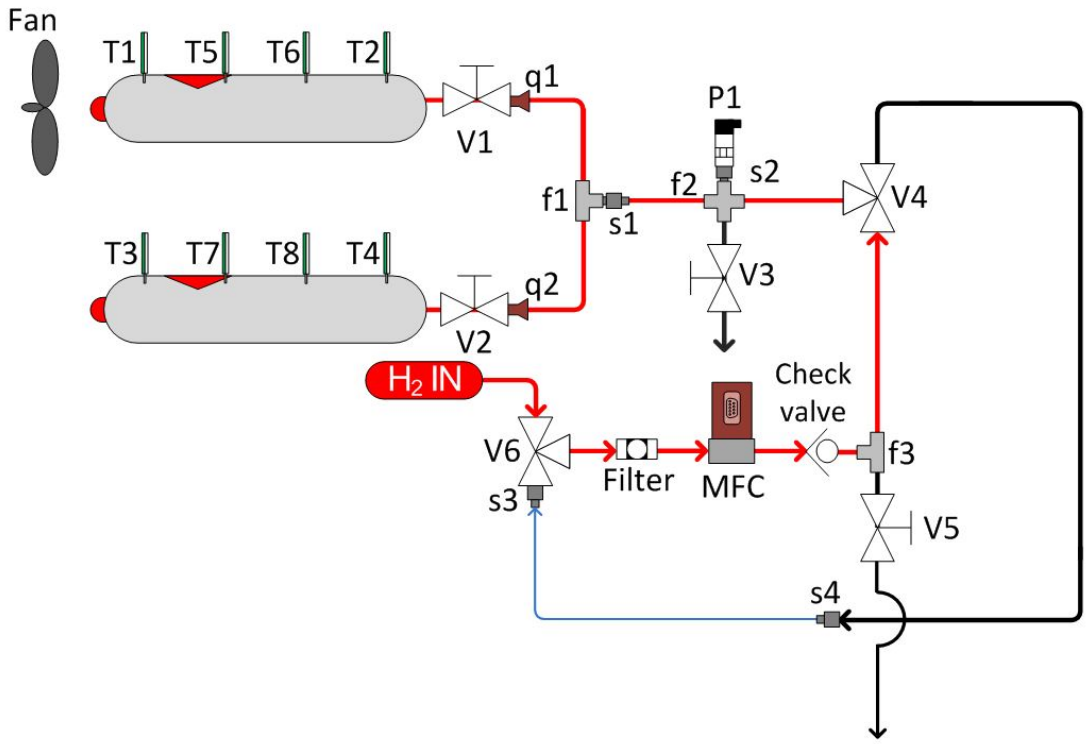

Figure 4.4: Charge scenario experimental scheme

4.2.2 Discharge protocol

First, it is necessary that the bottle that is going to be studied in each of the experiments is charged or partially charged with hydrogen. Also it is important that all valves are closed before starting the process.

Once the setup protocol is completed, the discharging process can start (Fig. 4.5). First, the valve corresponding to the selected bottle is opened, being it $V1$ or $V2$. Then, $V4$ is opened in the direction that allows hydrogen flow towards $V7$. Then, $V7$ is opened and hydrogen goes towards the MFC. Finally, the outlet of the system is opened using $V5$.

At this instant the bottle is in discharging mode, and the system will continue working until the hydrogen discharge curve is saturated, which means that it has reached a steady asymptotic situation in which a relatively small amount of hydrogen is released. At this point, the bottle is considered empty.

When the bottle is empty, discharge process is completed and so the bottle valve ($V1$ or $V2$), followed by $V4$, $V7$ and $V5$ are closed.

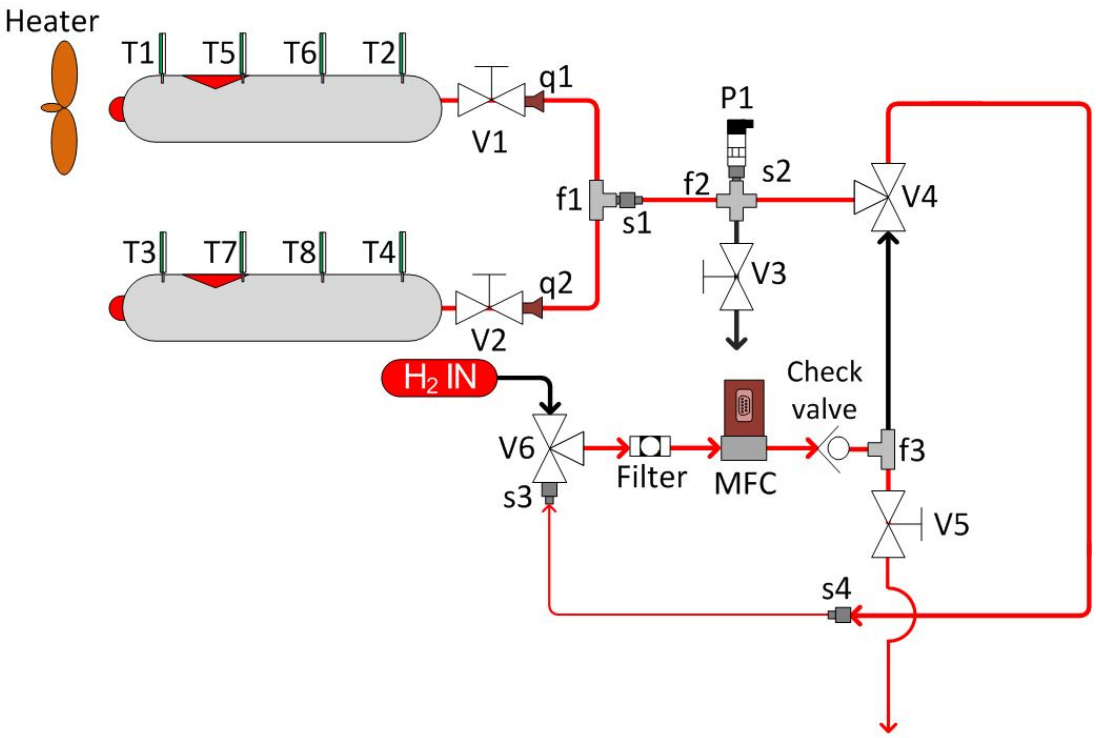

Figure 4.5: Discharge scenario experimental scheme

4.3 Control and data acquisition system

4.3.1 myRIO device and sensor connections

4.3.1.1 NI myRIO-1900

The National Instruments (NI) myRIO-1900 is a portable embedded design device based on NI's RIO technology, a re-configurable IO, like CompactRIO which is highly used in the industry. NI myRIO uses the Zynq chip from Xlinx, which has a dual core ARM real time processor and an FPGA.

Figure 4.6: NI myRIO-1900

Specifications:

- Analog Input (10 channels)
- Analog Output (6 channels)
- Analog Input and Output also available through 3.5 mm audio Jacks
- 40 Digital I/O lines; wireless enabled
- Accelerometer, LEDs and push button on-board
- 6 V to 16 V, 14 W power requirement

4.3.1.2 Sensor connections

In the following diagram (Fig. 4.7), an overview of the sensors and their connections can be seen. The complete connection diagram can be found in Appendix B.

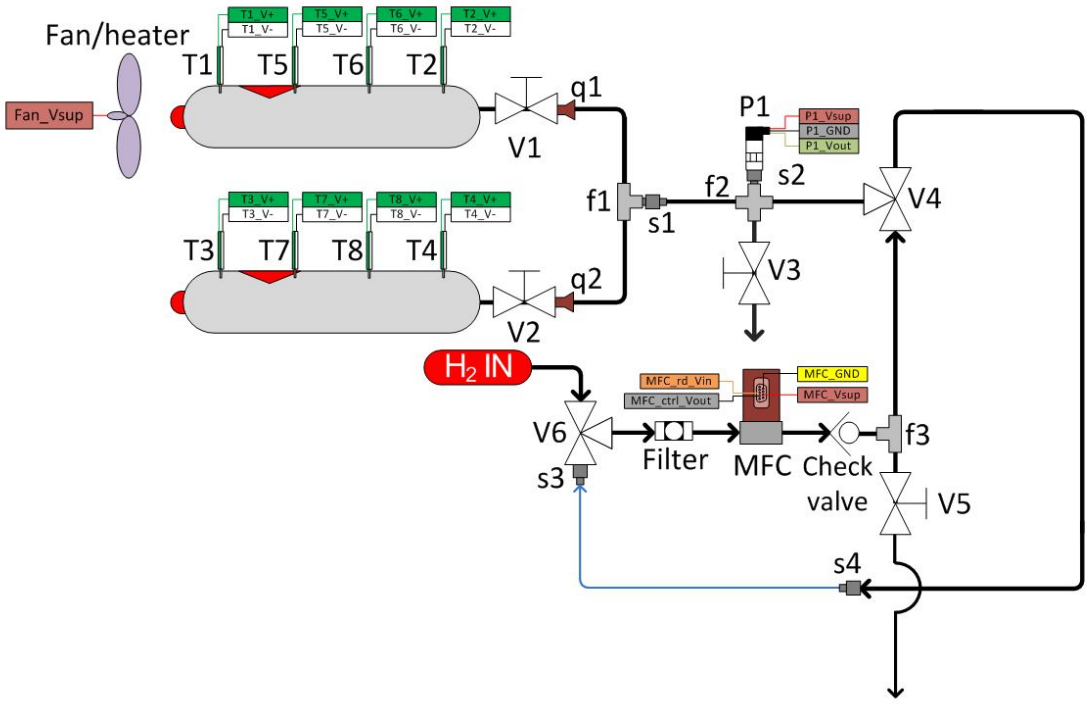

Figure 4.7: Sensor connections general diagram

Sensor	**Physical variable**	V_{supply}	**SP**	**RD**	**myRIO**
P1	Pressure	13-32V dc (15V)	-	0-10V (3 wire) 0-40 barg	1 AI (0-10V)
T (controller)	Temperature	230V ac	-	0-10V -0.5 to 300°C	4 AI (0-5V)
MFC	Mass flow	15-24V dc (15V)	0-5V	0-5V 0-5 nlpm H_2	1 AI, 1 AO (0-5V)

Table 4.1: Connection parameters for each sensor

Pressure

The pressure sensor is connected at the inlet/outlet of the bottles and will monitor charge and discharge pressure.

Connections: Connector C

Sensor	*myRIO*
HP_Vsup	Power supply (15 V)
HP_GND	C-Pin 6 (AGND)
HP_Vout	C-Pin 7 (AI0+)

Table 4.2: Connections of the pressure sensor

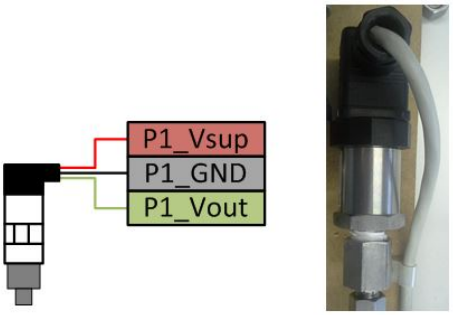

Figure 4.8: Pressure sensor connections

Mass flow

The Mass Flow Controller (MFC) works as a mass flow meter (during charge), which means that is only reading the mass flow going through the pipe, and also as a controller (during discharge), which means that will impose a certain mass flow limit to go through the pipe.

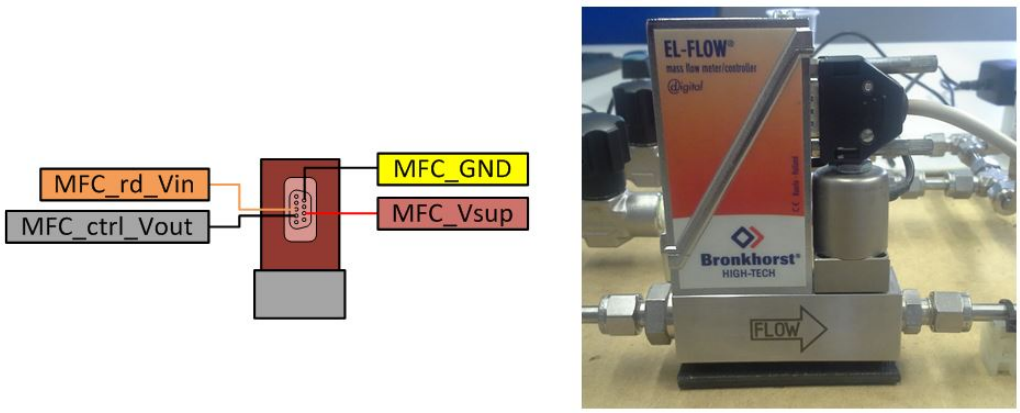

Figure 4.9: Mass flow controller connections

Connections: Connector C and B

Sensor	*myRIO*
MFC_Vsup	Power supply (15 V)
MFC_GND	B-Pin 6 (AGND)
MFC_rd_Vin	C-Pin 4 (AO0)
MFC_ctrl_Vout	B-Pin 3 (AI0)

Table 4.3: Connections of the Mass flow controller

Temperature

As it can be seen in the previous diagram 4.7, there are eight thermocouples distributed along the two metal hydride bottles. Among these eight thermocouples, four of them read and acquire temperature values, and the other four only read temperature values which are shown on screen.

The thermocouples used have a welded tip which is be attached to the surface of the bottle. These thermocouples provide a small voltage signal (mV) which has to be amplified. For that purpose Red Lion temperature controllers are used. These controllers can work as a PID controller but in this case they are only used as an amplifier of the voltage signal so that it can be acquired by the myRIO device as seen in figure 4.10.

Connections: Connector A

Controller	*myRIO*
T_Vsup	Power supply (230 V ac)
T_GND	A-Pin 6 (AGND)
T1_Vout	A-Pin 3 (AI0)
T2_Vout	A-Pin 5 (AI1)
T3_Vout	A-Pin 7 (AI2)
T4_Vout	A-Pin 9 (AI3)

Table 4.4: Connections of thermocouples and Red Lion controllers

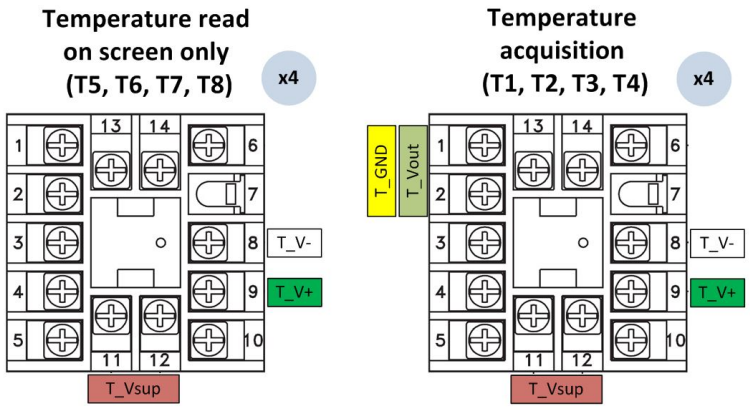

Figure 4.10: Connections of the Red Lion temperature controllers

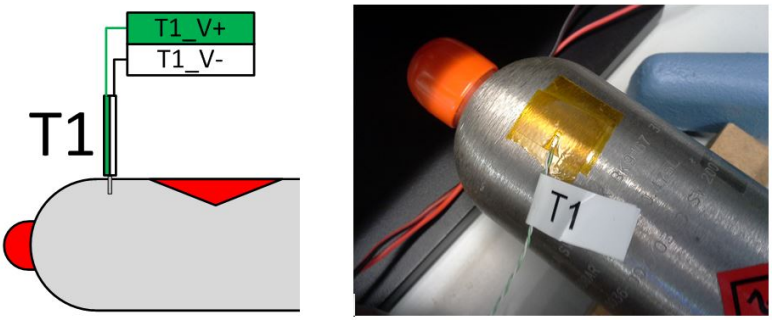

Figure 4.11: Thermocouple connections

4.3.2 LabVIEW program

To acquire and save all the data LabVIEW is used which is a graphical programming platform developed by National Instruments. Via LabVIEW, a link is created between the sensors and the user so that it is possible to interact with all the elements and also visualize the data obtained on a screen.

The LabVIEW program (which can be viewed in detail in Appendix C) is structured in three differentiated parts: Initialize, acquire and process data, and close.

4.3.2.1 Initialize

In this part of the program, the name (and also the path) of the file is set. Once the name and path are set, the *.tdms* file is opened (if it already exists) or created.

4.3.2.2 Acquire and process data

This part of the program is the core of the whole sequence of instructions. Here is where the myRIO intervenes with its inputs and outputs, connecting the physical device with the program and enabling the data to be acquired and processed.

The first thing that the program does is mainly to acquire the data basically through its analog inputs (pressure, mass flow and temperature) but also send signals via its analog outputs (mass flow controller).

Inputs

Analog inputs are acquired by means of voltage. Then, these values in volts have to be converted into the real physical magnitude, for example bars or Celsius degrees.

Knowing that the myRIO has an analog input range that goes from 0 to 10 V, and for example, the pressure sensor has a range from 0 to 40 bars, the conversion from volts to bars would be to multiply the acquired data by four, which is what the program is doing (Fig. 4.12a). This same process is implemented for all of the sensors.

When the data is converted into the right units, the program plots pressure and temperature so that they can be seen in the front panel. And finally all the variables are put into local variables which are collected together in a block and are saved on the previously created file .

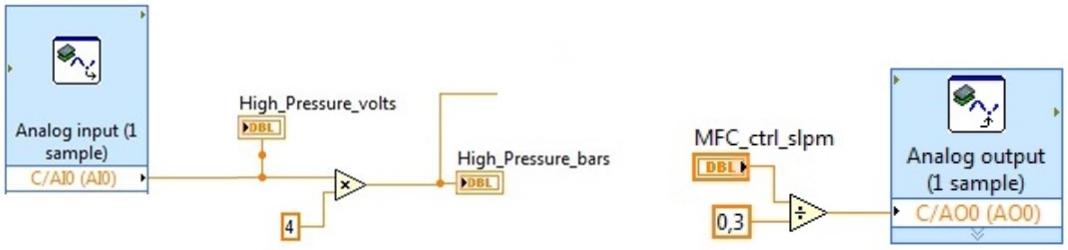

(a) Pressure transformation volts-bars in LabVIEW (b) MFC output in LabVIEW

Figure 4.12: Example of input and output on LabVIEW

Outputs

There is also one output, which is the mass flow on the MFC (Fig. 4.12b). The MFC sends signals to the outputs of the myRIO device. The program also saves the values of the control, the same way as before.

Get current time

Another thing that has to be saved into the file is the current time, so that all the variables can be related to a certain instant. For that, it has to be taken into account that the t=0 on LabVIEW and t=0 on Excel (where all the data will be analyzed) is different, so an offset needs to be added to make them match.

As before, this new variable will be saved along with the other experimental values.

Write file

Finally, all the data acquired has to be saved, which means that has to be written into a file. This file will be a *.tdms*, which is a spreadsheet format and therefore there are organized columns with titles, for example pressure, temperature, etc. The writing part of the program is inside a time loop set to save the data every 2 s, this way all the changes can be monitored.

Stop button

A very important thing that every LabVIEW program must have is a stop button, so that it allows the user to stop the program at any time without putting at risk the sensors and controllers. As it is a programmed stop it allows the sensors and controllers to reset to a desired position.

If a stop button is not added, the only way to stop the program is aborting which has the risk to put in danger the sensors or even ourselves, as the sensors and controllers will stop on the position they currently are, which may not be secure.

4.3.2.3 Close

Finally, the program ends and the file is closed.

Chapter 5

Numerical and experimental results

5.1 Numerical model results

5.1.1 Specifications and calibration of the simulations

As explained in Chapter 3, a two-dimensional axisymmetric model is developed to study hydrogen desorption in a metal hydride hydrogen storage canister.

That being said, there have been some limitations when trying to represent the numerical model to experimental conditions, that make it difficult to compare experimental and simulation data.

First and foremost, the bottle is like a black box, there is no information on the metal hydride material inside it, and so its properties are not known. Besides not knowing the metal hydride, its current state, quality or degree of degradation are unknown as well.

As the bottles are closed and so it is impossible to see inside, the morphology and internal distribution, porosity, permeability or available storage space are also unknown. It is also unknown if there is a hydrogen buffer region, the size of it, and also if there is some kind of manifold or other device that distributes the hydrogen within the bottle during charge or discharge.

5.1.1.1 Parameters that can be estimated

There are some parameters that can be obtained by theoretical calculations or from the experimental tests and measurements.

Ambient/heating temperature

As said, each experimental test considers only one bottle, but the temperature sensors on the bottle that is not being tested are connected as well. These measurements give an estimation of ambient temperature when the heater is not connected. If the heater is connected, heating temperature has been considered as the maximum acquired by the thermocouples during the experiment.

Initial pressure

Initial pressure can also be estimated, as it will be similar to the initial pressure value registered in the experimental tests. For all experimental tests except the one from 15/12/2016 whose initial pressure is around 5 bars, the initial pressure is around 3 bars.

Initial and saturated metal hydride density

Throughout the charging process, the hydrogen mass flow entering the bottle was measured, and so the amount of hydrogen stored inside the bottle is known. This allows an estimation on the initial metal hydride density. In fact, this is not actually a known parameter, but just an estimation considering a certain hydrogen-empty metal density. For the saturation metal hydride density the process is the same, but considering the maximum amount of stored hydrogen registered, and the conditions at which this experiment was performed. As the metal is unknown, the density of $LaNi_5$ has been taken as ρ^m_{emp}. These calculations are shown in section D.1 of Appendix D.

Equilibrium pressure

As this system has a lot of unknowns, it has been decided to use the simple expression of equilibrium pressure considering constant thermophysical properties (left part of equation (2.20)). ΔH has been taken as 35620 J mol^{-1}, ΔS as 108 J mol^{-1}K^{-1} and T_{ref} as ambient temperature. These values give adsorption equilibrium pressure, and to calculate the desorption equilibrium pressure the hysteresis relation $ln\left(\frac{p_{eq_a}}{p_{eq_d}}\right) = 0.13$ is used.

Convection heat transfer coefficient

A first estimation of the convection heat transfer coefficient can be done using correlations collected in *Handbook of Heat Transfer* from McGraw-Hill [32], and considering a horizontal cylinder (D= 50.8 mm) exposed to convection. It is necessary to take into account that there are two different cases: natural convection and forced convection using a heater.

These calculations are shown in detail in section D.2 of Appendix D, and the convection heat transfer coefficient for natural convection is estimated to be h= 4.3 W m^{-2}K^{-1}, whilst for forced convection is estimated as h= 18.6 W m^{-2}K^{-1} in the lateral surface and h= 66.2 W m^{-2}K^{-1} in the bottom surface.

It is also important to take into account that these are only initial estimations considering a cylinder totally exposed to convection, but in the real case there is a part of the lateral surface covered by the support system that will not receive as much convection as the rest of the surfaces.

Pressure loss coefficient

As there are experimental measures of pressure in a point quite close to the outlet of the bottle, and it is also known that the circuit is opened to ambient air, a pressure drop can be estimated for each time instant. Knowing the mass flow and applying equation (2.36), *grille* can be calculated as shown in section D.3 of Appendix D.

5.1.1.2 Unknown parameters

As said, the internal characterization of the bottle is a challenge, as the material as well as its morphology are unknown. This means that the material properties k^m, c_p^m, ρ_{emp}^m, ρ_{sat}^m, M^m, E_a, C_a, E_d, C_d, ΔH and $(H/M)_{sat}$, as well as the possible modification of these parameters due to the current quality of the metal and its degree of degradation, and the material thermodynamics in terms of equilibrium pressure (p_{eq_a} and p_{eq_d}) are not known. Also, the internal characterization of the bottle is unknown, and so porosity (ε), permeability (K) and available volume fraction (θ_m) are also unknown. Besides that, the existence and size of a buffer area as well as the possible existence of a hydrogen distributing manifold is also not known.

And that is the reason why a lot of parametric studies have been carried out to try to evaluate their influence on the model, and how it can be adapted to any other metal hydride material with different characteristics.

Regarding metal properties, the following parametric studies (section 5.1.2) have been performed. These parametric studies also give information on other unknowns as structural parameters and other working conditions that were not possible to measure.

5.1.2 Numerical sensitivity analysis of the metal properties and working conditions

In this section, a collection of parametric studies to analyze the sensitivity of the model to metal properties as well as working conditions is presented.

These parametric studies allow selecting suitable metal hydride materials for the desired hydrogen storage applications, as well as providing a solid base knowledge to study the degradation, in terms of total storage capacity.

The following plots show the effect of some properties to the desorption process, considering that the process is not enhanced using a heater. Nevertheless, these same parametric studies have been done considering the use of a heater, obtaining similar results, which will be explained also in the following sections (5.1.2.1 and 5.1.2.2).

5.1.2.1 Metal properties

Activation energy for desorption (E_d):

Fig. 5.1 shows the evolution of pressure, desorbed mass flow, temperature and desorbed hydrogen fraction for values of activation energy for desorption E_d=15000, 20000, 25000 and 30000 $Jmol^{-1}$. In the published literature, the value of E_d usually varies between 13000 and 59371.6 $Jmol^{-1}$, for different metal hydride materials [3, 7, 8, 10, 12, 25, 27, 29, 37, 42, 46].

From Fig. 5.1 it can be concluded that the desorption process becomes more effective if E_d decreases, which makes sense, as it is easier for the system to overcome that activation energy for the desorption process to start if its value is lower. This can be contrasted with the values of

pressure (5.1a), which are higher as E_d decreases. This means that the pressure gradient is larger and hydrogen will tend to desorbe. Desorbed mass flow increases as the pressure increases (5.1b) and temperature decreases as the desorbed mass flow increases (5.1c), because the endothermic reaction is more effective ($E_d \downarrow$). Obviously θ decreases faster when the reaction is more effective.

If a heater is used, the process is more effective and therefore it finishes sooner. The effects of E_d are the same, and the only significant difference is in the bottle temperature, which increases due to the heater.

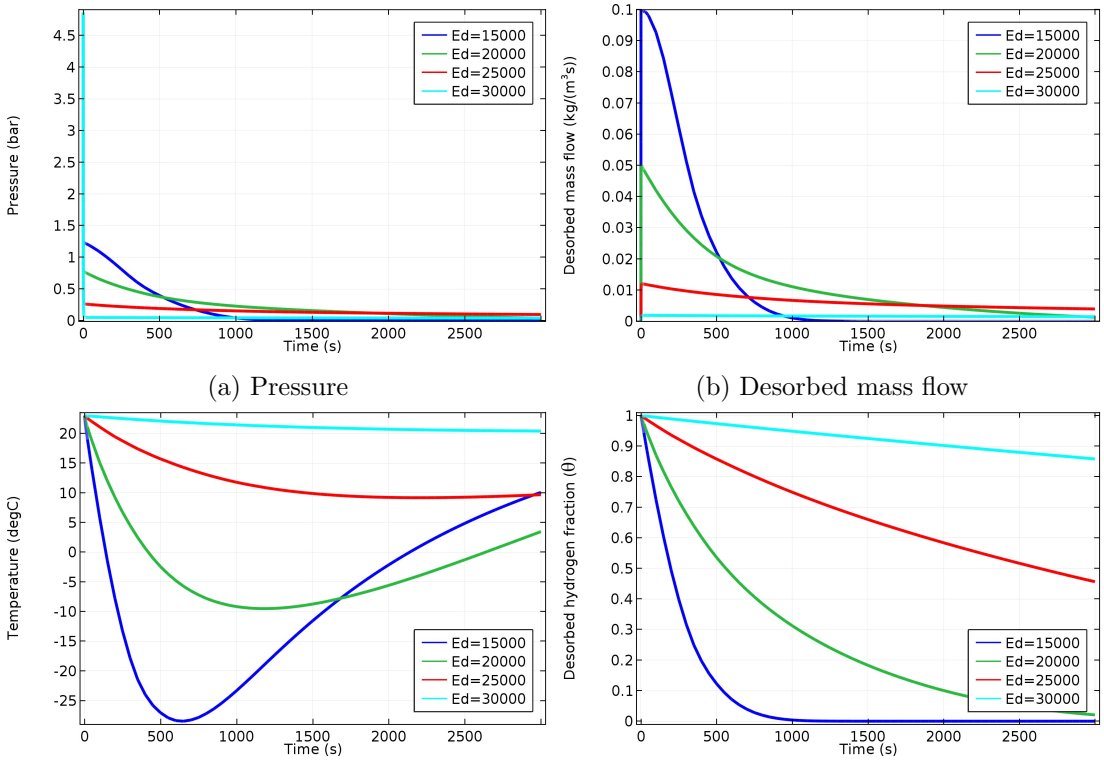

(a) Pressure

(b) Desorbed mass flow

(c) Temperature

(d) Desorbed hydrogen fraction (θ)

Figure 5.1: Evolution of different magnitudes for different values of activation energy for desorption (E_d = 15000, 20000, 25000, 30000 $Jmol^{-1}$), a) Pressure, b) desorbed mass flow, c) temperature, d) Desorbed hydrogen fraction

Desorption rate constant (C_d):

Fig. 5.2 shows the evolution of pressure, desorbed mass flow, temperature and desorbed hydrogen fraction for different values of desorption rate constant C_d=2, 5, 10, 15 s^{-1}. In the published literature, the value of C_d usually varies between 0.043 and 2127.3 s^{-1}, for different metal hydride materials [3, 7, 8, 10, 12, 25, 27, 29, 37, 42, 46].

In this case (Fig. 5.2), the desorption reaction is more effective when C_d increases, as it generates a higher desorption rate, according to equation (3.6).

Comparing these results with the ones obtained using a heater, the same as in the previous case (E_d) occurs. The desorption process is more effective and so it finishes sooner, and also temperature increases.

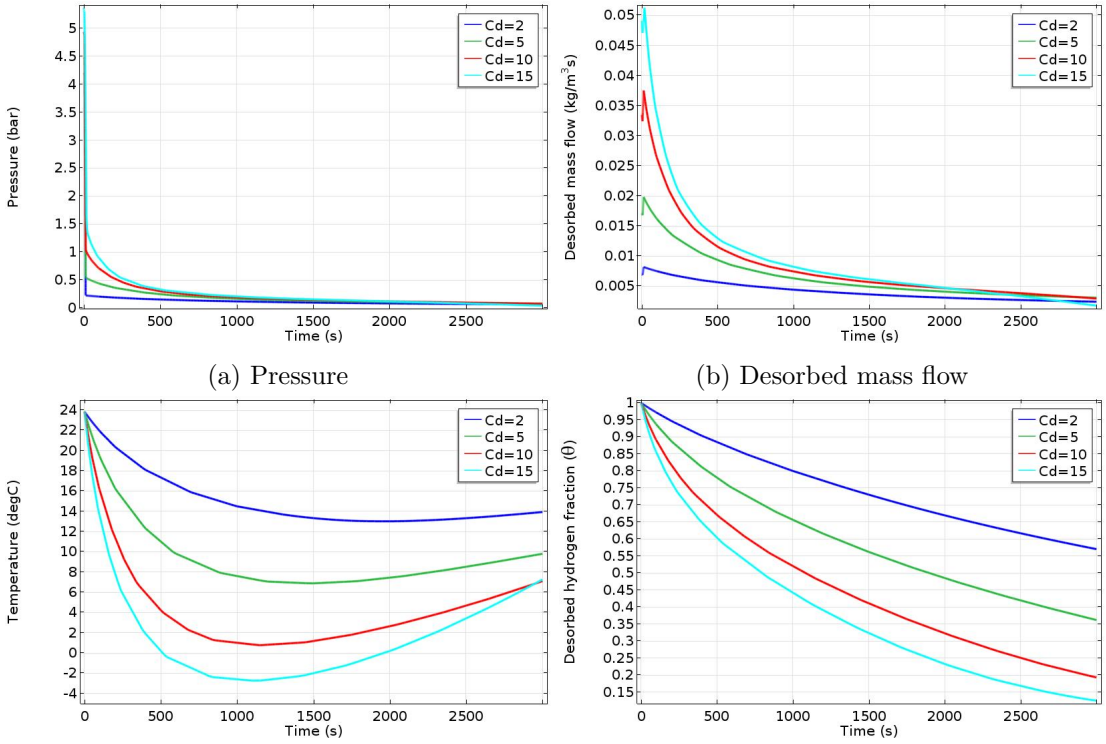

(a) Pressure

(b) Desorbed mass flow

(c) Temperature

(d) Desorbed hydrogen fraction (θ)

Figure 5.2: Evolution of different magnitudes for different values of desorption rate constant (C_d = 2, 5, 10, 15 s^{-1}), a) Pressure, b) desorbed mass flow, c) temperature, d) Desorbed hydrogen fraction

Reaction enthalpy (ΔH):

Fig. 5.3 shows the evolution of pressure, desorbed mass flow, temperature and desorbed hydrogen fraction for different values of reaction enthalpy ΔH=10000, 15000, 20000, 25000, 30000 $Jmol^{-1}$. In the published literature, the value of ΔH usually varies between 17600 and 64230.4 $Jmol^{-1}$, for different metal hydride materials [3, 7, 8, 10, 12, 25, 27, 29, 37, 42, 46].

ΔH is present in the equilibrium pressure expression, as well as in the heat source term. In this case (Fig. 5.3), pressure increases as ΔH decreases, and consequently the mass flow increases as well. At larger desorption mass flows, the process is faster and so θ decreases at a higher rate. Regarding temperature, and according to equation (3.17), as ΔH increases, S_T increases as well and so the temperature is lower.

Using a heater the process becomes more effective, and obviously temperature increases.

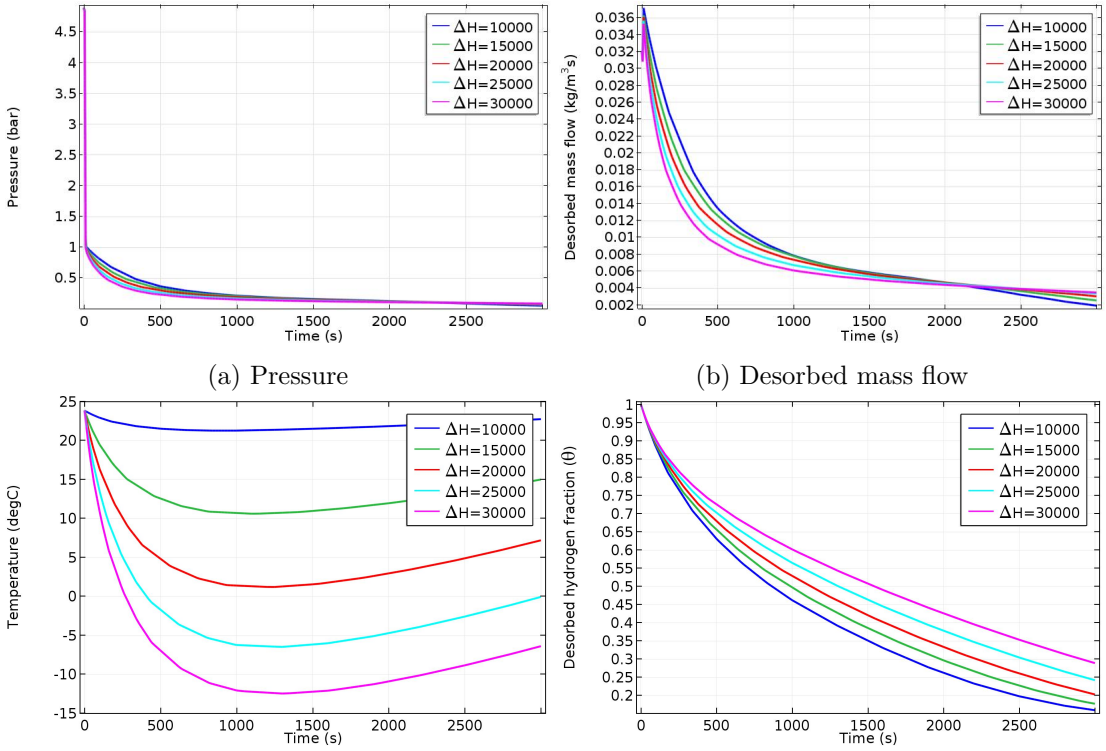

(a) Pressure

(b) Desorbed mass flow

(c) Temperature

(d) Desorbed hydrogen fraction (θ)

Figure 5.3: Evolution of different magnitudes for different values of reaction enthalpy (ΔH = 10000, 15000, 20000, 25000, 30000 $Jmol^{-1}$), a) Pressure, b) desorbed mass flow, c) temperature, d) Desorbed hydrogen fraction

Metal thermal conductivity (k^m):

Fig. 5.4 shows the evolution of pressure, desorbed mass flow, temperature and desorbed hydrogen fraction for different values of thermal conductivity of the metal k^m= 0.5, 1, 2, 3 $Wm^{-1}K^{-1}$. In the published literature, the value of k^m usually varies between 0.524 and 3.18 $Wm^{-1}K^{-1}$, for different metal hydride materials [3, 7, 8, 10, 12, 25, 27, 29, 37, 42, 46].

As expected, k^m only has a noticeable effect on the temperature (Fig. 5.4c). If the thermal conductivity of the metal is higher, it is easier to transfer the heat from outside (as the ambient temperature is higher) to the interior or the bottle, hence increasing the temperature.

As well as in the other cases, if a heater is used the effects of k^m on the desorption performance are the same as the ones without heater.

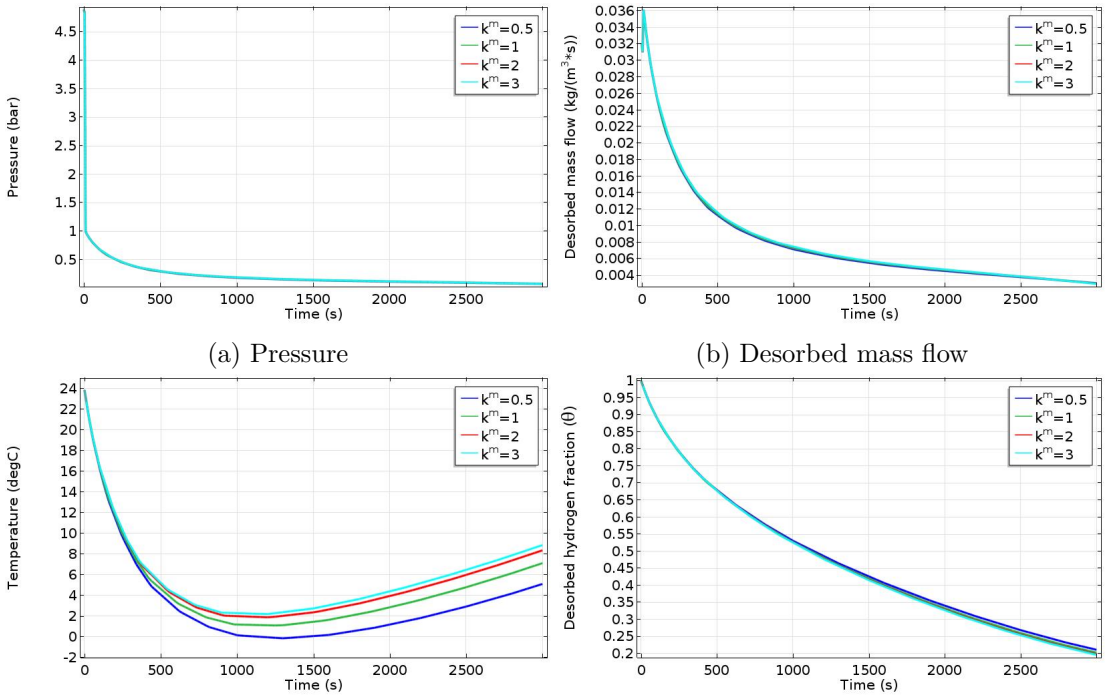

(a) Pressure

(b) Desorbed mass flow

(c) Temperature

(d) Desorbed hydrogen fraction (θ)

Figure 5.4: Evolution of different magnitudes for different values of thermal conductivity of the metal (k^m = 0.5, 1, 2, 3 $Wm^{-1}K^{-1}$), a) Pressure, b) desorbed mass flow, c) temperature, d) Desorbed hydrogen fraction

5.1.2.2 Working conditions and structural parameters

Convection heat transfer coefficient (h):

Fig. 5.5 shows the evolution of pressure, desorbed mass flow, temperature and desorbed hydrogen fraction for different values of convection heat transfer coefficient h= 5, 10, 50, 100, 1000 $Wm^{-2}K^{-1}$. A local heat transfer coefficient of up to 10 W m^{-2}K^{-1} represents the scenario in which the tank is cooled by natural convection, whilst 10< h <200 W m^{-2}K^{-1} represent forced air cooling scenarios and finally h >200 W m^{-2}K^{-1} represents liquid cooling scenarios.

As seen before in section 5.2, externally heating the system has a huge impact on desorption performance. At higher convection heat transfer coefficients, the process becomes more effective. Thus, pressure, desorbed mass flow, and obviously temperature inside the bottle increases and desorbed hydrogen fraction decreases.

In this case the use of a heater produces similar effects as in the previous cases. The desorption process is enhanced so the desorption time is reduced, and also temperature increases due to the heater.

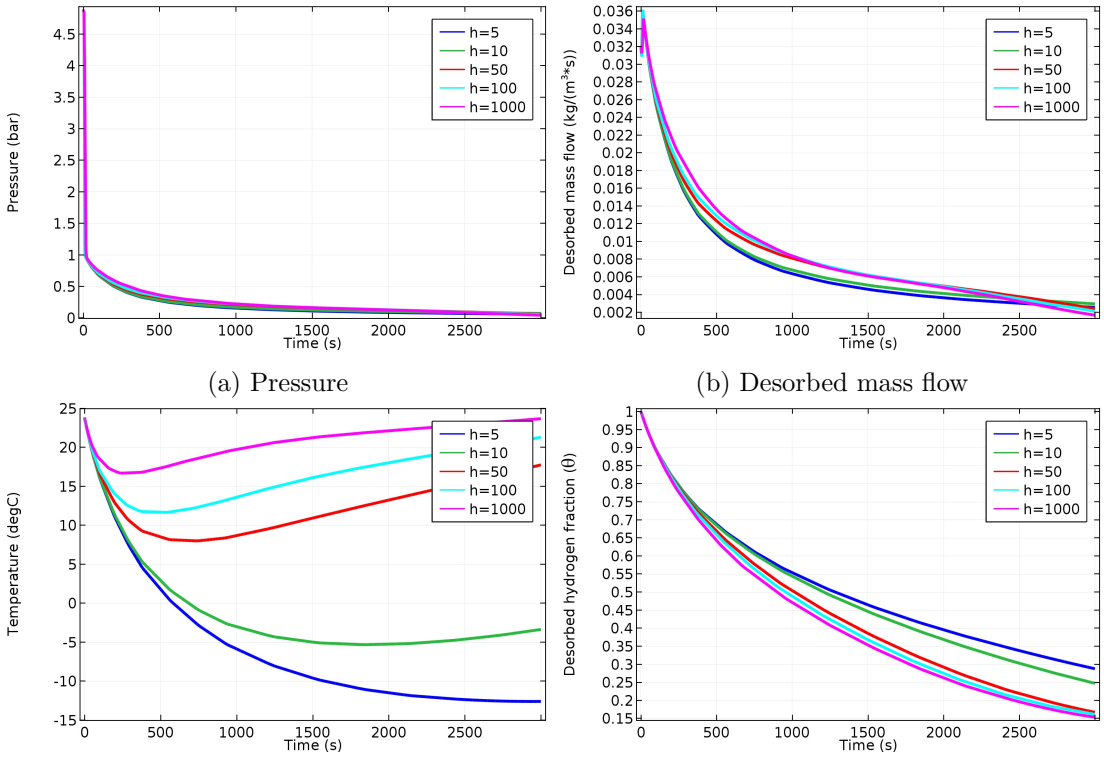

(a) Pressure

(b) Desorbed mass flow

(c) Temperature

(d) Desorbed hydrogen fraction (θ)

Figure 5.5: Evolution of different magnitudes for different values of convection heat transfer coefficient ($h = 5, 10, 50, 100, 1000\ Wm^{-2}K^{-1}$), a) Pressure, b) desorbed mass flow, c) temperature, d) Desorbed hydrogen fraction

Porosity (ε):

Fig. 5.6 shows the evolution of pressure, desorbed mass flow, temperature and desorbed hydrogen fraction for different values of porosity ε= 0.4, 0.5, 0.6, 0.7. In the published literature, the value of ε usually varies between 0.4 and 0.63 [3, 7, 8, 10, 12, 25, 27, 29, 37, 42, 46].

Focusing on porosity, it is important to bear in mind that the volume of the bottle does not change, and so, when porosity is high (ε= 0.7) there is less metal inside the bottle, and consequently less adsorbed hydrogen stored. As the amount of hydrogen stored is lower, the desorption process finishes sooner and the temperature increases until it reaches ambient temperature. On the other hand, when the metal is not very porous (ε= 0.4), the desorption process is slower, as there is a lot more metal inside the bottle and so more stored hydrogen.

As before, the heater produces similar effects, and the only substantial difference is that the temperature increases and the process if more effective.

The effect of the porosity on the metal hydride behavior can be useful for the design of hydrogen storage systems, with a trade-off between charge/discharge time and storage capacity.

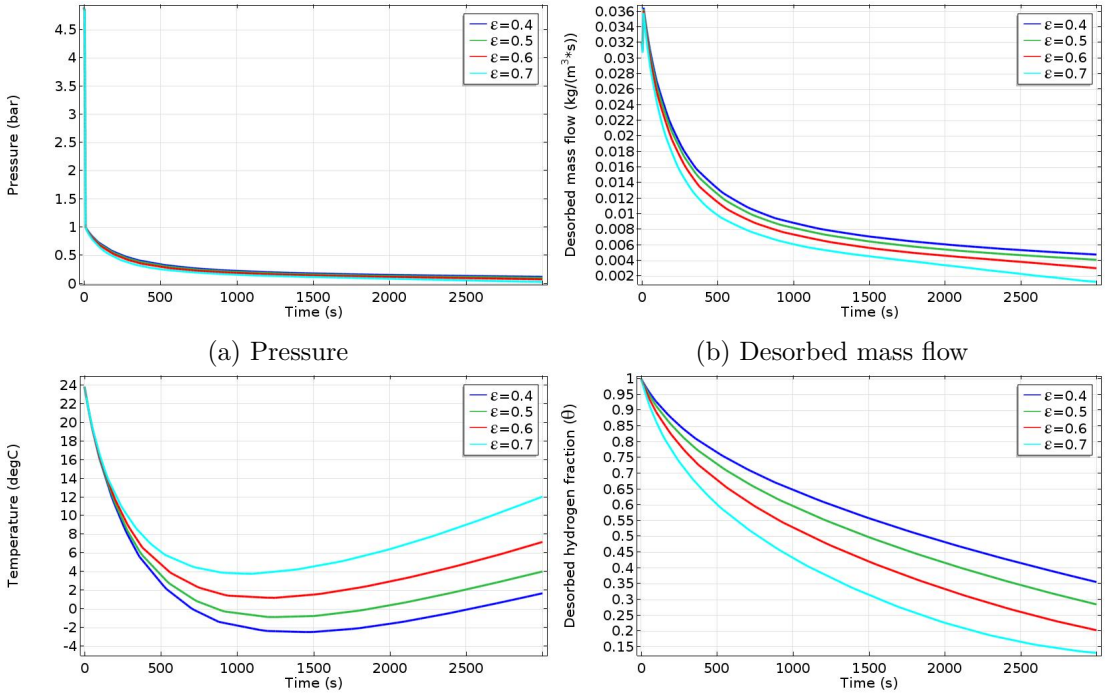

(a) Pressure

(b) Desorbed mass flow

(c) Temperature

(d) Desorbed hydrogen fraction (θ)

Figure 5.6: Evolution of different magnitudes for different values of porosity (ε = 0.4, 0.5, 0.6, 0.7), a) Pressure, b) desorbed mass flow, c) temperature, d) Desorbed hydrogen fraction

Pressure loss coefficient (*grille*):

Fig. 5.7 shows the evolution of pressure, desorbed mass flow, temperature and desorbed hydrogen fraction for different values of pressure loss coefficient *grille*= 5E8, 2E9, 8E9 $kgm^{-4}s^{-1}$.

As explained in section 3.2.2, at the outlet a flow resistance has been set to emulate the real pressure losses that occur throughout the experimental hydrogen circuit. Obviously this coefficient has a strong influence on the pressure (Fig. 5.7a), and these changes in pressure generate remarkable effects on all the other studied variables. If the *grille* coefficient increases, the pressure increases, as it requires more pressure to overcome the resistance and create the pressure gradient that allows the hydrogen evacuation.

If the pressure inside the bottle increases, it becomes similar to the equilibrium pressure, and so the reaction tends to slow down. If at some point the pressure inside the bottle becomes higher than the equilibrium pressure, the reaction is reversed and instead of desorbing it would start adsorbing. In this case, the equilibrium pressure has been modeled with the empirical curve fitting (eq. (2.20)) to see the real behavior of the system. That being said, S_m in figure 5.7b decreases as pressure increases. If the desorption mass flow is smaller, the temperature will be higher, because the reaction is not as effective and so, not as endothermic. Therefore, if *grille* is higher, the process is slower and so it takes longer to discharge.

If a heater is used, the overall effects are the same, but the process finishes sooner and the temperature increases.

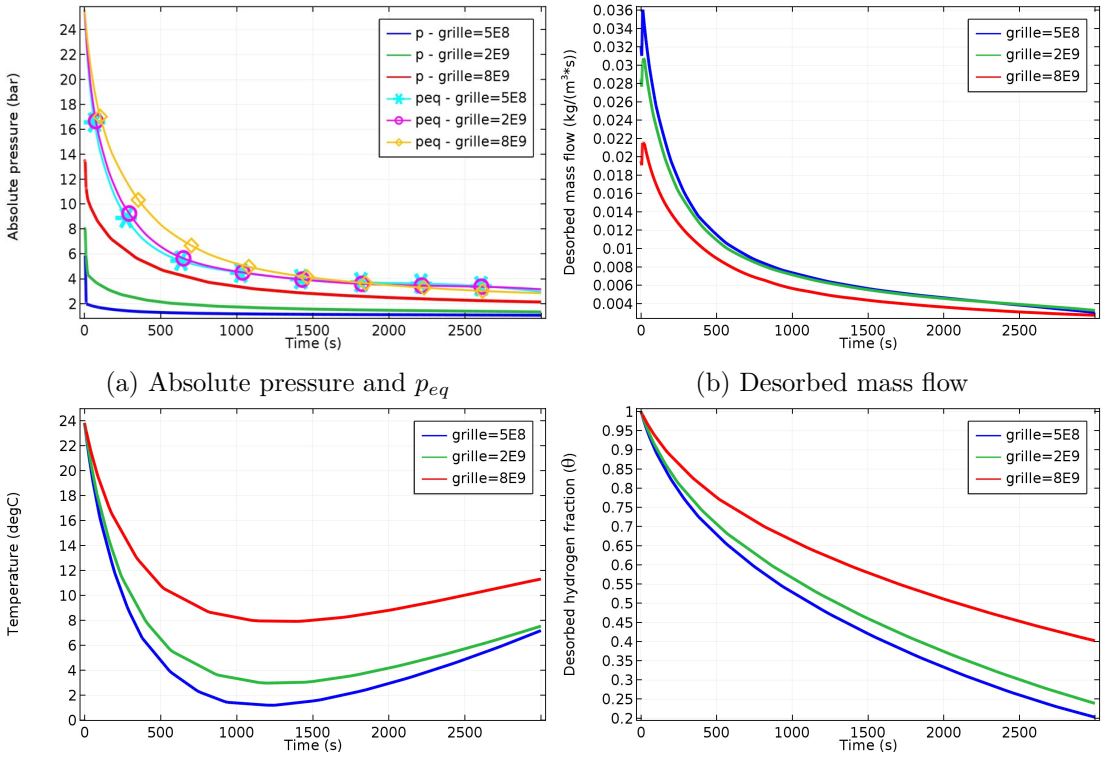

(a) Absolute pressure and p_{eq}

(b) Desorbed mass flow

(c) Temperature

(d) Desorbed hydrogen fraction (θ)

Figure 5.7: Evolution of different magnitudes for different values of pressure loss coefficient ($grille$ = 5E8, 2E9, 8E9 $kgm^{-4}s^{-1}$), a) Pressure, b) desorbed mass flow, c) temperature, d) Desorbed hydrogen fraction

5.1.3 Closed bottle equilibrium results

When the bottle is closed is when the adsorption/desorption equilibrium can be truly evaluated.

When the metal hydride is not completely saturated with hydrogen and the bottle is closed, if the equilibrium has not been reached, the system will adsorb or desorb hydrogen until the equilibrium pressure is reached at that temperature. This is the reason why in the experiments (explained in section 5.2), the bottles are charged at a constant pressure around 6.5 bars, but if they are given enough time to reach equilibrium, the initial discharge pressure is lower, as they continue adsorbing until they reach equilibrium conditions.

If the bottle was saturated and closed, the pressure would remain constant as all the available possible adsorption spaces would already be filled with hydrogen. So, the initial discharge pressure and temperature indicate the amount of hydrogen in gaseous state.

The following figures (5.8 and 5.9) show the pressure and temperature evolution at different conditions. It has been considered that ambient temperature is 24°C (297 K) and an external convection coefficient of 4.3 W $m^{-1}K^{-1}$. It has also been considered that the bottle is not saturated , and its initial metal hydride density is 5307.3 kg m^{-3}. Finally, for the equilibrium pressure expression (2.20) has been taken, as it reproduces the real behavior of a metal hydride during adsorption/desorption.

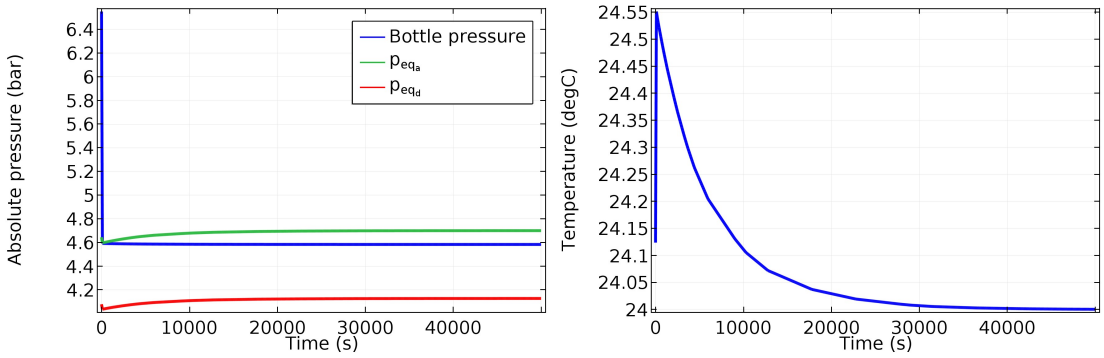

(a) Pressure (abs) - p>p_{eq}, T_{ini}=24 °C (b) Temperature - p>p_{eq}, T_{ini}=24 °C

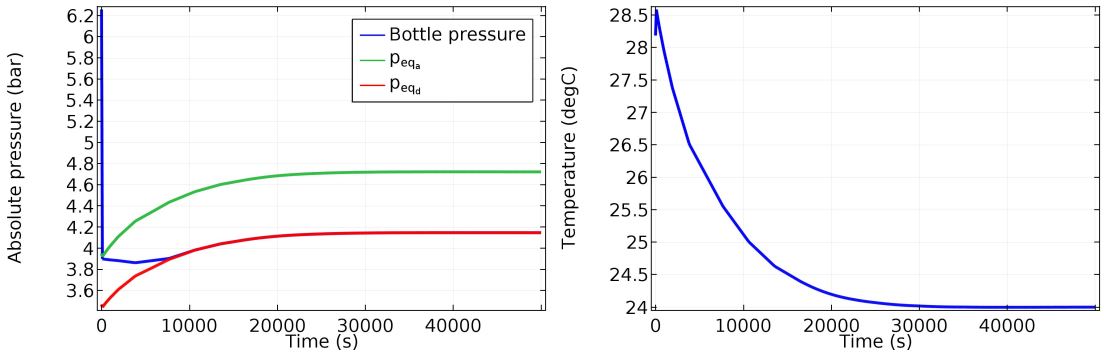

(c) Pressure (abs) - p>p_{eq}, T_{ini}=28 °C (d) Temperature - p>p_{eq}, T_{ini}=28 °C

Figure 5.8: Absolute pressure and temperature when the bottle is closed at p>p_{eq} and T_{ini}=24°C and 28°C

When pressure is higher than the equilibrium pressure (p_{eq_a} and p_{eq_d}), the reaction tends to adsorb reducing the internal bottle pressure so that it can reach equilibrium pressure. In figure 5.8a, pressure decreases until it reaches equilibrium pressure and then it remains constant. Regarding temperature in figure 5.8b it increases a bit at the beginning as the adsorption reaction is taking place to reduce pressure, and once equilibrium has been reached it returns to ambient conditions because of the external convection.

As equilibrium pressure depends on temperature, if the initial temperature changes, for example it increases as in figures 5.8c and 5.8d, the equilibrium will be slightly different. In figure 5.8c the system adsorbs hydrogen until it reaches the equilibrium pressure (green line) and then it remains constant. But, as there is an hysteresis between adsorption and desorption isotherms, as explained in section 2.3.2.3, and the system wants to remain in equilibrium it will follow the desorption equilibrium pressure isotherm (red line) and so it will desorb the necessary hydrogen to increase its pressure and remain in equilibrium. Regarding temperature in figure 5.8d, it increases a bit at the beginning due to the exothermic adsorption reaction and then in decreases mainly due to the convection with surrounding air.

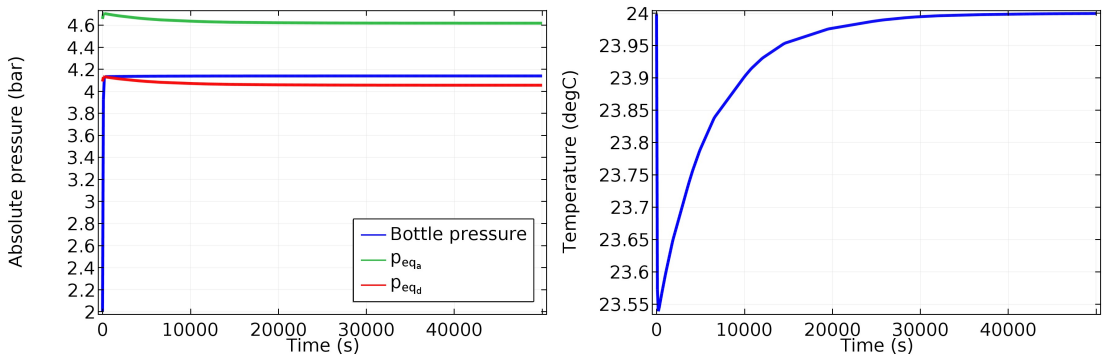

(a) Pressure (abs) - p<p_{eq}, T_{ini}=24 °C

(b) Temperature - p<p_{eq}, T_{ini}=24 °C

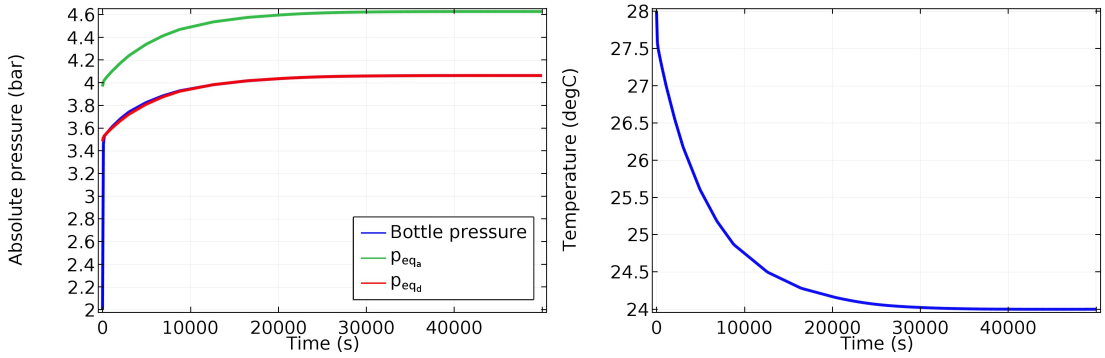

(c) Pressure (abs) - p<p_{eq}, T_{ini}=28 °C

(d) Temperature - p<p_{eq}, T_{ini}=28 °C

Figure 5.9: Absolute pressure and temperature when the bottle is closed at p<p_{eq} and T_{ini}=24°C and 28°C

In figures 5.9, the initial pressure is lower than the equilibrium pressure, and as before, two different temperature scenarios are presented. In figures 5.9a and 5.9b the bottle is initially at ambient temperature. Regarding pressure, as it is lower than the equilibrium pressure, the reaction shifts to the left and it desorbs hydrogen to increase its pressure and reach equilibrium. As it desorbs, internal temperature decreases and once the equilibrium is reached it returns to ambient temperature due to the external convection.

In figures 5.9c and 5.9d, initial temperature is 28 °C, this means that the equilibrium pressures are slightly modified and also that desorption is enhanced. As expected, the system desorbs to reach equilibrium and temperature decreases, faster at the beginning due to the endothermic reaction, and a bit slower after the equilibrium is reached due to convection with surrounding air.

5.2 Experimental results

5.2.1 Specifications

As explained in Chapter 4, there are two metal hydride canisters (B1 and B2) with different degrees of degradation, as their use previous to this study was different from one another. Besides that, there is also a fan/heater that may be used to improve the adsorption/desorption process. In the end, there are different combinations of these factors that result in different discharge behaviors.

In the table below (5.1), there is a summary of the four experiments analyzed in the following section, to understand why apparently analogous situations are not really the same.

	Bottle	**Charge**	**Discharge**
14/12/2016	B1	Natural convection (77 nL)	Natural convection
15/12/2016	B2	Forced convection (fan) (138 nL)	Natural convection
19/12/2016	B1	Forced convection (fan) (118 nL)	Heater
21/12/2016	B2	Natural convection (78 nL)	Heater

Table 5.1: Specifications of the performed experiments

All the experiments are performed charging the bottles at an inlet pressure of 6.5 bars and at an ambient temperature around 25 °C, as well as limiting the hydrogen mass flow entering/exiting the bottle to 1.5 nlpm. The fan and heater are both working with an air mass flow of 340 L/min, and the set point temperature of the heater is 70 °C.

It is also important to mention that the provider of the bottles recommends a charging pressure of 30 bar, higher than the one that was used for these experiments (around 6.5 bars), as these levels of pressure are not available in the laboratory environment and installation. That is the reason why the bottles were only partially charged. That being said, they were charged the maximum amount of hydrogen possible depending on the charge conditions used.

5.2.2 Results discussion

In figures 5.10 and 5.11 the temperature measurements with and without heater can be seen. As expected, when there is no heater (Fig. 5.10), the temperature on the surface of the bottles decreases, due to the endothermic desorption reaction at the beginning. Then the temperature reaches a plateau, and finally when the reaction has stopped, the temperature starts to increase until it reaches ambient temperature. As seen in Table 5.1, B2 had a larger amount of hydrogen stored and so the discharge process takes longer. It is important to mention that the system did not reach equilibrium at the beginning (temperature is higher than ambient temperature at the beginning), as the bottles did not have enough time to do so, because charge and discharge experiments were performed one after the other.

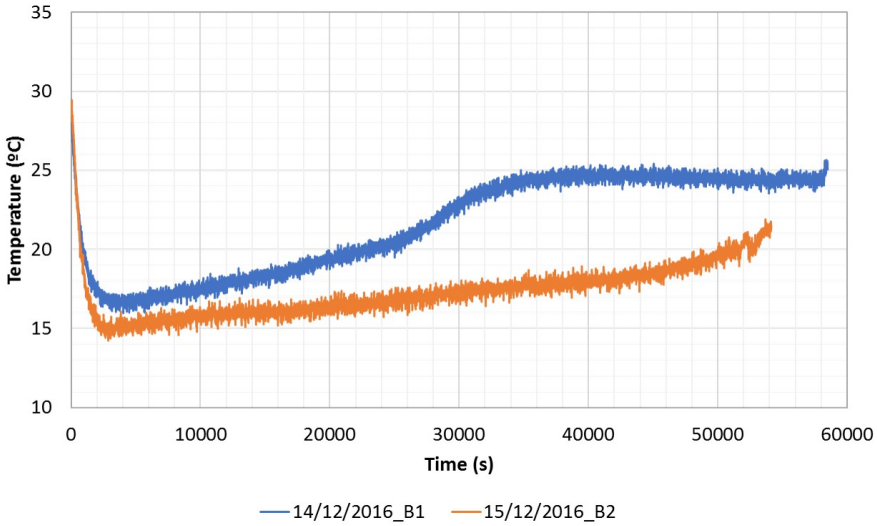

Figure 5.10: Experimental temperature without heater during discharge

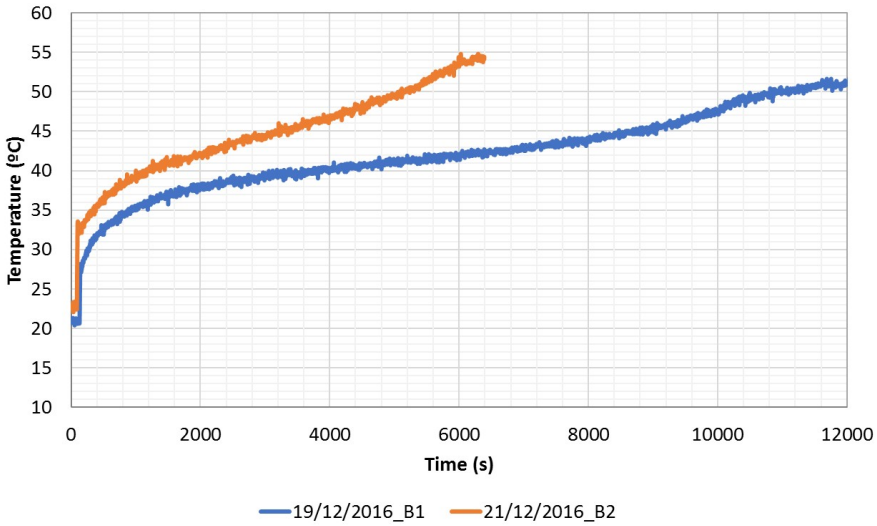

Figure 5.11: Experimental temperature with heater during discharge

On the other hand, when the heater is on (Fig. 5.11), temperature on the surface of the bottles increases. Again, it reaches a plateau, as there is a balance between the endothermic reaction and the heat supplied, and finally, when the reaction has finished, the temperature increases according to the set point temperature of the heater. In this case B1 had a larger amount of hydrogen stored, so the discharge process takes longer.

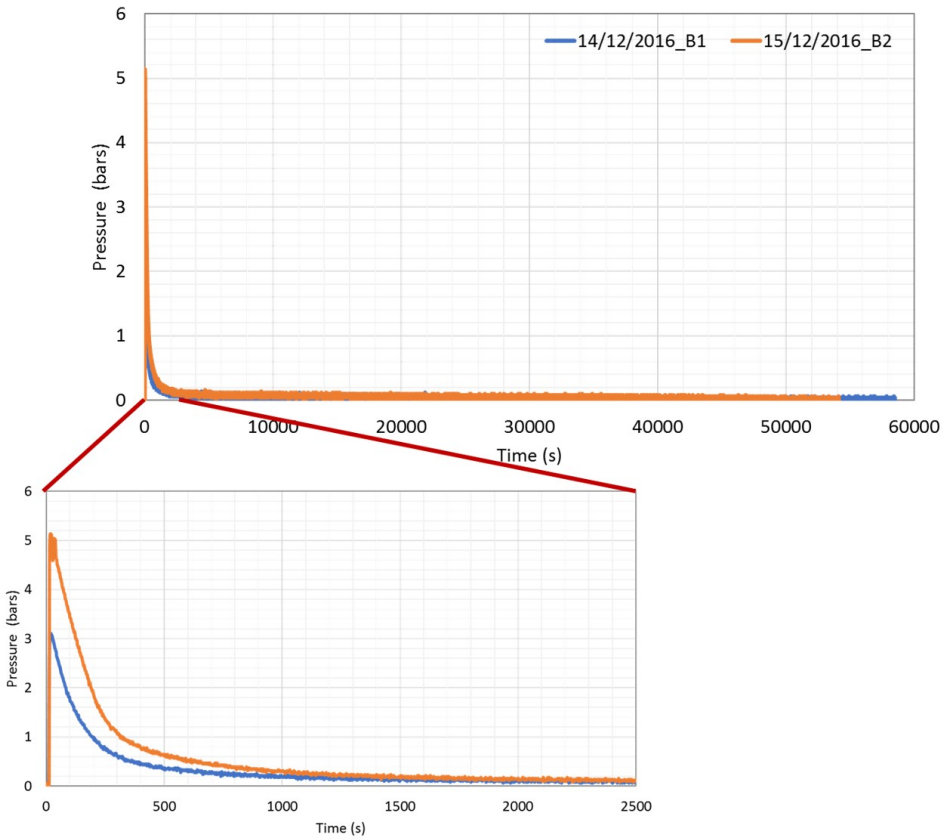

Figure 5.12: Experimental pressure without heater during discharge

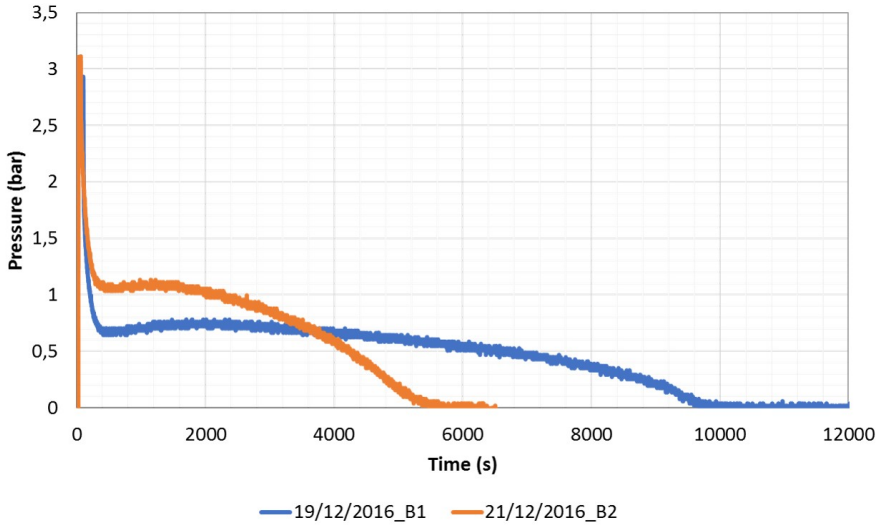

Figure 5.13: Experimental pressure with heater during discharge

This change in temperature has a great influence on the pressure. It can be seen that if temperature increases, the hydrogen molecules are more excited and increase the pressure inside the bottle. Consequently, a pressure gradient is produced from inside out, enabling the evacuation of hydrogen.

Analyzing the graphs (5.12 and 5.13), a sharp decrease on the pressure is observed at the

beginning, as the hydrogen that was not adsorbed and is stored in gas form comes out quickly, producing a huge drop in pressure. Then, the adsorbed hydrogen inside the metal starts to desorb. If this process is improved by raising the wall's temperature, the interior pressure will be higher, the pressure gradient that drives the evacuation of hydrogen will be stronger, and so, the discharge process will finish sooner (Fig. 5.13).

Again, it is important to mention that in 14/12/2016 and 15/12/2016 experiments the system was not in equilibrium at the beginning, and that is why initial pressures are not the same. The system did not have time to adsorb the necessary hydrogen to reach equilibrium.

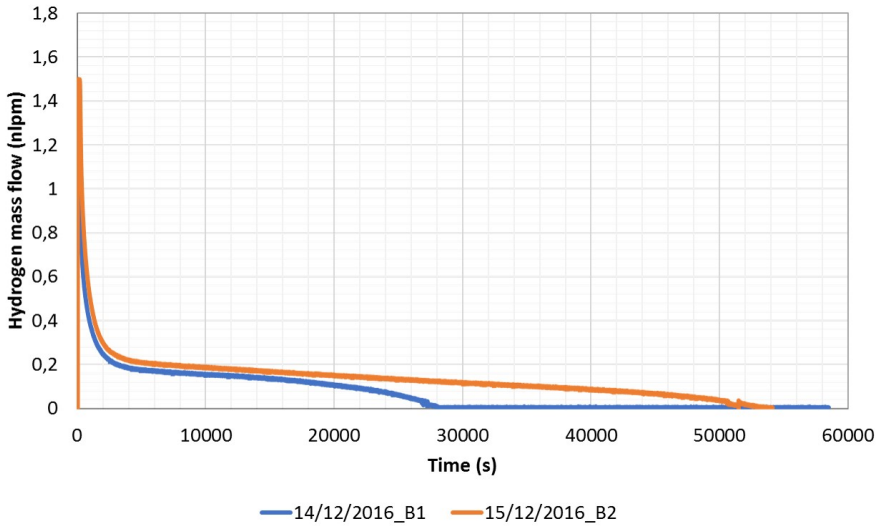

Figure 5.14: Experimental outlet mass flow without heater during discharge

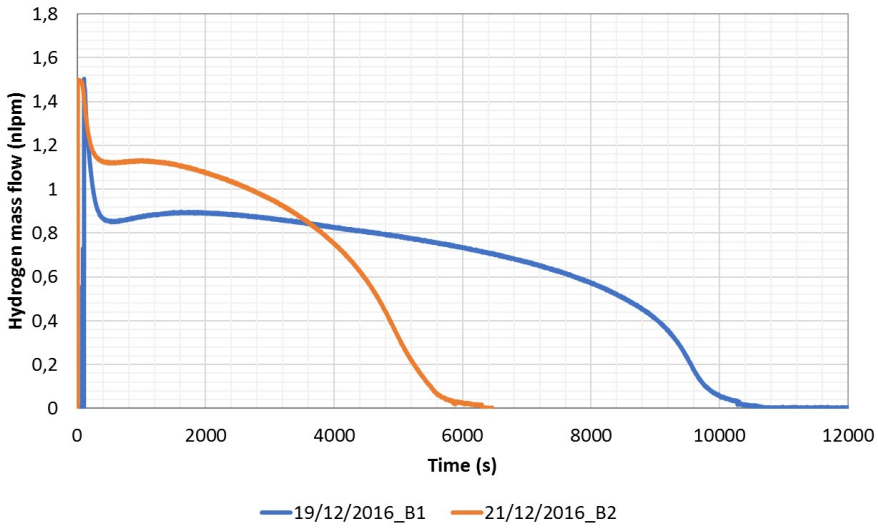

Figure 5.15: Experimental outlet mass flow with heater during discharge

As said, temperature and pressure have a huge impact on the hydrogen mass flow exiting the bottle (figures 5.14 and 5.15). Temperature produces a more efficient desorption process, so there is more hydrogen molecules ready to exit the bottle. Also, the increase in temperature

produces a rise in pressure and consequently a stronger pressure gradient that will force the desorbed hydrogen to exit the bottle at a much higher rate. If both the desorption rate and the discharge rate are higher, the discharge process will finish sooner.

Finally, it is important to mention that these experimental results have allowed developing an empirical metal hydride state of charge estimator, explained in Appendix F.

5.3 Simulation and experimental results comparison

5.3.1 Differences between simulation results and experimental tests

As thoroughly explained in Chapter 3, the numerical model faithfully represents the internal phenomena occurring inside the metal hydride canister (mass and heat transfer, and desorption kinetics). What happens inside the bottle consequently governs what can be experimentally measured outside of the bottle (Chapter 4), as displayed in figure 5.16.

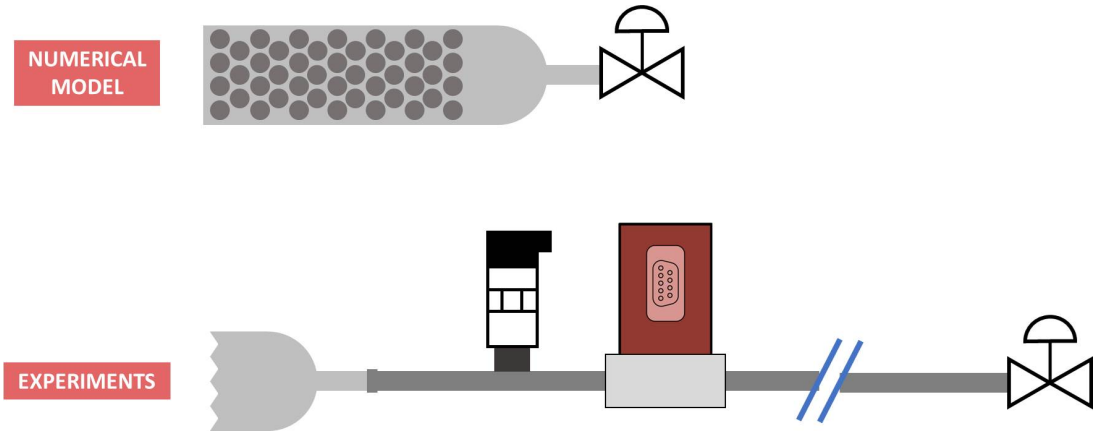

Figure 5.16: Scheme of the simulation and experimental setups

It is important to realize that what happens inside the bottle has direct consequences on the experimental measures, but not the other way around. Let's explain this in a bit more detail.

At the beginning the bottle is closed and considered charged, and so it is pressurized. Whilst the bottle is closed, all the possible available adsorption places are already filled and the hydrogen that was not able to get adsorbed is in gas form, maintaining the pressure level. This means that there is no net adsorption/desorption mass flow, and that the pressure inside is constant. At this point the temperature is not important, as the bottle has acclimated with the surrounding air. As the bottle is closed, nothing is coming out of it, and so there are not experimental measurements.

Once the outlet valve of the circuit is opened, at the end of the circuit pressure is atmospheric, and a pressure gradient is generated. Then, as explained in section 2.1, this difference in pressure will force the reaction to go to the left and release the adsorbed hydrogen, so a desorption mass flow is generated. These released hydrogen molecules (still inside the bottle), need to circulate through the porous media and once they reach the buffer region they can come out of the bottle.

As seen in section 2.5, the discharge of a pressurized tank is not simple, and while hydrogen is leaving the bottle is has to go through some major section changes, and so the fluid flow will not be fully developed yet at the outlet. To be accurately measured by the mass flow meter, the fluid flow must be developed and so it needs a certain amount of pipe length to do so.

That being said, it is important to keep in mind that in the real experimental setup there is a pipe circuit that goes from the outlet of the bottle to the exterior air, where hydrogen needs to go through dozens of connectors, pipe fittings, sensors and other elements, and this generates pressure losses. However, the numerical model only considers the bottle and, as seen in figure 5.16 includes a resistance at the outlet of the bottle. This resistance (*grille*) is a pressure drop that emulates the pressure losses in the whole experimental circuit. Nevertheless, the mass flow at the outlet of the bottle is not the same as the one that can be measured by the mass flow meter, as they are located in different positions.

The same thing happens with the pressure measurement, the outlet of the bottle and the sensor are located in different points of the system, and so the outlet pressure is higher than the one being acquired by the sensor, due to pressure losses.

Regarding temperature, it is even easier to see why the simulation and experimental measures are not the same. Thermocouples are placed outside the bottle, being very susceptible to ambient temperature (or temperature set point, if a heater is used), as well as the thermal conductivity of the exterior bottle material. In the numerical model, temperatures are monitored inside, being a good indicator of the adsorption/desorption reaction.

5.3.2 Simulation and experimental results comparison

As said before, the studied problem is extremely complex given the lack of information of what happens inside the bottle. There is no experimental data of the interior of the bottle, plus no information on morphology or material given by the provider.

That being said, it is important to select the most reliable information possible to be able to provide a good comparison with the model. As the experiments with natural convection (14/12/2016 and 15/12/2016) were not at equilibrium conditions at the initial discharge instant, it is much more complex to reproduce this behavior, taking into account all the other number of unknowns. That is the reason why it has been decided to check the validity of the model with the experimental data obtained using a heater, and only illustrate the natural convection case in terms of pressure and in a dimensionless way.

Experiments: 14/12/2016 and 15/12/2016

In figure 5.17, the results for the pressure at the outlet of the bottle obtained with the numerical model and the measured experimental pressure for the case without using a heater can be compared. As expected, the pressure at the outlet of the bottle is higher, and then it suffers some pressure losses that produce a lower pressure in the sensor.

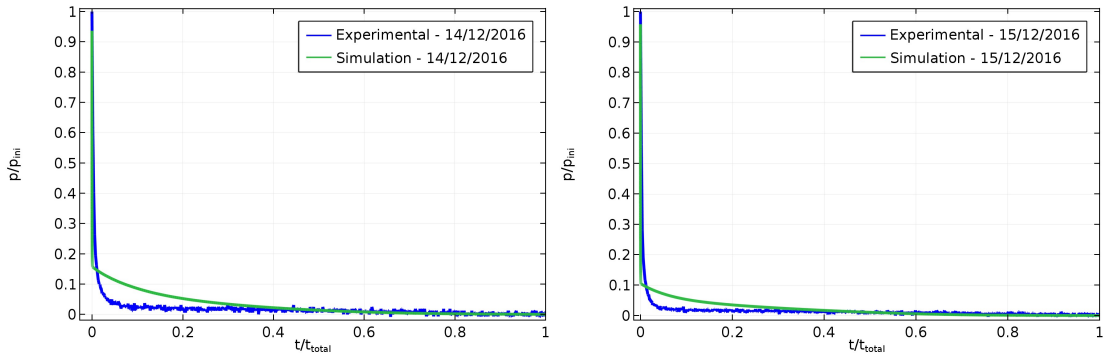

(a) Pressure (14/12/2016) (b) Pressure (15/12/2016)

Figure 5.17: Simulated and experimental pressure without heater (dimensionless)

Experiment: 19/12/2016, Bottle 1

In this case, the simulated bottle is B1 and the model has been calibrated using the parameters in table E.1.2 of Appendix E.

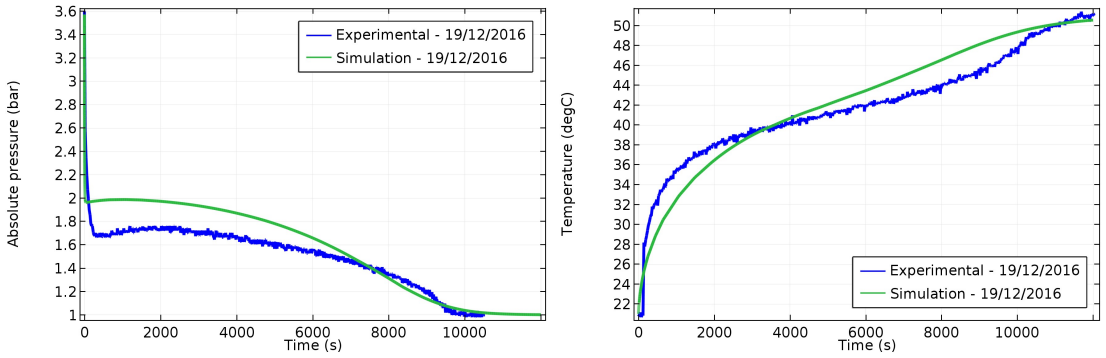

(a) Absolute pressure (bar) (b) Temperature (°C)

Figure 5.18: Simulation and experimental results comparison (19/12/2016)

Figure 5.18a shows the comparison between experimental pressure measured outside of the bottle and simulation results modeled inside the bottle. As can be seen, both curves match, and the small deviations are a consequence of the pressure difference by pressure losses explained in section 5.3.1, plus the many uncertainties explained throughout the project report.

On figure 5.18b, the temperature evolution at the surface of the bottle is depicted. In this case, temperature is not a good indicator of the desorption reaction, because a heater is being used and so the temperature measurement and the simulation results at the surface of the bottle basically give information on the heater temperature. That being said, both curves match well and so the validity of the model is checked once again.

More simulation results can be found in section D.4 of Appendix D.

Experiment: 21/12/2016, Bottle 2

In this case, the simulated bottle is B2 and the model has been calibrated using the parameters in table E.1.2 of Appendix E.

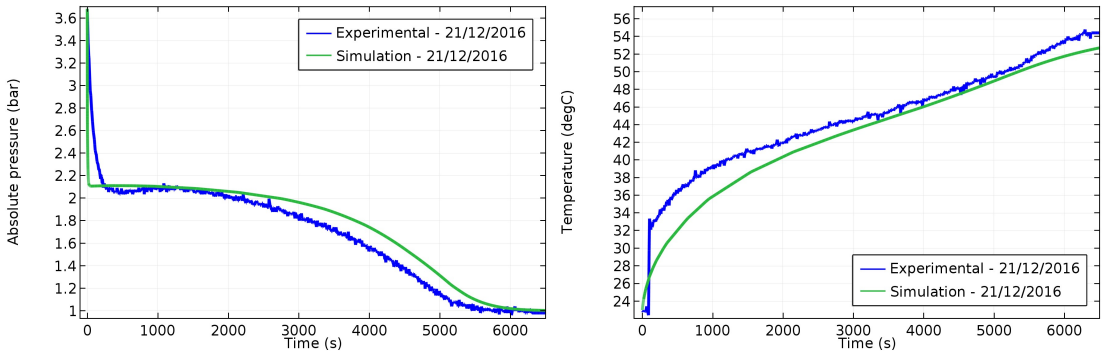

(a) Absolute pressure (bar) (b) Temperature (°C)

Figure 5.19: Simulation and experimental results comparison (21/12/2016)

Figure 5.19a shows the pressure evolution in absolute terms both experimentally and numerically. As in the previous case, both curves match perfectly and the small deviations that may appear are due to the unknown nature of the metal hydride inside and the internal configuration of the bottle.

Regarding temperature, figure 5.19b, shows a good agreement as well, but again it has to be taken into account that this temperature evolution is not a good indicator of the endothermic reaction occurring inside the bottle.

More simulation results can be found in section D.4 of Appendix D.

Chapter 6

Budget

6.1 Budget broken down into sections

The first part of the budget is divided on the following sections:

- Hydrogen storage system
- Valves and piping
- Data acquisition system
- Sensors and controllers
- Electronics
- Gases
- Support structures
- Computer and software
- Professional fees

6.1.1 Hydrogen storage system

Units		Unit cost	Total cost
2	MHS-225. Metal Hydride Storage Tank with 225 nl of Hydrogen storage capacity	950.00 €	1900.00 €
2	Adapter with outage tube	33.00 €	66.00 €
			1966.00 €

6.1.2 Valves and piping

Units		Unit cost	Total cost
2	1/4” Stainless Steel 3-way ball valves	85.40 €	107.80 €
2	1/4” Stainless Steel 2-way ball valves	84.40 €	168.80 €
1	1/4” Stainless Steel 7μm in-line particulate filter	61.60 €	61.60 €
1	1/4” Stainless Steel Poppet Check valve	46.40 €	46.40 €
2	1/4” Nonrotating-Stem Needle valve	105.70 €	211.40 €
2	1/4” Stainless Steel Quick-connects	31.90 €	63.80 €
2	1/4” Stainless Steel Union Tee	25.70 €	51.40 €
1	1/4” Stainless Steel Union Cross	38.80 €	38.80 €
2	1/4” Stainless Steel Straight Union	9.79 €	19.58 €
25	1/4” Stainless Steel Nuts	1.83 €	45.75 €
25	1/4” Stainless Steel Front Ferrule	1.04 €	26.00 €
2	1/4” Stainless Steel Plug	5.20 €	10.40 €
1	1.5 m of 1/4” Stainless Steel pipe	8.40 €	8.40 €
			860.13 €

6.1.3 Data acquisition system

Units		Unit cost	Total cost
1	NI myRIO device	250.00 €	250.00 €
1	Host computer	850.00 €	850.00 €
			1100.00 €

6.1.4 Sensors and controller

Units		Unit cost	Total cost
1	1.5 nlpm H_2 Mass Flow Controller	1430.00 €	1430.00 €
1	Industrial pressure transmitter 40 bar	194.00 €	194.00 €
8	Welded Tip PFA Thermocouple	3.94 €	31.52 €
4	Temperature controllers. Data acquisition	400.00 €	1600.00 €
4	Temperature controllers. Data visualization	350.00 €	1400.00 €
1	Hot air blower	1017.00 €	1017.00 €
			5672.52 €

6.1.5 Electronics

Units		Unit cost	Total cost
1	Power Source	71.00 €	71.00 €
1	Signal wiring	15.00 €	15.00 €
			86.00 €

6.1.6 Gases

Units		Unit cost	Total cost
1	900 L of hydrogen (H_2)	15.08 €	15.08 €
1	150 L of nitrogen (N_2)	2.21 €	2.21 €
			17.29 €

6.1.7 Support structures

Units		Unit cost	Total cost
1	85x70 mm wood board	10.00 €	10.00 €
1	0.5 m of DIN rail	2.10 €	2.10 €
			12.10 €

6.1.8 Computer and software

6.1.8.1 Computational costs

Units		Unit cost	Time used	Total cost
1	Asus laptop	700.00 €		700.00 €
1	Cluster	0.15 €/h	580 h	87.00 €
				787.00 €

6.1.8.2 Licenses and software

Units		Unit cost	Total cost	
1	COMSOL Multiphysics 5.2	5000 €		5000 €
1	LabVIEW 2014 and myRIO Toolkit	3376.00 €	250 h	1688.00 €
1	SolidWorks 2014	3995.00 €	5 h	332.92 €
				7020.92 €

In order to make the project more competent, it is important to take into account that some of the programs' licenses are floating, so they are shared and not used all year long. That is the reason why in the project it is considered a derived cost of the licenses proportional to the hours used and considering a 6 month contract for LabVIEW, and a month for SolidWorks.

6.1.9 Professional fees

	Cost per hour	Hired hours	Total
Junior engineer	15.00 €/h	800 h	12000.00 €
Senior engineer	35.00 €/h	150 h	5250.00 €
			17250.00 €

The justification for the payment of salaries is:

	Junior engineer	**Senior engineer**
Accruals		
Base salary	15.00 €	35.00 €
Total accrued	12000.00 €	5250.00 €
Deductions		
4.7 % Social Security	564.00 €	246.25 €
1.55 % General unemployment rate	186 €	81.38 €
Withholding tax (IRPF) 13.21 % for junior 2 % for senior	1585.20 €	105.00 €
	9664.80 €	4817.37 €

6.2 Total Budget

Hydrogen storage system	1966.00 €
Valves and piping	860.13 €
Data acquisition system	1100.00 €
Sensors and controller	5672.52 €
Electronics	86.00 €
Gases	17.29 €
Support structures	12.10 €
Computer and software	7807.92 €
Professional fees	14714.25 €
TOTAL	**32236.21 €**

Chapter 7

Environmental impact

There is increasing interest in the role that hydrogen-based energy systems may play in the future, especially in the transport sector, where metal hydride hydrogen storage will play a key role. Hydrogen-based systems seem to be an attractive alternative to current fossil fuel-based energy systems, since these have been proven to affect climate due to the greenhouse gases emissions. Nevertheless, any future hydrogen-based economy would need to assess the possible global environmental impacts of such alternative energy production [45].

Derwent et al. [16] and van Ruijven et al. [43] reviewed the fate and behavior of hydrogen in the atmosphere, and characterized its major sources and sinks. From their study it is concluded that, contrary to most expectations, hydrogen is an indirect greenhouse gas with potential global warming effect.

Then, the global warming potential of hydrogen in comparison to CO_2 and the global warming consequences of replacing the current fossil fuel-based economy with one based on hydrogen were quantified.

The results suggest that because hydrogen reacts in the atmosphere with tropospheric OH radicals, the emission of hydrogen into the atmosphere would disrupt the distribution of methane and ozone, the second and third most important greenhouse gases. Emissions of hydrogen lead to increased burdens of methane and ozone and hence to an increase in global warming. Therefore hydrogen can be considered as an indirect greenhouse gas with the potential to increase global warming.

It was also estimated that the potential effects on climate from hydrogen-based energy systems would be much lower than those from fossil fuel-based energy systems. However, such impacts will depend on the rate of hydrogen leakage during its synthesis, storage and use. The researchers [16] have calculated that a global hydrogen economy with a leakage rate of 1 % of the produced hydrogen would produce a climate impact of 0.6 % of the fossil fuel system it replaces. If the leakage rate was 10 %, then the climate impact would be 6 % of that of the fossil fuel system.

These studies conclude that using hydrogen as an energy carrier can help reduce air pollution and greenhouse gas (GHG) emissions associated with fossil fuels. However, if used on a large-scale, it is important that hydrogen does not leak significantly into the atmosphere as it might have some negative environmental effects, such as increasing the lifetime of methane, increasing climate effects and causing some depletion of the ozone layer.

Chapter 8

Project planning

For the development of this project, a collection of activities and tasks (represented in a Gantt diagram 8.1) have been carried out, being the most important ones:

- State of the art:
  - Desorption in metal hydride hydrogen storage canisters
  - Transport in porous media
  - Adsorption and desorption between fluids and solids
  - Compressible flow and discharge of pressurized tanks
- Numerical model
  - Adapt charge model to discharge situation using cylindrical geometry
  - Adjust the geometry to the real metal hydride canisters in the lab
  - Mesh independence test
  - Parametric studies
  - Post-processing and results analysis
- Experimental testing
  - Plan the experimental tests
  - Re-assemble the experimental setup
  - Test the data acquisition system
  - Test the whole experimental setup and purge the circuit
  - Discharge the metal hydride bottles completely, so that both are approximately at the same level
  - Experimental tests
  - Post-processing and data analysis
- Budget
- Environmental impact
- Write the Master's Thesis

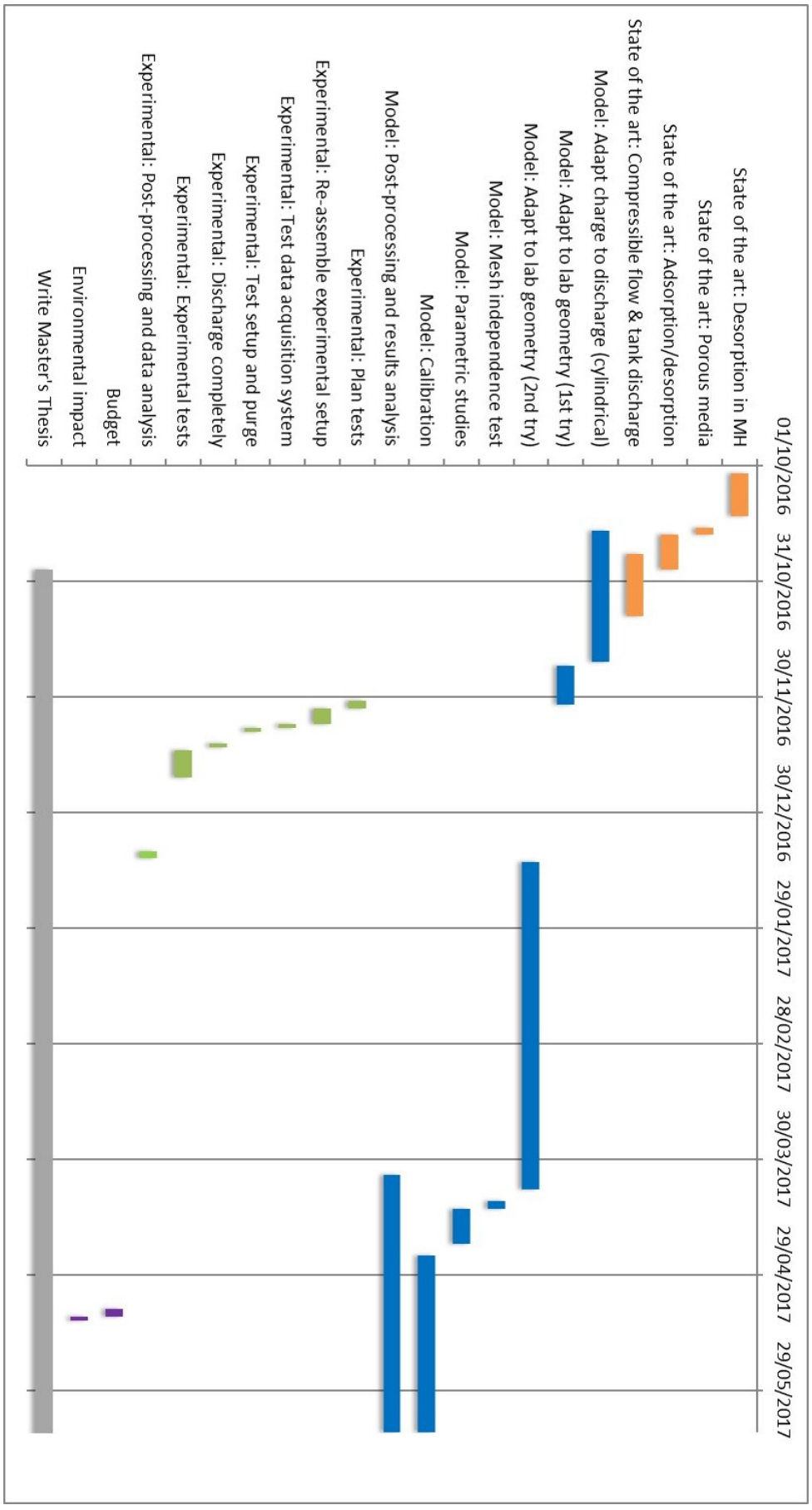

Figure 8.1: Gantt diagram of the project

Chapter 9

Conclusions

Present storage techniques for hydrogen include compressed gas, cryogenic liquid and adsorbed solid (for example metal hydrides). To store hydrogen as a compressed gas, energy must be consumed to reach the high pressure. Considering hydrogen compressed at 680 bars, the system would require around 47 MJ/kg, which corresponds to the 40 % of the low heat value (LHV) of hydrogen [22]. So, storing hydrogen as a compressed gas is quite energy intensive.

To store hydrogen as a liquid, the energy to cool hydrogen to the liquid state is critical, considering inefficiencies of the refrigeration system at extremely low temperatures. The total required energy to store hydrogen as a liquid would be 50.4 MJ/kg, which is 42 % of the LHV, so liquid hydrogen storage is as energy intensive as the compressed hydrogen [22].

As seen, the use of metal hydrides to store hydrogen requires charge (and adsorption) and discharge (and desorption) processes. A typical charge process requires a supply of hydrogen at a moderate pressure and the removal of heat from the adsorption. A similar amount of heat would be needed to desorb the hydrogen, but this can be provided by the waste heat of the fuel cell, if a good strategy of the energy re-utilization is designed. For a typical system, the total energy required to operate the metal hydride storage system is therefore about 15 MJ/kg, or about 12.5 % of LHV [22]. This is the lowest operating energy compared to those of compressed hydrogen and liquid hydrogen. Therefore, metal hydride for hydrogen storage has the advantage of low operating energy, moderate pressure and temperature and high volumetric density.

In this context, a mathematical model, which rigorously accounts for the principles of mass, momentum and energy conservation, and adsorption and desorption kinetics, is developed to simulate the hydrogen desorption process in a metal hydride tank. The effects of metal properties as well as structural and working conditions are analyzed, through extensive parametric studies.

In addition, an experimental setup using commercially available metal hydride bottles is designed, assembled and a data acquisition system using a NI myRIO device is programmed on LabVIEW, in order to obtain the required experimental data to be compared with the numerical model.

As explained before, what happens inside the bottle is simulated, and determines what can be measured in the proposed experimental system.

During natural convection, pressure follows an exponential relaxation, similar to the ones obtained in the discharge of pressurized tanks, and as said, pressure inside the tank is higher than the one being measured because of pressure losses. If a heater is connected, the shape of the curve changes slightly. At the beginning it follows an exponential relaxation until it reaches a pressure plateau, as the reaction is enhanced and the released hydrogen molecules inside the bottle increase the internal pressure. Then, pressure progressively decreases as there is less hydrogen inside the bottle, until it reaches atmospheric conditions.

Regarding mass flow, in the numerical model the desorbed mass flow can be monitored, whilst in the experimental measurements only the exiting mass flow is acquired. These two mass flows are not the same, and obviously the exiting mass flow will depend on the desorbed mass flow, but not the other way around. Connecting a heater, both mass flows increase, as the desorption reaction is more effective and more hydrogen is able to leave the canister.

Regarding temperature, it is difficult to compare simulation and experimental results, as the thermocouples are placed at the surface of the bottle, being very sensitive to ambient conditions or the heater temperature.

All in all, the simulation results show the same tendencies in comparison with experimental data, and so it is demonstrated that the model successfully captures the essential trends that occur in the system.

The results and observations of this Master's Thesis as well as the numerical model can be used for the characterization of a metal hydride storage system. Therefore, an effective design of the storage system can be implemented, maximizing the mass flow for a certain application. Besides that, the simulations and experimental data can also be used as a tool for selecting metal hydride materials and also for monitoring the current status of the bottle and the supervision of its performance, evaluating aspects such as degradation of the metal hydride material due to fatigue or wear, or reduction of the hydrogen absorption capacity of the metal due to contamination (for example presence of air and water vapor).

As future works, it would be highly suggested to test the numerical model developed with a known metal hydride material, and also have information on the internal structure, support systems and morphology, to reproduce exactly the experimental system. Another important point would be to perform the discharge experimental tests starting with adsorption/desorption equilibrium in the bottle, as this fact (among others) generated calibration problems. It would be even better if the sensors could be placed inside of the bottle, but, as commercially available bottles were used, this was not possible.

It would also be very interesting to use the model to perform an optimization problem and obtain the optimal metal hydride for a given application. Moreover, as the model is able to reproduce adsorption and desorption phenomena, a good idea would be to try to model cyclic charge and discharge processes, as it is likely that a real application would use a hydrogen storage system cyclically.

Finally, use the acquired knowledge and data to develop a metal hydride state of charge estimator.

References

[1] "NTP 385: Fugas en recipientes: emisión en fase gaseosa (1995)," Instituto Nacional de Seguridad e Higiene en el Trabajo, Tech. Rep., 1995, http://www.insht.es/InshtWeb/Contenidos/Documentacion/FichasTecnicas/NTP/Ficheros/301a400/ntp_385.pdf.

[2] "ISO 6358-1:2013. Pneumatic fluid power – Determination of flow-rate characteristics of components using compressible fluids - Part 1: General rules and test methods for steady-state flow," International Organization for Standardization," Standard, May 2013.

[3] O. Akanji and A. Kolesnikov, "Modeling of hydrogen absorption/desorption in a metal hydride bed reactor - a theoretical study," *InTech*, 2013.

[4] F. Askri, A. Jemni, and S. B. Nasrallah, "Study of two-dimensional and dynamic heat and mass transfer in a metal-hydrogen reactor," *International Journal of Hydrogen Energy*, vol. 28, pp. 537–557, 2003.

[5] M. Auset and A. A. Keller, "Pore-scale processes that control dispersion of colloids in saturated porous media," *Water Resources Research*, vol. 40, 2004.

[6] F. Barbir, *PEM Fuel Cells. Theory and practice.* Elsevier Inc, 2005.

[7] H. Ben-Maad, F. Askri, and S. Ben-Nasrallah, "Numerical investigation of heat and mass transfer during the desorption process of an Mg2Ni-H2 reactor," *International Journal of Hydrogen Energy*, vol. 38, pp. 4597–4610, 2013.

[8] H. BenMaad, F. Askri, and S. BenNasrallah, "Numerical simulation of absorption-desorption cyclic processes for metal-hydrogen reactor with heat recovery using phase-change material," *Applied Thermal Engineering*, vol. 96, pp. 267–276, 2015.

[9] R. Busqué, "Metal hydride state of charge estimator. Development and experimental validation of the hydrogen storage system model," Bachelor's Thesis, EUETIB, Universitat Politècnica de Catalunya, Barcelona, 2015.

[10] C. A. Chung and C.-J. Ho, "Thermal-fluid behavior of the hydriding and dehydriding processes in a metal hydride hydrogen storage canister," *International Journal of Hydrogen Energy*, vol. 34, pp. 4351–4356, 2009.

[11] COMSOL Multiphysics, "COMSOL Multiphysics Version 4.3a Documentation, Subsurface Fluid Flow Module," pp. 1–16, 2012.

[12] A. A. R. Darzi, H. H. Afrouzi, A. Moshfegh, and M. Farhadi, "Absorption and desorption of hydrogen in long metal hydride tank equipped with phase change material jacket," *International Journal of Hydrogen Energy*, vol. 41, pp. 9595–9610, 2016.

[13] S. de las Heras, *Mecánica de fluidos en ingeniería*. Iniciativa Digital Politècnica, 2012.

[14] R. V. Denys, A. B. Riabov, V. A. Yartys, M. Sato, and R. G. Delaplane, "Mg substitution effect on the hydrogenation behavior, thermodynamic and structural properties of the La2Ni7-H(D)2 system," *Journal of Solid State Chemistry*, vol. 181, pp. 812–821, 2008.

[15] R. V. Denys and V. A. Yartys, "Effect of magnesium on the crystal structure and thermodynamics of the $La_{3-x}Mg_xNi_9$ hydrides," *Journal of Alloys and Compounds*, vol. 509, pp. 540–548, 2011.

[16] R. Derwent, P. Simmonds, S. O'Doherty, A. Manning, W. Collins, and D. Stevenson, "Global environmental impacts of the hydrogen economy," *International Journal of Nuclear Hydrogen Production and Application*, vol. 1, pp. 57–67, 2006.

[17] H. Dhaou, F. Askri, M. B. Salaha, A. Jemni, S. B. Nasrallah, and J. Lamloumi, "Measurement and modelling of kinetics of hydrogen sorption by $LaNi_5$ and two related pseudobinary compounds," *International Journal of Hydrogen Energy*, vol. 32, pp. 576–587, 2007.

[18] M. Dornheim, "Thermodynamics of metal hydrides: Tailoring reaction enthalpies of hydrogen storage materials," *Thermodynamics - Interaction Studies - Solids, Liquids and Gases*, pp. 891–918, 2011.

[19] E. R. G. Eckert and J. R. M. Drake, *Analysis of heat and mass transfer*. McGraw-Hill, 1972.

[20] Florida Solar Energy Center (FSEC), "Metal Hydride Storage," http://www.fsec.ucf.edu/en/consumer/hydrogen/basics/documents/task2_solid_h2.pdf.

[21] M. R. Gopal and S. S. Murthy, "Experiments on a metal hydride cooling system working with $ZrMnFe/MmNi_{4.5}Al_{0.5}$ pair," *International Journal of Refrigeration*, vol. 22, pp. 137–149, 1999.

[22] L. K. Heung, "Using Metal Hydride to Store Hydrogen," *U.S. Department of Energy*, 2003.

[23] K. Jiao, X. Li, Y. Yin, Y. Zhou, S. Yu, and Q. Du, "Effects of various operating conditions on the hydrogen absorption processes in a metal hydride tank," *Applied Energy*, vol. 94, pp. 257–269, 2012.

[24] E. A. Kumar, M. P. Maiya, and S. S. Murthy, "Influence of transient operating conditions on pressure-concentration isotherms and storage characteristics of hydriding alloys," *International Journal of Hydrogen Energy*, vol. 32, pp. 2382–2389, 2007.

[25] S. Kyoung, S. Ferekh, G. Gwak, A. Jo, and H. Ju, "Three-dimensional modeling and simulation of hydrogen desorption in metal hydride hydrogen storage vessels," *International Journal of Hydrogen Energy*, vol. 40, pp. 14 322–14 330, 2015.

[26] S. S. Mohammadshahi, E. M. Gray, and C. J. Webb, "A review of mathematical modeling of metal-hydride systems for hydrogen storage applications," *International Journal of Hydrogen Energy*, vol. 41(5), pp. 3470–3484, 2016.

[27] P. Muthukumar, A. Singhal, and G. K. Bansal, "Thermal modeling and performance analysis of industrial-scale metal hydride based hydrogen storage container," *International Journal of Hydrogen Energy*, vol. 37(19), pp. 14 351–14 364, 2012.

[28] J. Nam, J. Ko, and H. Ju, "Three-dimensional modeling and simulation of hydrogen absorption in metal hydride hydrogen storage vessels," *Applied Energy*, vol. 89(1), pp. 164–175, 2012.

[29] M. Odysseos, P. De Rango, C. N. Christodoulou, E. Hlil, T. K. Steriotis, G. Karagiorgis, G. Charalambopoulou, T. Papapanagiotou, A. Ampoumogli, V. Psycharis, E. Koultoukis, D. Fruchart, and A. Stubos, "The effect of compositional changes on the structural and hydrogen storage properties of $(La{-}Ce)Ni_5$ type intermetallics towards compounds suitable for metal hydride hydrogen compression," *Journal of Alloys and Compounds*, vol. 580, pp. 268–270, 2013.

[30] R. O'Hayre, S. W. Cha, W. Colella, and F. B. Prinz, *Fuel cell fundamentals*. John Wiley & Sons, 2016.

[31] S. Patil and M. R. Gopal, "Analysis of a metal hydride reactor for hydrogen storage," *International Journal of Hydrogen Energy*, vol. 38, pp. 942–951, 2013.

[32] W. M. Rohsenow, J. P. Hartnett, and Y. I. Cho, *Handbook of Heat Transfer*. McGraw-Hill, 1998.

[33] N. A. A. Rusman and M. Dahari, "A review on the current progress of metal hydrides material for solid-state hydrogen storage applications," *International Journal of Hydrogen Energy*, vol. 41, pp. 12 108–12 126, 2016.

[34] B. Sakintuna, F. Lamari-Darkrim, and M. Hirscher, "Metal hydride materials for solid hydrogen storage: A review," *International Journal of Hydrogen Energy*, vol. 32, pp. 1121–1140, 2007.

[35] G. Sandrock, "Panoramic overview of hydrogen storage alloys from a gas reaction point of view," *Journal of Alloys and Compounds*, vol. 293, pp. 877–888, 1999.

[36] O. Z. Sharaf and M. F. Orhan, "An overview of fuel cell technology: Fundamentals and applications," *Renewable Sustainable Energy Reviews*, vol. 32, pp. 810–853, 2014.

[37] K. Song and H. Knickle, "Study of hydrogen release from metal hydride bed," *Excerpt from the Proceedings of the COMSOL Conference 2009 Boston*, 2009.

[38] G. A. Truskey, F. Yuan, and D. F. Katz, *Transport Phenomena in Biological Systems*. Pearson Prentice Hall, 2004.

[39] I. Tunón, "Fenómenos de superfície," http://www.uv.es/tunon/QFIII/tema_5.pdf.

[40] Universidad Nacional Autónoma de Mexico (UNAM), "Fenómenos de superfície. Adsorción," http://depa.fquim.unam.mx/amyd/archivero/Unidad3Adsorcion_19664.pdf.

[41] Uniwersytet Marii Curie-Skłodowskiej (UMCS), Lublin, "Adsorption at the solid/gas interface."

[42] M. Valizadeh, M. A. Delavar, and M. Farhadi, "Numerical simulation of heat and mass transfer during hydrogen desorption in metal hydride storage tank by lattice boltzmann method," *International Journal of Hydrogen Energy*, vol. 41, pp. 413–424, 2016.

[43] B. van Ruijven, J.-F. Lamarque, D. P. van Vuuren, T. Kram, and H. Eerens, "Emission scenarios for global hydrogen economy and the consequences for global air pollution," *Global Environmental Change*, vol. 21, pp. 983–994, 2011.

[44] F. M. White, *Fluid Mechanics*. McGraw-Hill, 1998.

[45] C. Wulf and M. Kaltschmitt, "Environmental impacts of hydrogen use in vehicles," *Compendium of Hydrogen Energy*, vol. 4, pp. 337–358, 2015.

[46] H. Yoo, J. Ko, S. hun Yun, M. ho Chang, H. goo Kang, W. Kim, and H. Ju, "A numerical investigation of hydrogen desorption phenomena in ZrCo based hydrogen storage beds," *International Journal of Hydrogen Energy*, vol. 38, pp. 6226–6233, 2013.

Master's Thesis

Màster en Enginyeria de l'Energia

Numerical modeling and experimental analysis of the desorption process in a metal hydride hydrogen storage system

APPENDICES

Author: Raquel Busqué Somacarrera
Directors: Attila Husar, Ricardo Torres Cámara

Call: June 2017

Escola Tècnica Superior
d'Enginyeria Industrial de Barcelona

CONTENTS

Appendix A

Detailed list of elements

The main components of the system are two metal hydride hydrogen storage bottles. The container has the following characteristics:

Description/Specifications

- Stainless Steel Container (Swagelok)
- 304L-HDF4-500-PD
- 1.19 kg
- 0.475 L
- $V_{int} = 500cm^3 \pm 5\%$

A detailed list introducing each element is shown below:

Num.	Code	PRESSURE SENSOR	Description/Specifications
1	P1		• Industrial Pressure Transmitter (Impress. Sensors and systems) • IMP-G4002-7A4-BCV-00-000 • Pressure range: 0-40 bar • Accuracy: ± 0.25% FS

Num.	Code	MASS FLOW CONTROLLER	Description/Specifications
1	MFC		• EL-FLOW base Mass flow controller (Bronkhorst High Tech) • F-201C-AAA-22V • Range: 0-1.5 nlpm H_2 • Analog output: 0-5V dc

Num.	Code	THERMOCOUPLES	Description/Specifications
8	T-1, T-2, T-3, T-4, T-5, T-6, T-7, T-8		• Welded Tip PFA Thermocouple (tc direct) • 401-301 • Temperature range: $-75°C$ to $+250°C$

Num.	Code	PARTICLE FILTER	Description/Specifications
1	Filter		• Stainless Steel In-Line Particulate Filter (Swagelok) • SS-4F-7 • 7 micron pore size • 1/4” connection

Num.	Code	CHECK VALVE	Description/Specifications
1	Check-valve		• Stainless Steel Poppet Check Valve (Swagelok) • SS-4C-1/3 • 0.03 bar • 1/4” connection

Num.	Code	QUICK-CONNECTS	Description/Specifications
2	q1, q2		• Stainless Steel Quick-connects (Swagelok) • SS-QC4-B-4PM • 1/4” male NPT

Num.	Code	BOTTLE FLOW VALVE	Description/Specifications
2	V1, V2		• Nonrotating-Stem Needle valves (Swagelok) • SS-16DPM-F4-BC-PD • Inlet: 1/4” male NPT • Outlet: 1/4” female NPT

Num.	Code	2-WAY FLOW VALVE	Description/Specifications
2	V3, V5		• Stainless Steel Ball valve (Swagelok) • SS-42S4 and SS-42S4-SC11 • 1/4” connection

Num.	Code	3-WAY FLOW VALVE	Description/Specifications
2	V4, V6		• Stainless Steel 3 way Ball valve (Swagelok) • SS-42GXS4 and SS-42XS4 • 1/4” connection

Num.	Code	STAINLESS STEEL UNION TEE	Description/Specifications
2	f1, f3		• Stainless Steel Union Tee (Swagelok) • SS-400-3 • 1/4” tube fitting

Num.	Code	STAINLESS STEEL UNION CROSS	Description/Specifications
1	f2		• Stainless Steel Union Cross (Swagelok) • SS-400-4 • 1/4” tube fitting

Num.	Code	STAINLESS STEEL STRAIGHT UNION	Description/Specifications
2	s1, s2		• Stainless Steel Straight Union (Swagelok) • SS-400-7-2 • 1/4” Tube OD x 1/4” Female NPT

Appendix B

Experimental connection diagram

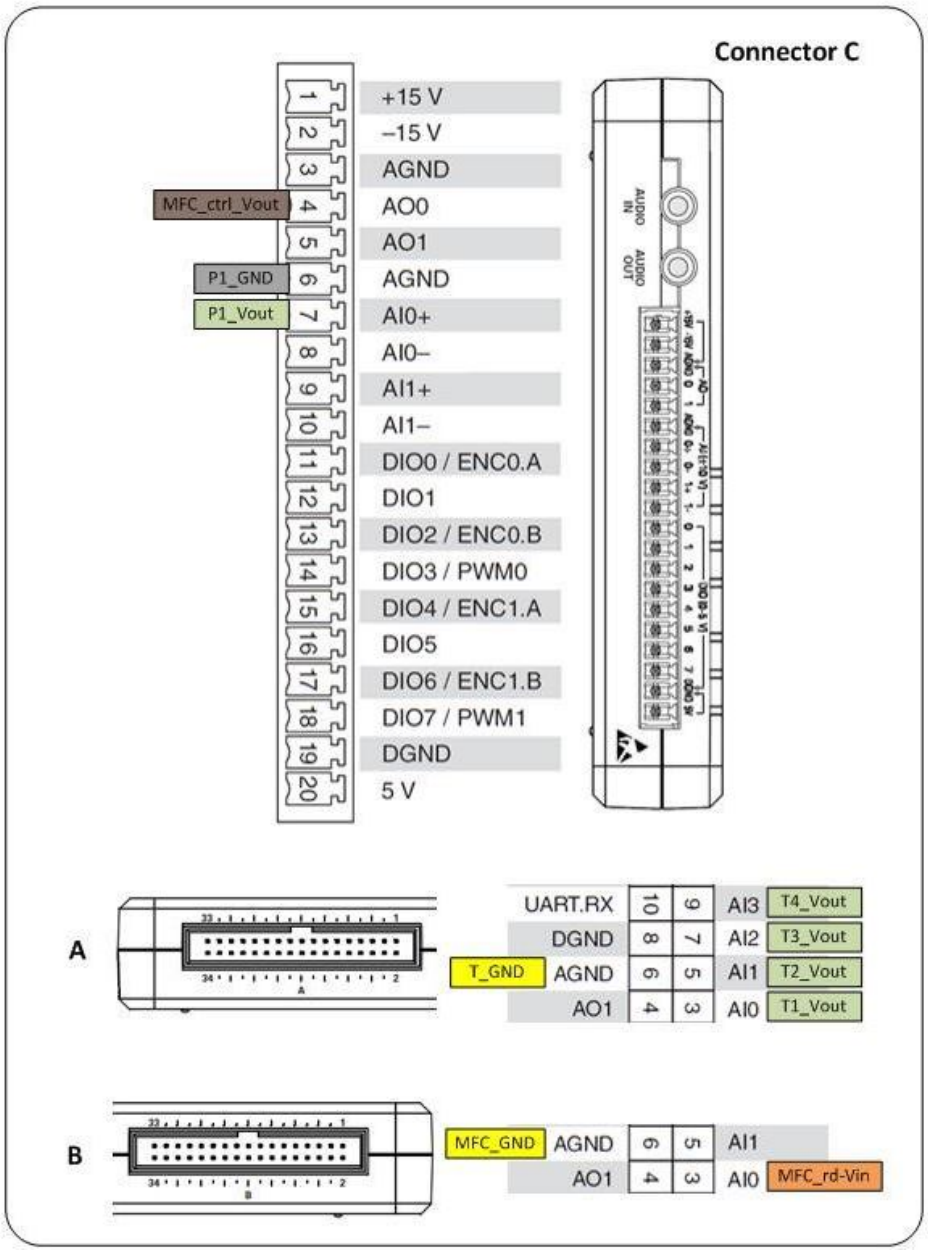

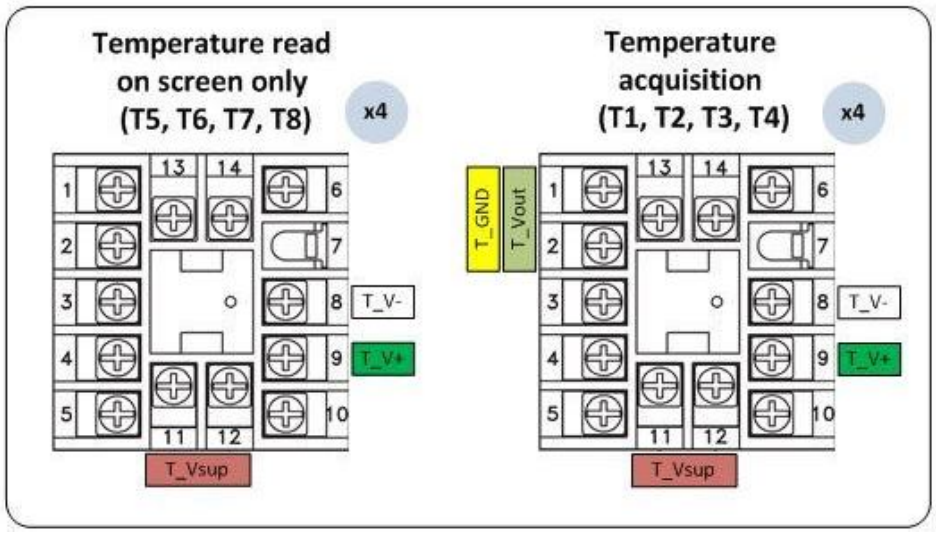
Temperature read on screen only (T5, T6, T7, T8)
x4
Temperature acquisition (T1, T2, T3, T4)
x4
T_GND
T_Vout
T_V-
T_V+
T_Vsup

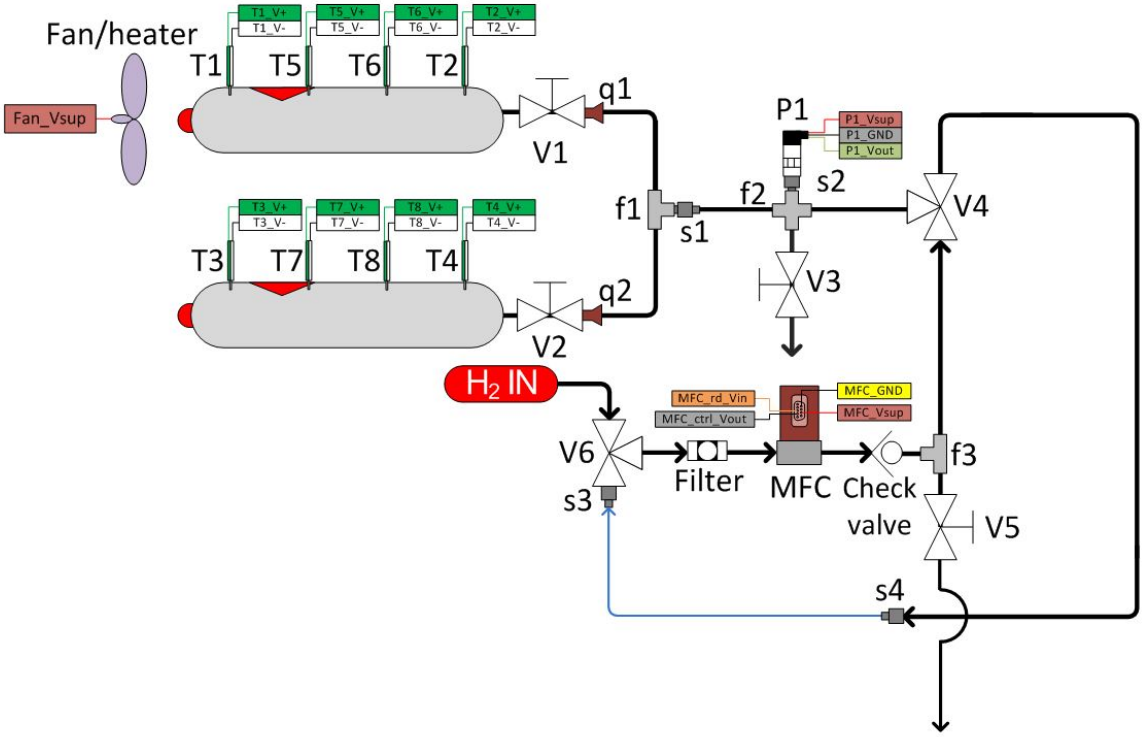
Fan/heater
Fan_Vsup
T1
T5
T6
T2
T3
T7
T8
T4
q1
q2
V1
V2
f1
s1
P1
P1_Vsup
P1_GND
P1_Vout
f2
s2
V3
V4
H2 IN
V6
s3
MFC_rd_Vin
MFC_ctrl_Vout
MFC_GND
MFC_Vsup
Filter
MFC
Check valve
f3
V5
s4

Appendix C

LabVIEW program

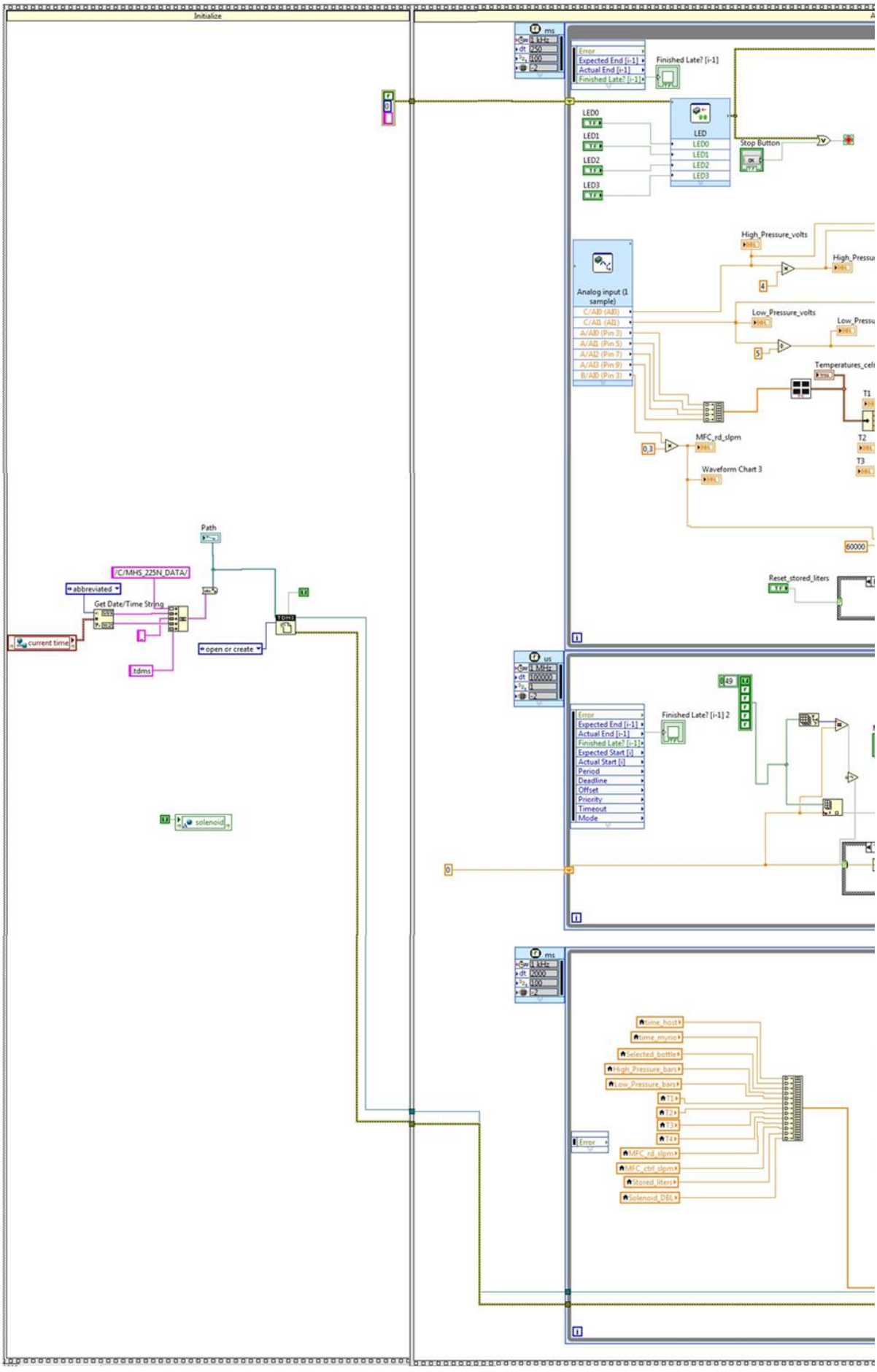
Initialize
ms
Error
Expected End [i-1]
Actual End [i-1]
Finished Late? [i-1]
LED0
LED1
LED2
LED3
LED
Stop Button
High_Pressure_volts
Analog input (1 sample)
C/AI0 (AI0)
C/AI1 (AI1)
A/AI0 (Pin 3)
A/AI1 (Pin 5)
A/AI2 (Pin 7)
A/AI3 (Pin 9)
B/AI0 (Pin 3)
Low_Pressure_volts
Temperatures_celsius
T1
T2
T3
MFC_rd_slpm
Waveform Chart 3
Reset_stored_liters
Path
/C/MHS_225N_DATA/
abbreviated
Get Date/Time String
current time
tdms
open or create
solenoid
us
Finished Late? [i-1] 2
Expected Start [i]
Actual Start [i]
Period
Deadline
Offset
Priority
Timeout
Mode
time_host
time_mytio
Selected_bottle
High_Pressure_bars
Low_Pressure_bars
T4
MFC_ctrl_slpm
Stored_liters
Solenoid_DBL

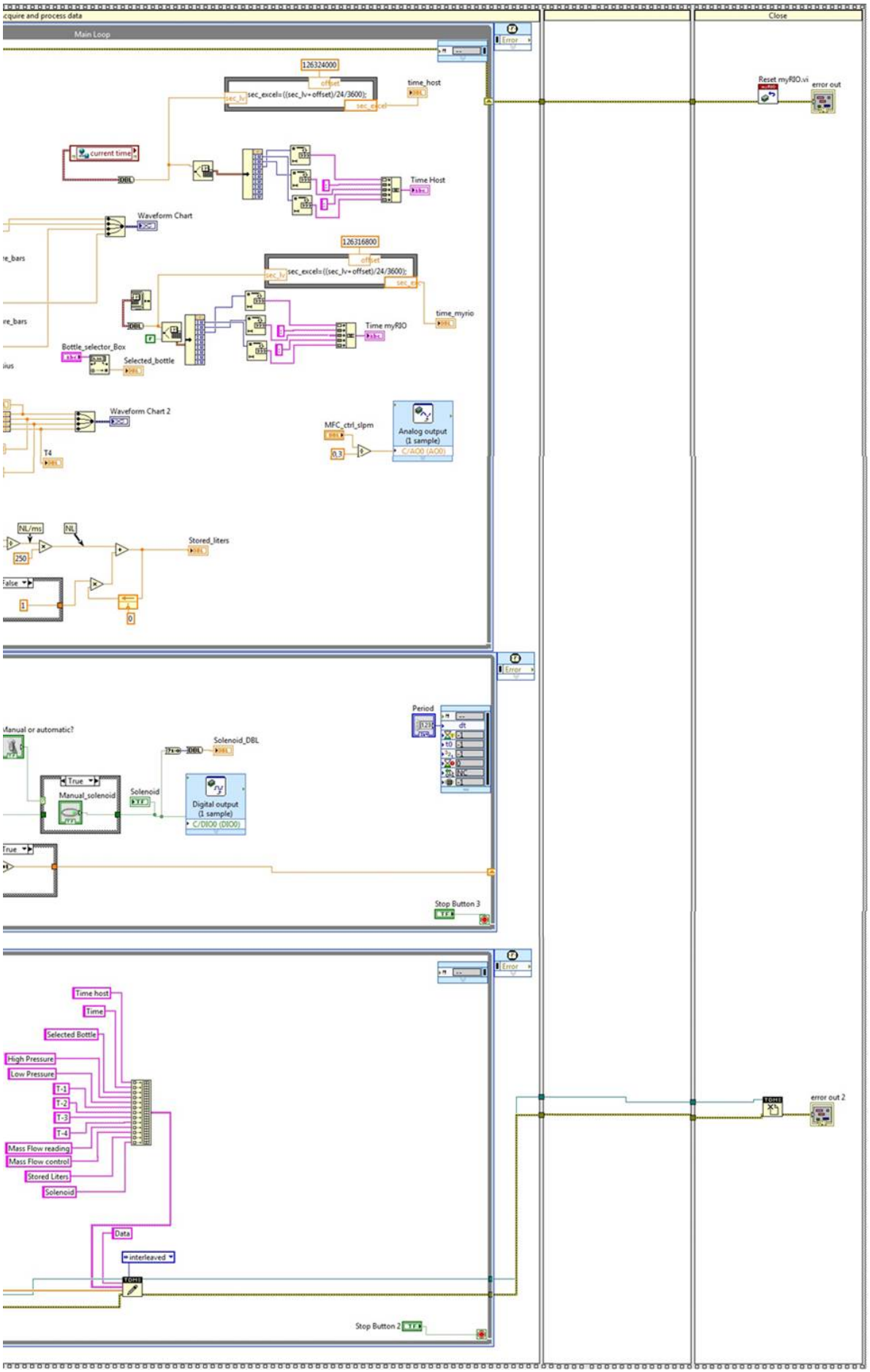
cquire and process data
Main Loop
Close
126324000
offset
sec_excel=((sec_lv+offset)/24/3600);
time_host
current time
Time Host
Waveform Chart
126316800
time_myrio
Time myR3O
Bottle_selector_Box
Selected_bottle
Waveform Chart 2
T4
MFC_ctrl_slpm
Analog output
(1 sample)
C/AO0 (AO0)
NL/ms
NL
250
Stored_liters
Reset myR3O.vi
error out
Error
Period
dt
Manual or automatic?
Solenoid_DBL
True
Manual_solenoid
Solenoid
Digital output
(1 sample)
C/DIO0 (DIO0)
Stop Button 3
Time host
Time
Selected Bottle
High Pressure
Low Pressure
T-1
T-2
T-3
T-4
Mass Flow reading
Mass Flow control
Stored Liters
Solenoid
Data
interleaved
error out 2
Stop Button 2

Appendix D

Complementary calculations and extra results

D.1 Volume, mass and density calculation

Volume

The data sheet of the containers indicates the internal volume of the empty bottle (without metal), which is 500 cm^3. As the internal distribution, morphology and amount of metal hydride inside the bottle is unknown, different percentages of the total metal volume have been calculated.

% Metal	% H2	$\mathbf{V_{metal}(m^3)}$	$\mathbf{V_{H_2}(m^3)}$
95	5	4.75E-4	2.50E-5
90	10	4.50E-5	5.00E-5
85	15	4.25E-5	7.50E-5
80	20	4.00E-5	1.00E-4
75	25	3.75E-5	1.25E-4

Table D.1: Metal and hydrogen volume at different metal percentages

Mass

To estimate the mass of the metal, the hydrogen-empty bottle has been weighted, and the weight of the bottle itself and other fitting elements have been subtracted.

$$\begin{aligned} m_{bottle+metal} &= 2.925kg \\ m_{bottle} &= 1.2kg \\ m_{valve} &= 0.08kg \\ m_{quick-connect} &= 0.074kg \\ m_{union} &= 0.048kg \end{aligned}$$

The mass of the metal is:

$$m_{metal} = 1.523kg$$

Free hydrogen gas at the beginning of the discharge experiments can be estimated applying ideal gas law:

$$m_{H2_{gas}} = \frac{p_{ini} V_{H2} M_{H2}}{R T_{ini}}$$

So, for each of the experiments and metal percentages, hydrogen in gaseous state mass is the following:

Experiment	p_{ini} (bar)	T_{ini} (K)	% H2	H2 gas mass (kg)
14/12/2016	3	301	5	7.99E-6
14/12/2016	3	301	10	1.60E-5
14/12/2016	3	301	15	2.40E-5
14/12/2016	3	301	20	3.20E-5
14/12/2016	3	301	25	4.00E-5
15/12/2016	5	301	5	1.20E-5
15/12/2016	5	301	10	2.40E-5
15/12/2016	5	301	15	3.60E-5
15/12/2016	5	301	20	4.80E-5
15/12/2016	5	301	25	5.99E-5
19/12/2016	3	296	5	8.21E-6
19/12/2016	3	296	10	1.64E-5
19/12/2016	3	296	15	2.46E-5
19/12/2016	3	296	20	3.28E-5
19/12/2016	3	296	25	4.11E-5
21/12/2016	3	296	5	8.13E-6
21/12/2016	3	296	10	1.63E-5
21/12/2016	3	296	15	2.44E-5
21/12/2016	3	296	20	3.25E-5
21/12/2016	3	296	25	4.06E-5

Table D.2: Initial hydrogen in gaseous state mass

The total amount of hydrogen inside the bottle at the beginning was measured in normal liters. In the following table these values have been transformed into kilograms.

Experiment	Bottle	H2 measurement (nl)	m_{H2} (kg)
14/12/2016	B1	77	6.32E-3
15/12/2016	B2	138	1.13E-2
19/12/2016	B1	118	9.69E-3
21/12/2016	B2	78	6.40E-3

Table D.3: Initial total hydrogen mass

Knowing the total hydrogen mass and also the part that is in gaseous state, it is easy to calculate the amount of hydrogen adsorbed in the metal.

$$m_{H2-m} = m_{H2} - m_{H2_{gas}}$$

Experiment	% H2	Adsorbed H2 (kg)
14/12/2016	5	6.31E-3
14/12/2016	10	6.31E-3
14/12/2016	15	6.30E-3
14/12/2016	20	6.29E-3
14/12/2016	25	6.28E-3
15/12/2016	5	1.13E-2
15/12/2016	10	1.13E-2
15/12/2016	15	1.13E-2
15/12/2016	20	1.13E-2
15/12/2016	25	1.13E-2
19/12/2016	5	9.68E-3
19/12/2016	10	9.6E-3
19/12/2016	15	9.66E-3
19/12/2016	20	9.66E-3
19/12/2016	25	9.65E-3
21/12/2016	5	6.40E-3
21/12/2016	10	6.39E-3
21/12/2016	15	6.38E-3
21/12/2016	20	6.37E-3
21/12/2016	25	6.36E-3

Table D.4: Initial adsorbed hydrogen

Density

Assuming an hydrogen-empty density of the metal of ρ^m_{emp}=5300 kg/m^3, the initial density of the metal hydride can be calculated as follows, and displayed in table D.5.

$$\rho^m_{ini} = \frac{\rho^m_{emp} V_{metal} + m_{H2-m}}{V_{metal}}$$

The same method has been used to obtain the saturation metal hydride density for both bottles. For Bottle 1 it has been considered a maximum storage capacity of 200 nl of hydrogen, as it was the maximum amount of hydrogen that we were able to store. The storage final pressure (when the system was stabilized) was 10 bars at ambient temperature. With this conditions ρ^m_{sat}=5340.49 kg/m^3. For Bottle 2, the maximum amount was 167 nl, at a pressure of 5.7 bar, so ρ^m_{sat}=5328.70 kg/m^3

Experiment	% H2	Initial metal hydride density (kg/m^3)
14/12/2016	5	5313.29
14/12/2016	10	5314.01
14/12/2016	15	5314.82
14/12/2016	20	5315.72
14/12/2016	25	5316.75
15/12/2016	5	5323.83
15/12/2016	10	5325.12
15/12/2016	15	5326.57
15/12/2016	20	5328.21
15/12/2016	25	5330.05
19/12/2016	5	5320.38
19/12/2016	10	5321.49
19/12/2016	15	5322.74
19/12/2016	20	5324.14
19/12/2016	25	5323.73
21/12/2016	5	5313.46
21/12/2016	10	5314.19
21/12/2016	15	5315.01
21/12/2016	20	5315.93
21/12/2016	25	5316.97

Table D.5: Initial metal hydride density

D.2 Convection heat transfer coefficient calculation

A first estimation of the convection heat transfer coefficient can be done using correlations collected in *Handbook of Heat Transfer* from McGraw-Hill [32], and considering a horizontal cylinder (D= 50.8 mm) exposed to convection. It is necessary to take into account that there are two different cases: natural convection and forced convection using a heater.

First step is to calculate the air properties at the mean temperature between the wall and exterior air. For the case with natural convection is has been estimated a mean temperature of 294 K, and for the heater case 318 K.

Thermophysical properties are calculated using the expressions from *Analysis of Heat and Mass Transfer* by Eckert and Drake [19], and are shown in table D.6.

Property	Natural conv.	Forced conv.
Density (ρ_{air}) [kgm^{-3}]	1.1851	1.0957
Thermal conductivity (k_{air}) [$Wm^{-1}K^{-1}$]	0.0258	0.0277
Specific heat at constant pressure (cp_{air}) [$Jkg^{-1}K^{-1}$]	1006.069	1007.656
Dynamic viscosity (μ_{air}) [$kgm^{-1}s^{-1}$]	1.8175E-5	1.9300E-5
Expansion coefficient (β_{air}) [K^{-1}]	3.401E-3	-

Table D.6: Air properties for the convection heat transfer coefficient

D.2.1 Natural convection

First, it is necessary to know if the air flow is laminar or turbulent, it is quite expected for the flow to be laminar, but let's calculate it.

It is considered laminar flow if $10^4 < Gr * Pr < 10^9$ and turbulent if $Gr * Pr > 10^9$.

Prandlt number is calculated as follows:

$$Pr = \frac{\mu_{air} cp_{air}}{k_{air}} = 0.7087 \tag{D.1}$$

And Grashof number includes $\Delta\theta$ which is the difference between ambient temperature and the temperature of the wall, which has been estimated.

$$Gr = \frac{g\beta_{air}\rho^2\Delta\theta D^3}{\mu^2} = 148802.285 \tag{D.2}$$

So, $Gr * Pr$= 1.05E5, which indicates that the air flow is laminar, and that the needed parameters to calculate the Nusselt number are: C=0.47, n=0.25 and K=1.

$$\bar{Nu} = C(Gr * Pr)^n K = 8.470 \tag{D.3}$$

Knowing the expression for the Nusselt number, the convection heat transfer coefficient can be estimated.

$$\bar{Nu} = \frac{hD}{k_{air}} \tag{D.4}$$

Finally, the convection heat transfer coefficient for natural convection is estimated to be h= 4.3 W $m^{-2}K^{-1}$.

D.2.2 Forced convection

For this case, two different convection coefficients will be considered: one for the lateral walls of the bottle; and another for the bottom part, as the heater directly hits this part before surrounding the bottle.

For both cases, it is necessary to know the velocity of the heating air. The heater data sheet indicates that it has an air mass flow of 340 nl/min. As the outlet section of the heater is known (diameter of 62 mm), the velocity can be estimated to u_{air}= 1.877 m/s.

Then, the Reynolds number can be calculated.

$$Re = \frac{\rho_{air} u_{air} D}{\mu_{air}} = 5413.278 \tag{D.5}$$

Lateral surface

This value of Reynolds number allows obtaining the following parameters to calculate the Nusselt number: C= 0.148 and m= 0.633.

$$\bar{Nu} = CRe^m = 34.162 \tag{D.6}$$

And again, using equation (D.4), the heat transfer coefficient can be estimated to h= 18.6 W $m^{-2}K^{-1}$.

Bottom surface

Using the Reynolds number previously calculated, and the parameters for this type of convection, the values to calculate Nusselt number are: C=0.227 and m=0.731.

$$\bar{Nu} = CRe^m = 121.672 \tag{D.7}$$

So finally: h=66.24 W $m^{-2}K^{-1}$.

D.3 Pressure drop calculation (*grille*)

To estimate a value for the pressure drop in the circuit (*grille*), the experimental data can be used. If the flow is laminar, as the one being studied, pressure losses can be estimated using equation (2.36).

Δp can be estimated calculating the difference between measured pressure and atmospheric pressure. $\dot{V}$ corresponds to the measurement of the mass flow meter. Using all variables in international system, an estimation of the grille coefficient can be done:

$$grille = \frac{\Delta p}{\dot{V}} \tag{D.8}$$

Experiment	**Bottle**	**grille($kgm^{-4}s^{-1}$)**
14/12/2016	B1	8.56E9
15/12/2016	B2	8.66E9
19/12/2016	B1	1.05E10
21/12/2016	B2	4.34E10

Table D.7: Estimation of the *grille* coefficient

D.4 Other results

Experiment: 19/12/2016, Bottle 1

Figure D.1 shows metal hydride density, desorbed hydrogen mass flow and generated heat over time. As expected, metal hydride density decreases from the initial value calculated in section D.1 until it reaches the hydrogen-free metal density, which means that the metal is completely empty of hydrogen.

Regarding desorbed hydrogen mass flow (figure D.1b), it increases at the beginning and while the reaction lasts it tries to remain constant but, as time goes by there is less hydrogen inside the bottle to be desorbed, so the mass flow decreases until it reaches zero, as there is no more hydrogen inside the bottle.

Related with the desorbed hydrogen there is the heat generated, or in this case, as the reaction is endothermic, heat absorbed by the reaction. As expected it has a very similar curve to the desorbed hydrogen mass flow (but opposite), as the absorbed heat will be higher as the reaction is more active and so the desorption mass flow is higher.

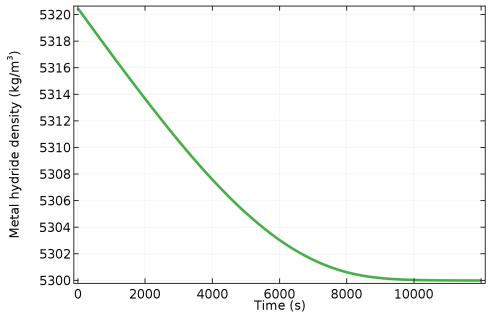

(a) Metal hydride density (kg/m^3)

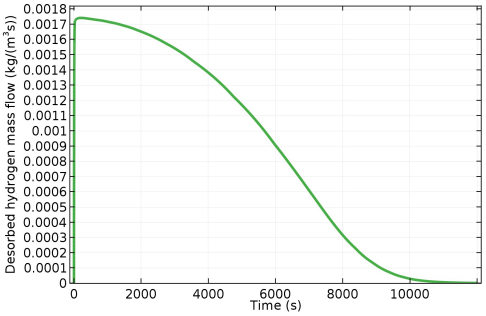

(b) Desorbed hydrogen mass flow (kg/(m^{3}s))

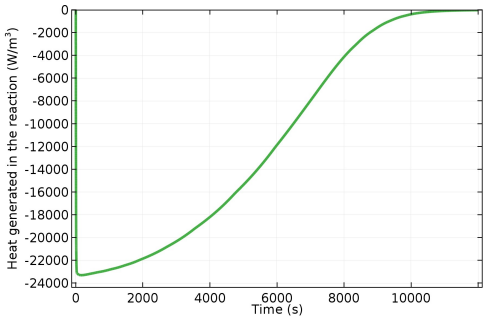

(c) Heat generated in the reaction (W/m^3)

Figure D.1: Metal hydride density, desorbed mass flow and generated heat simulation results (19/12/2016)

Experiment: 21/12/2016, Bottle 2

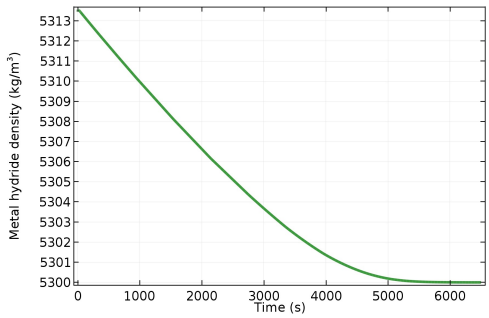

(a) Metal hydride density (kg/m^3))

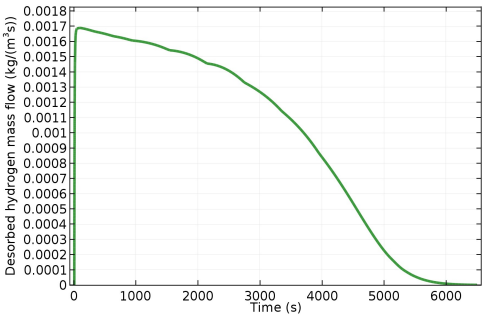

(b) Desorbed hydrogen mass flow (kg/(m^{3}s)

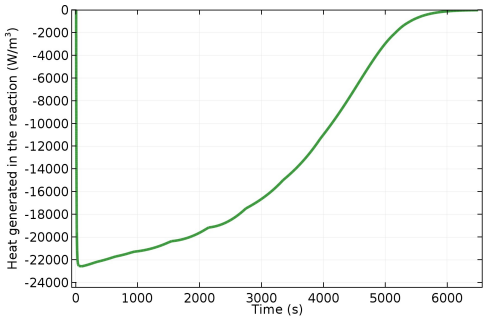

(c) Heat generated in the reaction (W/m^3)

Figure D.2: Metal hydride density, desorbed mass flow and generated heat simulation results (21/12/2016)

Figure D.2b shows the metal hydride density evolution, as in the previous case, it increases at the beginning then it decreases progressively until it reaches zero, as there is no more hydrogen inside the bottle.

Desorbed hydrogen mass flow and generated heat curves are very similar to the previous case ones as well.

Appendix E

COMSOL Multiphysics model

E.1 Global definitions

E.1.1 Global settings and used products

- COMSOL version: COMSOL 5.2
- Used modules:
  - COMSOL Multiphysics
  - Batteries & Fuel Cells Module
  - Heat Transfer Module

E.1.2 Parameters

Name	Description	Expression	Value
K	Permeability	1E-8 [m^2]	1E-8 m^2
mu	Dynamic viscosity of H_2	8.411E-6 [Pa*s]	8.411E-6 Pa s
kg	Thermal conductivity of H_2	0.1672 [W/m/K]	0.1672 W $m^{-1}K^{-1}$
km	Thermal conductivity of the metal	1.04 [W/m/K]	1.04 W $m^{-1}K^{-1}$
k_eff	Effective thermal conductivity	(1-epsilon)*km+epsilon*kg	0.60636 W $m^{-1}K^{-1}$
cpg	Heat capacity of H_2	14.89 [kJ/kg/K]	14890 J $kg^{-1}K^{-1}$
cpm	Heat capacity of the metal	0.419 [kJ/kg/K]	419 J $kg^{-1}K^{-1}$
cp_eff	Effective heat capacity	(1-epsilon)*cpm+epsilon*cpg	7654.5 J $kg^{-1}K^{-1}$
rho_metal_emp	Metal density without H_2	5300 [kg/m^3]	5300 kg m^{-3}
R	Universal gas constant	8.314 [J/mol/K]	8.314 J $mol^{-1}K^{-1}$
M_H2	H_2 molecular weight	2.01588 [kg/kmol]	0.0020159 J kg mol^{-1}
M_metal	Metal molecular weight	432 [kg/kmol]	0.432 J kg mol^{-1}
p_atm	Atmospheric pressure	1 [bar]	1E5 Pa

p_ref	Reference pressure	10 [bar]	1E6 Pa
A	1st equilibrium pressure constant	12.99	12.99
B	2nd equilibrium pressure constant	4284.34 [K]	4284.34 K
Ea	Activation energy for adsorption	21179.6 [J/mol]	21179.6 J mol^{-1}
Ca	Equilibrium pressure pre-exponential factor (adsorption)	59.187 [1/s]	59.187 s^{-1}
delta_H	Reaction enthalpy	35620 [J/mol]	35620 J mol^{-1}

Table E.1: List of default parameters introduced in COMSOL

Name	**Description**	**Expression**	**Value**
epsilon	Porosity	0.5	0.5
rho_metal_sat	Metal density saturated with H_2	5334.1 [kg/m^3]	5334.1 kg m^{-3}
rho_metal_ini	Initial metal density	5313.3 [kg/m^3]	5313.3 kg m^{-3}
T_ref	Reference temperature	24.5 [degC]	297.65 K
T_amb	Ambient temperature	24.5 [degC]	297.69 K
p_ini	Initial pressure	2.8 [bar]	2.8E5 Pa
H_M_sat	Saturated hydrogen to metal ratio	(2*(rho_metal_sat-rho_metal_emp)/M_H2) /(rho_metal_emp/M_metal)	2.7795
Ed	Activation energy for desorption	23879.6 [J/mol]	23880 J mol^{-1}
Cd	Equilibrium pressure pre-exponential factor (desorption)	9.57 [1/s]	9.57 s^{-1}
grille	Fluid flow resistance	3E9 [kg/m^4/s]	3E9 kg $m^{-4}s^{-1}$
Tf	Heating temperature	24.5 [degC]	297.65 K
frac_m	Metal volume fraction	0.95	0.95
hht	Lateral surface convection heat transfer coefficient	10 [W/(m^2K)]	10 W $m^{-2}K^{-1}$
hht1	Bottom surface convection heat transfer coefficient	10 [W/(m^2K)]	10 W $m^{-2}K^{-1}$

Table E.2: List of parameters for 14/12/2016

Name	**Description**	**Expression**	**Value**
epsilon	Porosity	0.55	0.55
rho_metal_sat	Metal density saturated with H_2	5328.7 [kg/m^3]	5328.7 kg m^{-3}
rho_metal_ini	Initial metal density	5323.8 [kg/m^3]	5323.8 kg m^{-3}

T_ref	Reference temperature	24.19 [degC]	297.34 K
T_amb	Ambient temperature	24.19 [degC]	297.34 K
p_ini	Initial pressure	4.8 [bar]	4.8E5 Pa
H_M_sat	Saturated hydrogen to metal ratio	(2*(rho_metal_sat-rho_metal_emp)/M_H2) /(rho_metal_emp/M_metal)	2.3393
Ed	Activation energy for desorption	20000 [J/mol]	20000 J mol^{-1}
Cd	Equilibrium pressure pre-exponential factor (desorption)	5 [1/s]	5 s^{-1}
grille	Fluid flow resistance	4E9 [kg/mˆ4/s]	4E9 kg $m^{-4}s^{-1}$
Tf	Heating temperature	24.19 [degC]	297.34 K
frac_m	Metal volume fraction	0.95	0.95
hht	Lateral surface convection heat transfer coefficient	10 [W/(mˆ2K)]	10 W $m^{-2}K^{-1}$
hht1	Bottom surface convection heat transfer coefficient	10 [W/(mˆ2K)]	10 W $m^{-2}K^{-1}$

Table E.3: List of parameters for 15/12/2016

Name	**Description**	**Expression**	**Value**
epsilon	Porosity	0.5	0.5
rho_metal_sat	Metal density saturated with H_2	5334.1 [kg/mˆ3]	5334.1 kg m^{-3}
rho_metal_ini	Initial metal density	5320.4 [kg/mˆ3]	5320.4 kg m^{-3}
T_ref	Reference temperature	23.24 [degC]	296.39 K
T_amb	Ambient temperature	23.24 [degC]	296.39 K
p_ini	Initial pressure	2.6 [bar]	2.6E5 Pa
H_M_sat	Saturated hydrogen to metal ratio	(2*(rho_metal_sat-rho_metal_emp)/M_H2) /(rho_metal_emp/M_metal)	2.7795
Ed	Activation energy for desorption	23879.6 [J/mol]	23880 J mol^{-1}
Cd	Equilibrium pressure pre-exponential factor (desorption)	9.57 [1/s]	9.57 s^{-1}
grille	Fluid flow resistance	2E10 [kg/mˆ4/s]	2E10 kg $m^{-4}s^{-1}$
Tf	Heating temperature	51 [degC]	324.15 K
frac_m	Metal volume fraction	0.95	0.95
hht	Lateral surface convection heat transfer coefficient	20 [W/(mˆ2K)]	20 W $m^{-2}K^{-1}$
hht1	Bottom surface convection heat transfer coefficient	70 [W/(mˆ2K)]	70 W $m^{-2}K^{-1}$

Table E.4: List of parameters for 19/12/2016

Name	Description	Expression	Value
epsilon	Porosity	0.55	0.55
rho_metal_sat	Metal density saturated with H_2	5328.7 [kg/m^3]	5328.7 kg m^{-3}
rho_metal_ini	Initial metal density	5313.5 [kg/m^3]	5313.5 kg m^{-3}
T_ref	Reference temperature	23.12 [degC]	296.27 K
T_amb	Ambient temperature	23.12 [degC]	296.27 K
p_ini	Initial pressure	2.7 [bar]	2.7E5 Pa
H_M_sat	Saturated hydrogen to metal ratio	(2*(rho_metal_sat-rho_metal_emp)/M_H2) /(rho_metal_emp/M_metal)	2.3393
Ed	Activation energy for desorption	20000 [J/mol]	20000 J mol^{-1}
Cd	Equilibrium pressure pre-exponential factor (desorption)	5 [1/s]	5 s^{-1}
grille	Fluid flow resistance	2.5E10 [kg/m^4/s]	2.5E10 kg $m^{-4}s^{-1}$
Tf	Heating temperature	55 [degC]	328.15 K
frac_m	Metal volume fraction	0.95	0.95
hht	Lateral surface convection heat transfer coefficient	20 [W/(m^2K)]	20 W $m^{-2}K^{-1}$
hht1	Bottom surface convection heat transfer coefficient	70 [W/(m^2K)]	70 W $m^{-2}K^{-1}$

Table E.5: List of parameters for 21/12/2016

E.2 Model

E.2.1 Definitions

E.2.1.1 Variables

Name	Description	Expression	Unit
H_M	Hydrogen to metal ratio	(2*(rho_metal - rho_metal_emp)/M_H2) /(rho_metal_emp/M_metal)	-
Sm_a	Mass source term for adsorption	Ca*exp(-Ea/R/T) *log((p3+p_atm)/peq_a) *(rho_metal_sat-rho_metal)	kg $m^{-3}s^{-1}$
ST_a	Energy source term for adsorption	Sm_a*(delta_H/M_H2-T*(cpg-cpm))	W m^{-3}
Sm_d	Mass source term for desorption	Cd*exp(-Ed/R/T))*(((p3 + p_atm) - peq_d)/peq_d)*(rho_metal - rho_metal_emp)	kg $m^{-3}s^{-1}$
ST_d	Energy source term for desorption	Sm_d*(delta_H/M_H2-T*(cpg-cpm))	W m^{-3}

peq_a	Equilibrium pressure for adsorption	p_ref*exp(A-B/T_ref)	Pa
peq_d	Equilibrium pressure for desorption	peq_a/exp(0.13)	Pa

Table E.6: List of variables introduced in COMSOL

E.2.1.2 Funcions

Step

- Parameters
  - Location: -0.5
  - From: 0, To: 1
- Smoothing: Size of transition zone: 1

E.2.1.3 Geometry

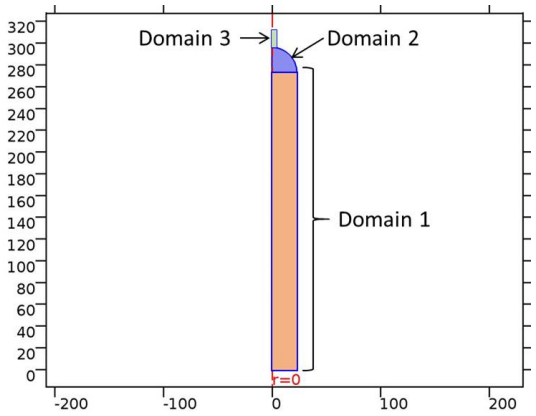

Figure E.1: Geometry domains

E.2.1.4 Materials

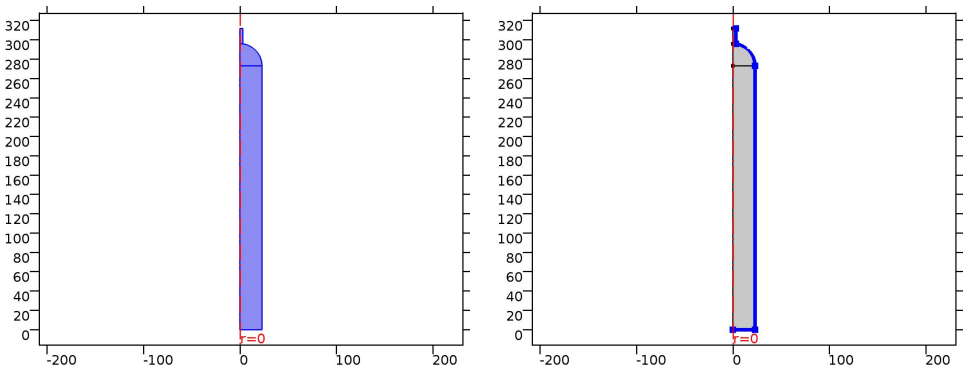

(a) **Hydrogen**: domains 1-3

(b) **304L (UNS S30403) (SUS 304L) [solid,polished]**: boundaries 2,8-10

Figure E.2: Materials implemented in COMSOL

E.2.2 Heat transfer in Fluids

- Module used: COMSOL Multiphysics, Heat Transfer Module
- Domains: 1-3
- Variable: Temperature T [K]
- Domain, boundary and initial conditions:
  - Heat Transfer in Fluids 1: Domains 2-3; fluid type ideal gas
  - Axial symmetry 1: Boundaries 1,3,5
  - Initial Values 1: Domains 1-3; T_ref
  - Heat Flux 1: Boundaries 2, 8-10; convective heat flux (hht, hht1 and T_amb or Tf)
  - Heat source 1: Domain 1; if((p3 + p_atm)<peq_d, ST_d, if((p3 + p_atm)<peq_a, 0, ST_a))
  - Outflow 1: Boundary 7
  - Heat transfer in porous media 1: Domain 1; fluid type ideal
  - Thin Layer: 304L, Thickness 2.4 mm

E.2.3 Laminar Flow

- Modules used: COMSOL Multiphysics, Batteries & Fuel Cells Module, Heat Transfer Module
- Domains: 1-3
- Variable: Pressure p3 [Pa], velocity field u2, v2, w2 [m/s]
- Compressibility: Compressible flow (Ma<0.3)
- Domain, boundary and initial conditions:
  - Fluid properties 1: Domains 2-3
  - Initial Values 1: Domains 1-3; p_ini, velocity field 0
  - Axial symmetry 1: Boundaries 1,3,5
  - Wall 1: Boundaries 2, 8-10; no slip
  - Fluid and Matrix Properties 1: Domain 1
  - Mass Source 1: Domain 1; if((p3 + p_atm)<peq_d, -Sm_d, if((p3 + p_atm)<peq_a, 0, -Sm_a))
  - Grille 1: Boundary 7
    - Flow direction: outlet
    - Exit pressure: p_ini*(1-step(t[1/s]))
    - Static pressure curve: linear loss
    - Linear loss coefficient: grille

E.2.4 Domain ODEs and DAEs

- Module used: COMSOL Multiphysics
- Domain: 1
- Variable: rho_metal [kg/m^3]
- Distributed ODE 1:
  - Source term: if((p3 + p_atm)<peq_d, Sm_d, if((p3 + p_atm)<peq_a, 0, Sm_a))
  - Damping or mass coefficient: (1-epsilon)
  - Mass coefficient: 0
- Initial values 1:
  - Initial value for rho_metal: rho_metal_ini
  - Initial time derivative of rho_metal: 0

E.2.5 Mesh

Explained in section 3.3.

E.3 Study

- **Solver configurations**
  - Absolute tolerance: 5.0E-4
  - Fully coupled:
    - Linear solver: direct
    - Damping factor: 0.9
    - Jacobian update: Once per time step
    - Maximum number of iterations: 6

Appendix F

Empirical state of charge estimator

The experimental data obtained, allows developing an estimator of the state of charge of the bottles, i.e. a way to know the amount of H_2 inside the bottle at any time of the discharge.

The idea is to relate the pressure at the outlet of the bottle with the outlet mass flow rate, and hence the amount of hydrogen discharged.

It is important to mention, that is has been considered that the discharge process has finished when the outlet mass flow is below 0.01 nlpm during at least 20 s.

F.1 Without heater

As detailed in section 5.2, two different experimental tests are performed without using a heater. Focusing on the pressure results (Fig. 5.12), it can be seen that the range of variation of the pressure is different, as the experimental test performed on 15/12/2016 has an initial higher pressure, consequence of the cooled charging process.

For that reason, the results of this experiment are used to find a relationship between pressure and mass flow rate, and the results of the other experiment (14/12/2016) are used to check the obtained estimation.

To obtain a relationship between the studied variables, mass flow rate has been plotted over pressure (Fig. F.1). Then, a polynomial trend-line has been added, to obtain an empirical equation relating pressure and mass flow (Eq. (F.1)).

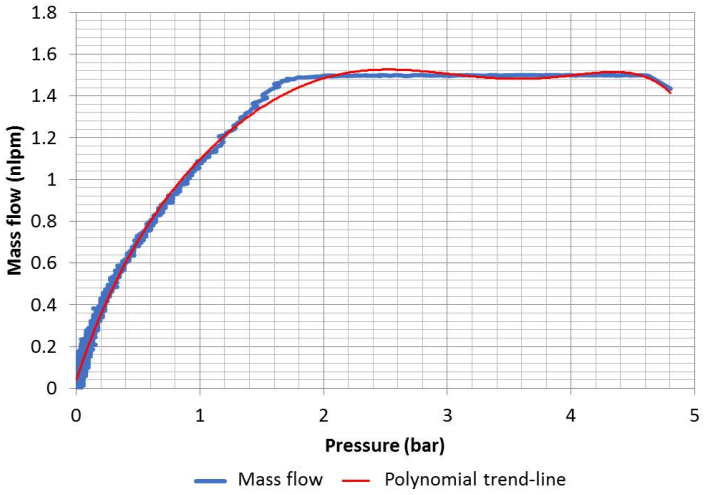

Figure F.1: Experimental mass flow over pressure on exp. 15/12/2016

The relationship between pressure and mass flow is obtained from the following equation:

$$\dot{m}_d = -0.0035p^6 + 0.0478p^5 - 0.2493p^4 + 0.6658p^3 - 1.1963p^2 + 1.7923p + 0.0397 \qquad \text{(F.1)}$$

Knowing the pressure at any time instant, it is possible to calculate the mass flow with the proposed equation. Also knowing the time step used to acquire pressure (in this case $\Delta t = 2$ s) it is possible to calculate the amount of H_2 exiting the bottle.

To check the validity of the proposed empirical equation, the experimental results obtained in test 14/12/2016 have been used. Fig. F.2, shows the experimental mass flow rate compared with the one obtained by the empirical estimation in equation (F.1).

As can be seen, the experimental and empirical results match perfectly. It has to be taken into account that the empirical estimation was obtained using experimental test 15/12/2016 which differs from 14/12/2016 in the way the bottle was charged. That being said, it can be demonstrated that the empirical estimation is able to reproduce the experimental results regardless of the way the bottle was charged.

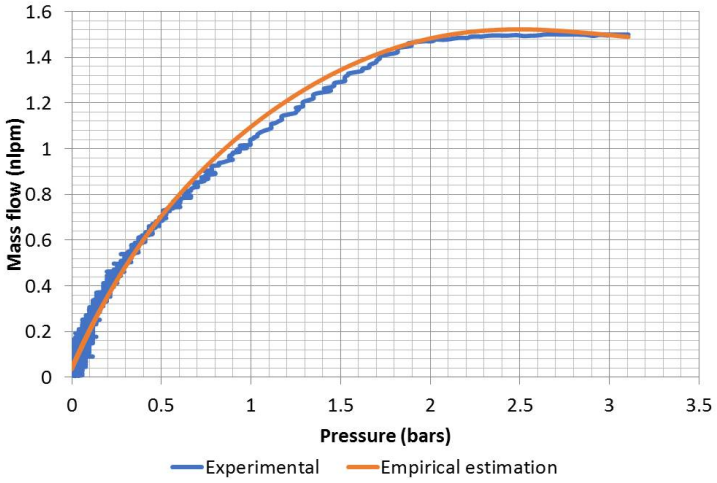

Figure F.2: Exp. and empirical estimation of mass flow and over pressure on exp. 14/12/2016

The idea of a state of charge estimator is to obtain the amount of hydrogen inside the bottle at a certain instant. The procedure would be the following:

1. With a manometer connected at the outlet measure the pressure.
2. Use equation (F.1) to obtain the mass flow.
3. Knowing the time step between measurements (in this case $\Delta t = 2$ s) calculate the desorbed hydrogen:
$$m_d = \dot{m}\Delta t$$
4. Knowing the initial amount of hydrogen in the bottle, the amount of hydrogen left can be calculated as well.

Using pressure measurements from experiment 14/12/2016, the amount of hydrogen discharged can be estimated and compared with experimental measurements (Fig. F.3). As shown in this figure, the measured amount of discharged hydrogen and the estimated one are almost the same. The measured amount of hydrogen discharged is 71.6 nl, and the estimated one is 68.3 nl.

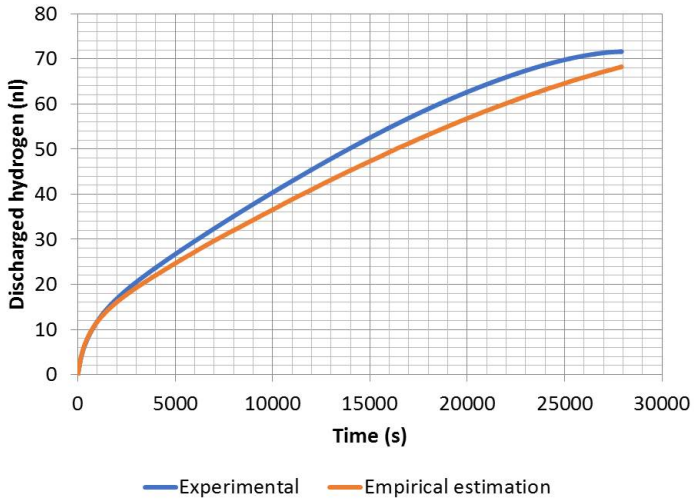

Figure F.3: Experimental and empirical estimation of discharged hydrogen without heater

F.2 With heater

For the experiments performed with the help of a heater, the procedure to obtain an empirical estimation is the same, using 21/12/2016 (from 5.2) as a base to obtain the equation.

Fig. F.4, shows mass flow over pressure, as well as the added trend-line. The relationship between pressure and mass flow is obtained from the following equation:

$$\dot{m}_d = 0.1501p^5 - 1.0076p^4 + 2.4098p^3 - 2.7221p^2 + 2.201p + 0.0368 \tag{F.2}$$

As before, knowing the pressure at any time instant, it is possible to calculate the mass flow with the proposed equation. And, also knowing the time step used to acquire pressure (in this case $\Delta t = 2$ s) it is possible to calculate the amount of H_2 exiting the bottle.

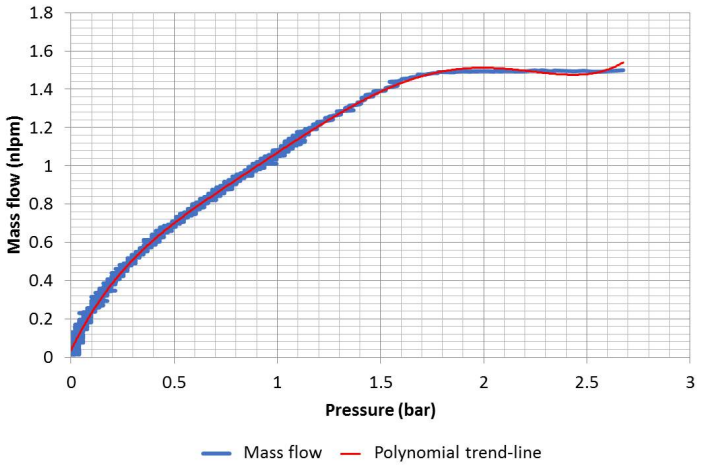

Figure F.4: Experimental mass flow over pressure on exp. 21/12/2016

Again, to check the validity of the proposed empirical equation, the experimental results obtained in test 19/12/2016 have been used. Fig. F.5 , shows the experimental mass flow rate compared with the one obtained by the empirical estimation in equation (F.2).

The experimental and empirical results match, demonstrating again that the empirical estimation is able to reproduce the experimental results regardless of the way the bottle was charged.

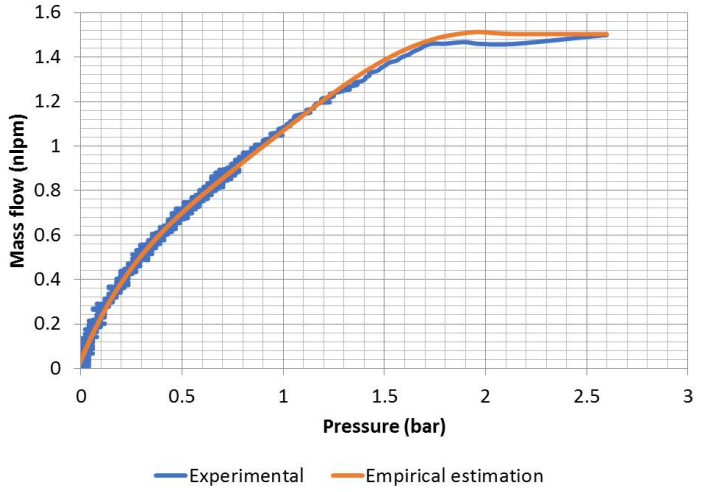

Figure F.5: Exp. and empirical estimation of mass flow and over pressure on exp. 19/12/2016

Using pressure measurements from experiment 19/12/2016, the amount of hydrogen discharged can be estimated and compared with experimental measurements (Fig. F.6). As shown in this figure, the measured amount of discharged hydrogen and the estimated one are almost the same. The measured amount of hydrogen discharged is 118.0 nl, and the estimated one is 117.8 nl.

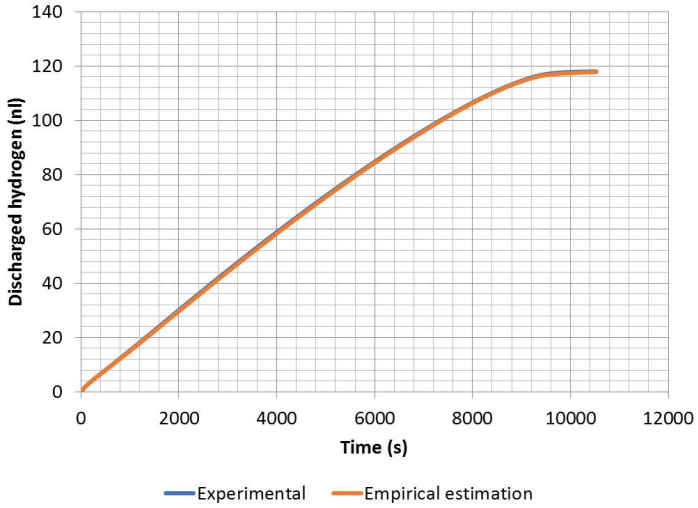

Figure F.6: Experimental and empirical estimation of discharged hydrogen with heater